Hauptreferent:
Prof. Dr.-Ing. U. Nackenhorst

Korreferent:
Asst. Prof. Dr. L. Chamoin

Doktorand:
M.Sc. Ole Stegen

A Fully Micro-mechanically Motivated Material Law for Filled Elastomer

A Fully Micro-mechanically Motivated Material Law for Filled Elastomer

M.Sc. Ole Stegen
geboren am 30.08.1984, in Hamburg

2015

Kurzfassung

In der vorliegenden Arbeit wird ein Materialmodell für partikel gefüllte Elastomere entwickelt und dessen FE-Implementierung wird aufgezeigt. Die Mikromechanik spielt eine entscheidende Rolle für die Materialeigenschaften von Partikel gefüllten Elastomeren. Der innere Aufbau und die Synthese von Elastomeren wird ausführlich erklärt. Das grundlegende Konzept der Steifigkeit von Elastomeren, die Entropie Elastizität, wird hergeleitet.

Ausgehend von der Entropie Elastizität werden die mikromechanischen Gleichungen von etablierten Modellen erweitert. Die Mikromechanik gliedert sich in drei Teile, das elastische-, das schädigungs- (auch als Mullins Effekt bekannt) und das zeitabhängige viskose Verhalten. Beim Mullins Effekt wird besonderer Fokus auf die dehnungsinduzierte Anisotropie gelegt.

Die konstitutiven Gleichungen aus der Mikromechanik können zunächst nur für den eindimensionalen Fall hergeleitet werden, was einer FE-Implementierung im Wege steht. Hierzu werden die mikromechanischen Gleichungen in eine Form gebracht, die eine effiziente Auswertung mit dem Computer ermöglicht. Mit Hilfe des Mikro-Sphären Konzeptes werden die Gleichungen in einem dreidimensionalen kontinuumsmechanischen Sinne verallgemeinert. Ausgehend von dieser Verallgemeinerung werden die konstitutiven Gleichungen in ein bekanntes FE-Framework eingebettet.

Für das Materialmodell wird anhand von Parameterstudien gezeigt, welchen Einfluss die einzelnen mikromechanischen Parameter haben. In einem weiteren Schritt wird das Materialmodell mit Testdaten aus der Literatur verglichen. Hierzu zählen unter anderem mehrachsige Zugversuche und der Relaxationstest. Es ist anzumerken, dass das Materialmodell in der Lage ist, permanentes Setzen abzubilden ohne Plastizität zu verwenden.

Stichworte: Finite-Elemente-Methode, Partikel gefüllte Elastomere, Mikromechanik, Entropie Elastizität, Anisotropie, zeitabhängiges Materialverhalten, Mullins Effekt, Mikro Sphären Modell

Abstract

In the present thesis, a material law for particle filled elastomer is derived and its finite element implementation is shown. The micromechanics has an important influence on the material behaviour of particle filled elastomer, whereby the inner structure and synthesis are described. The main concept for the stiffness - namely the entropy elasticity - is derived.

Starting from entropy elasticity, the micro-mechanical equations from established models are extended. The micromechanics is divided into three parts: the elastic, the damage (also known as Mullins effect) and the time dependent viscous material behaviour. For the Mullins effect, the main focus is placed upon the strain introduced anisotropy.

In a first step, the micro-mechanical constitutive equations can only be derived for the one-dimensional case, which impedes a finite element implementation. The equations are transferred in a form that enables an efficient computational implementation. With the use of the micro-sphere concept, the equations are generalised in a three-dimensional continuum. This generalisation is implemented in an existing finite element framework.

The influence of the micro-mechanical parameters are shown within parameter studies for the presented material model. In a further step, the material model is compared with test data from literature, such as multi axial tension tests and the relaxation test. It is mentionable that the material model can predict a permanent set without using the concept of plasticity.

Keywords Finite Element Method, Particle Filled Elastomer, Micromechanics, Entropy Elasticity, Anisotropy, Time Depended Material Behaviour, Mullins effect, Micro Sphere Model

Danksagung

Diese Arbeit entstand während meiner Arbeit als Wissenschaftlicher Mitarbeiter am Institut für Baumechanik und Numerische Mechanik der Leibniz Universität Hannover. Ich hatte das Glück, meine Arbeit im Rahmen des internationalen Graduiertenkollegs 1627 anfertigen zu dürfen.

Besonders dankbar bin ich meinem Doktorvater, Herrn Prof. Dr.-Ing. habil. Udo Nackenhorst, er hat mir nicht nur die Anfertigung meiner Arbeit ermöglicht, sondern war jederzeit bereit, mir wissenschaftliche Anleitung zu geben und hat damit zum Gelingen meiner Arbeit beigetragen.

Aufgrund meines Promotionsstipendiums konnte ich ein halbes Jahr an der ENS Cachan im LMT arbeiten. Hier wurde die wissenschaftliche Betreuung von Herrn Dr. Ludovic Chamoin übernommen. Besonders gefreut hat mich, dass Herr Chamoin auch das Referat meiner Arbeit übernommen hat und noch kurz vor Weihnachten nach Hannover gereist ist, hierfür einen herzlichen Dank.

Meinen Kollegen am IBNM, meinen Mitstreitern aus dem GRK1627 möchte ich für die gemeinsame Zeit und ihre Hilfsbereitschaft danken. Die Seminarfahrten mit den GRK werde ich sehr vermissen. Danken möchte ich auch Alena Rosenberger als Sekretärin am IBNM und Dorit Schulte als GRK Koordinatorin, sie haben mich immer bei unseren zahlreichen Reiseanträgen tatkräftig unterstützt. Herrn Prof. em. Dr.-Ing. habil. Dr.-Ing. E.h. Dr. h.c. mult. Erwin Stein möchte ich ganz besonders für die Weinseminare danken, bei denen ich mit den Kollegen und ehemaligen Kollegen viel Spaß hatte.

Der Deutschen Forschungsgemeinschaft möchte ich für die Finanzierung meiner Arbeit und insbesondere auch meines Forschungsaufenthaltes an der ENS Cachan danken. In diesem Rahmen gebührt auch ein herzlicher Dank an Prof. Dr.-Ing. habil. Dr. h.c. mult. Peter Wriggers, der das GRK1627 geleitet hat.

Ein besonderer Dank gilt meiner Familie und Freunden, die mich bei meiner Promotion immer unterstützt und motiviert haben.

Contents

1. Introduction

The history of elastomer dates back to the 17th century, when the main part of nowadays used elastomer, natural rubber was discovered. Francois Fresneau, on his travel to South America discovered the milk of the hevea tree, which is called natural rubber. In 1751, a paper of him was presented, in which he described many properties of rubber, see Chauvin [1999]. He tried to find some applications for this kind of material, but since it has almost no elastic stiffness, he could only show in a theoretical way, how to make it liquid with turpentine.

The first useful rubber was invented by Charles Goodyear in 1839, as mentioned in Goodyear [1844]. He developed the vulcanisation of natural rubber with sulphur. This newly developed material now had an elastic stiffness, but an incredible strain at failure up to 700%. Accordingly, the material became increasingly interesting for many industrial applications. Owing to economic growth, the demand for rubber products could not be supplied by natural rubber. In order to obtain an alternative and enhanced material properties, synthetic rubber was developed. In Germany, the first synthetic rubber was produced by Rohm and Hass using the method patented by Plauson [1937].

After 1950, the rubber industry became increasingly important, whereby the range of applications dramatically increased. The next important step of elastomer development was reinforcement to improve the stiffness. The basic idea was to fill rubber with small spheric particles to increase the local stretch during macroscopic stretching. Commonly used filler particles are carbon black and silica particles with modified surfaces. Inspired by Einstein [1911], who introduced the hydrodynamic reinforcement factor for viscous liquids, similar formulas for filled elastomer were developed by Mullins and Tobin [1965].

It was soon discovered that filled elastomers show more phenomenological effects than simply an increased modulus. In Mullins [1969], the famous Mullins effect was published, which describes the successive damage in virgin loading. From this point, it was clear that understanding of elastomer required a deeper look inside the material to understand the underlying micro-mechanical processes. The first theories that describe the micro-mechanical basics were published in Bueche [1960], while a more precise model derived from the statistics of chain-filler networks was published by Govindjee and Simo [1991]. Since computer-aided design was used in development process, suitable material models for elastomer were developed. This thesis is intended to close the gap between phenomenological material models and the micro-mechanical processes.

1.1. State of the Art

The phenomenological material models for elastomer have been available since long, capturing large strain and rotations. Most of these models use the principal invariants of the stretch tensor. The free energy function is split additively into deviatoric and volumetric parts. A general model was proposed by Rivlin [1948]. It contains an

infinite sum of terms having first and second invariants. If only the first term is considered, the so-called Neo-Hookean material by Treloar [1943] is obtained, which is the most simple material model. By keeping the second term of the Rivlin model, the first material equation derived by Mooney [1940] is obtained. This model is also known as the Mooney-Rivlin model. The Odgen-Material uses the principal stretches. Another model of this type is Yeoh [1993], which considers the first three powers of the first invariant. All these models are only able to describe the elastic material behaviour. Besides, as they are easy to implement, one can find them in almost all non-linear finite element codes. All these material models can be fitted to test data by tuning the material parameters, although these parameters have no physical meaning.

In order to describe damage, continuum approaches were developed. Almost all of these models use the concept of internal variables. These variables can be interpreted as a memory of the material. A simple model was introduced by Ogden and Roxburgh [1999], which uses only a single internal variable to describe the permanent set. In Ihlemann [2003], a set of eight variables was used depending on the load history. Another model was introduced by Dorfmann and Ogden [2004], which focuses on the dissipation function. A more general concept was introduced by Besdo and Ihlemann [2003], which also describes the effect of ongoing permanent set in cyclic loading. A step into a micro-mechanical motivation was undertaken by Cantournet et al. [2009], who use the internal sliding of elastomer chains as a material parameter. All of these models used parameters, which cannot be calculated by micromechanics, rather they have to be fitted to the material response in some way. Another major problem is that these approaches use an isotropic damage function, which cannot describe strain introduced anisotropy.

Elastomers show a strong rate dependent behaviour. The first studies were conducted by Fletcher [1953]. Payne [1962] conducted an extensive study of elastomer under cyclic loading with small strain amplitudes. He divided the Young's modulus in two parts, namely the storage modulus and the loss modulus, where the storage modulus describes the reversible part and the loss modulus the dissipation. A computational model was present by Simo [1987], which uses a set of Maxwell elements to describe the frequency dependent damping. This model counts among the class of fading memory models, which are commonly solved with the convolution integral.

In literature, a number of thermo-mechanical coupled models can be found in Holzapfel and Simo [1996], Boukamel et al. [2001], [Dal and Kaliske, 2009], Drozdov and Christiansen [2009]. All these models use the dissipation as a heat source and linear or non-linear dependence for the shear modulus on the temperature. These models are important for the development of tires and bearings, because they are used in cyclic loading. An approach for the stationary rolling was published by Suwannachit and Nackenhorst [2013]. A more micro-mechanical motivated model is described in Miehe and Göktepe [2005], which assumes the existence of three distinct time scales for relaxation. A two-scale approach dealing with viscosity was published by Tang et al. [2012].

Molecular dynamic methods are widely established in elastomer science and they allow predicting the time evolution for a system of interacting molecules. Usually, the simulation comprises of three parts: first, a set of initial conditions for the molecules; second, an interacting potential, e.g. Lennard-Jones, Mores, Born-Mayer, whereby the choice is obtained by the accuracy and the computational speed demands; and third, the time evolution of a system by solving a set of classical Newtonian equations

of motion for each particle in the system. The first molecular dynamics simulation was carried out by Alder and Wainwright [1957] using only 100 atoms to simulate a phase transition. The limiting factor is always the calculation power. For molecular dynamics simulation, the first standard finite elements like rod, beam or shell elements were used. An application for nanocomposits can be found in Zeng et al. [2008], whereby especially the interactions between the nanofillers and the polymermatrix are investigated. In Nasdala et al. [2005], a molecular dynamic FEM simulation is suggested, which can describe the hysteresis effects of linked polymer chains. For this purpose, a four-node finite element with only translational degree of freedom was developed. The advantage of this type of elements is the possibility to describe different non-linear force field potentials in an exact way. These models have a length scale much smaller than required for technical application. Some models use homogenization methods to find the material parameters for phenomenological models described before.

The micromechanics of elastomer is a wide research field with the micromechanics of the length scale of elastomer chains and filler particles. In Bueche [1961], the mechanism inside the material for the Mullins effect was described. Govindjee and Simo [1991] found a statistical distribution for the chain-filler interaction. Based upon this theory, Dargazany and Itskov [2009] developed a micro-mechnanical motivated constitutive relation, however, a FE implementation is missing.

1.2. Goal of this Thesis

In this thesis, a fully micro-mechanical motivated material law for particle filled elastomer will be developed and implemented into a FE framework.

All the material parameters have a physical expression or can be derived by the statistical distribution of elastomer chains and filler particles. This work is a step in the development of virtual material, which means a new material created on the computer and the response can be tested in a virtual material test. Moreover, a better understanding will be gained concerning what is going on inside the material.

Starting with the physical and chemical backgrounds, the micro-mechanical structure of filled elastomer will be investigated. The structure and mechanical behaviour is modelled within a micromechanics framework on the microstructure. Due to suitable upscaling techniques, a continuum mechanics description will be obtained, which can be implemented in an existing finite element framework. The main focus is placed upon the anisotropic Mullins effect and the viscous behaviour of filled elastomer. In Figure 1.1, the advances in virtual material modelling are shown.

State of the art workflow	Future workflow
new material	specifications for new material
material testing	micromechanical modeling
material model	validation
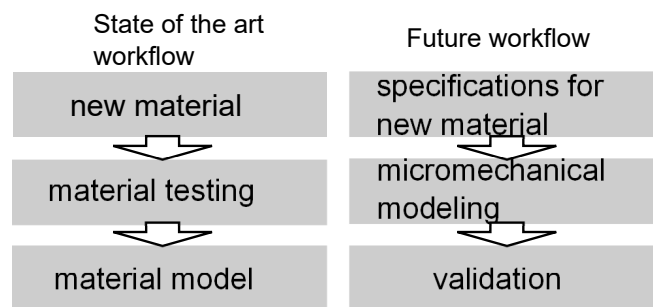
Figure 1.1.: Comparison between the state of the art workflow and the future workflow in material design process

2. Physical and Chemical Properties of Elastomer

In this chapter, the chemical and the physical properties are discussed. The elements of interest are the polymer chains, filler particles and the bonding points. For modelling, these elements are treated using the methods of statistical physics. The chemical structure of the chain segments and bondings is very important for the physical and mechanical behaviour.

2.1. Structure of Elastomer

To understand the structure of elastomer, a chain element is considered as the smallest element. This length scale is approximately $10\,\text{Å} = 10^{-9}\,\text{m}$.

2.1.1. Elastomer Chain

A single elastomer chain comprises of n chain elements, where each chain element is a macromolecule. The structure or chemical formula of the macromolecule is not yet of interest. The chain elements are bounded by chemical reactions and the most important is that this the bonding is not straight, which implies there is always a valence bond angle between two chain elements. If the first element is fixed in space, the second element will be connected with the valence bond angle, although there is one degree of freedom left, namely the rotation. This is called the freely rotating chain, because the rotation is random. If a sufficient number of chain elements are connected, the elastomer chain appears as a random walk, which is very similar to coiled spaghetti.

For a proper description of the elastomer chain, the following definitions are provided: length of a segment l and the chain end to end vector $\boldsymbol{R}$. With the direction vector $\boldsymbol{d}$ of the chain end to end vector, $\boldsymbol{R}$ is calculated by the following formula

$$\boldsymbol{R} = r\boldsymbol{d} \tag{2.1}$$

with the absolute value of end to end distance r, see Figure 2.1. To measure the end to end distance in a dimensionless way, the relative end to end distance

$$\bar{r} = \frac{r}{l} \tag{2.2}$$

is introduced, which means the measured length in chain elements.
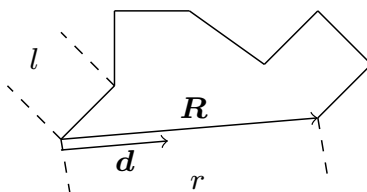
Figure 2.1.: Description of an elastomer chain
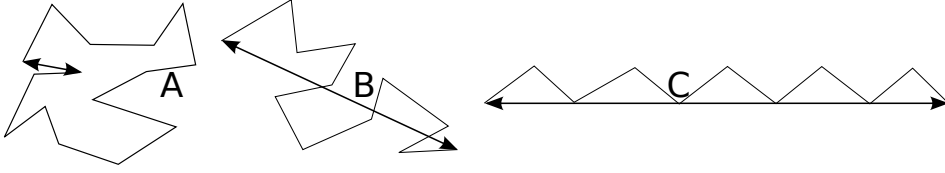
Figure 2.2.: Stretching of an elastomer chain: A) fully random chain, B) slightly stretched chain and C) fully stretched chain, the chain is not straight due to valence angle at the bondings

2.1.2. Entropy of an Elastomer Chain

For the description of elasticity of the elastomers, the entropy changes during stretching becomes important. For an unconstrained and unstretched chain, the rotation angle of each connected elastomer chain element is random, which form the state of maximum entropy. In this state, the chain has the maximum number of possible conformations, whereby it can be seen as the state of the lowest order. During stretching, the number of possible conformations decreases. In case of a fully stretched chain, there is only one possible conformation left, whereby the entropy reaches its minimum, see Figure 2.2.

A quantitative description of the entropy for small deformation using the Gaussian theory for rubber elasticity has been shown by Treloar [1943], which is illustrated in the following section. Imagine an elastomer with one end fixed in the origin and the other end is free to move on x_1 coordinate. The probability to find the free end in the infinitesimal range of $\mathrm{d}x_1$ can be calculated in the following way:

$$p(x_1)\mathrm{d}x_1 = \frac{b}{\pi^{\frac{1}{2}}} \exp(-b^2 x_1^2)\mathrm{d}x_1, \tag{2.3}$$

with the model parameter b. If one end is entirely free in space, the probability is calculated as

$$p(x_1, x_2, x_3)\mathrm{d}x_1\mathrm{d}x_2\mathrm{d}x_1 = \frac{b^3}{\pi^{\frac{3}{2}}} \exp(-b^2 r_1^2)\mathrm{d}x_1\mathrm{d}x_2\mathrm{d}x_3, \tag{2.4}$$

with the quadratic end to end distance $r^2 = x_1^2 + x_2^2 + x_3^2$. In spherical coordinates, equation (2.4) reads as

$$p(r)\mathrm{d}v = \frac{b^3}{\pi^{\frac{3}{2}}} 4\pi r^2 \exp(-b^2 r_1^2)\mathrm{d}r. \tag{2.5}$$

Now the Boltzmann equation can be applied, the entropy η_i of an elastomer is calculated as follows

$$\eta_i = a + k_\mathrm{B} \ln p(r), \tag{2.6}$$

with the constant entropy a and the Boltzmann constant $k_\mathrm{B} = 1.3806488 \times 10^{-23}$ J/K. By using (2.5), the entropy is calculated to

$$\eta_i = \underbrace{a + k_\mathrm{B} \ln \left(\frac{b^3}{\pi^{\frac{3}{2}}} \right)}_{\text{const}} - k b^2 r^2, \tag{2.7}$$

where the constant part can be neglected. The model parameter b is calculated by mean-square value of the radius

$$b^2 = \frac{3}{2\overline{r^2}}. \tag{2.8}$$

Now, the entropy for an incompressible network is investigated. A homogeneous deformation can be expressed with the principal stretches, which leads to the change of entropy

$$\Delta\eta_i = -Kb^2[(\lambda_1 - 1)X_1^2 + (\lambda_2 - 1)X_2^2 + (\lambda_3 - 1)X_3^3]. \tag{2.9}$$

In the reference configuration (unstretched state), the vector r has no preference direction, which means the isotropic state. Now, the sum over all elastomer chains per unit volume N is calculated

$$\sum_i^N X_1^2 = \sum_i^N X_2^2 = \sum_i^N X_3^2 = \frac{1}{3}N\overline{r^2}. \tag{2.10}$$

It result in the the change of entropy

$$\Delta\eta = -\frac{1}{2}Nk_B(\lambda_1^2 + \lambda_2^2 + \lambda_3^2 - 3). \tag{2.11}$$

For an isothermal process, the Helmholtz free energy function has the following simple form

$$\psi = -T\Delta\eta, \tag{2.12}$$

with the thermodynamic temperature T. After combining to two last equations finally ends up with

$$\psi = \frac{1}{2}Nk_BT(\underbrace{\lambda_1^2 + \lambda_2^2 + \lambda_3^2}_{I_1} - 3). \tag{2.13}$$

This is exactly the Neo-Hookean material model with the shear modulus of $\mu = Nk_BT$ and the first invariant of stretch tensor I_1. This simple example shows the concept of entropy elasticity. More general models are obtained with the non-Gaussian statistical theory. One example is the later used theory based upon the Langevin distribution function. It turns out that this theory is equal to the Gaussian statistical theory for small deformation.

2.1.3. Elastomer Network

Elastomer comprises coiled elastomer chains. For unvulcanised elastomers, they simply have physical bondings due to the attractive forces. The single chains are in their thermodynamic preferred state. During stretching, the chains will slip to each other. If the deformation is kept constant, they will return in their thermodynamic preferred state and the stress relaxes. This kind of material shows viscous behaviour like honey but not the elastic behaviour.

The chains are commonly vulcanised with sulphur, which leads to chemical bondings, which are much stiffer than the physical ones. The chains are no longer free, rather

they build a network with chains and bonding points. If the chains and bonding points are randomly distributed, the network is called amorphous. This network prevents the elastomer chains from sliding to each other. If the force on a specimen is released, the elastomer turns into its former state, where the elastomer now shows the elastic behaviour. The vulcanisation follows the statistical laws, which leads to microscopic inhomogeneities and anisotropy, although at the macroscopic length scale, it yields a homogeneous and isotropic material behaviour.

The amorphous network is not the only network form that can appear in elastomers, rather there can be sections of chains having a preferred direction. This leads in physical bondings between the elastomer chains. This kind of network is called semi crystalline. If all chains have the same preferred direction, the network is called crystalline, see Figure 2.3.

The phenomenon during stretching is the strain-introduced crystallisation. For high strains, about 500% of the elastomer chains are close to their fully stretched state. This leads to clusters of chains that have the same direction and are physically bounded with each other. This phenomenon is called strain-introduced crystallisation, see also Treloar [1975]. The recent results on this phenomenon can be found in Toki et al. [2009].
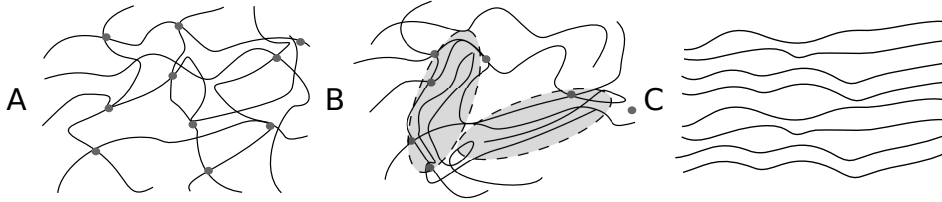
Figure 2.3.: Types of elastomer network: A) amorphous, B) semi crystalline (crystalline sections are marked with grey ellipsoids) and C) crystalline

2.1.4. Filler Reinforcement

To increase the shear modulus of the elastomers, filler particles are added. As these particles are much stiffer than the elastomer chain matrix, therefore they are treated as rigid. This leads to a deformation of only the elastomer matrix during loading. The filler particles decrease the deformable volume of the elastomer matrix. If the global deformation is the same as in unfilled elastomers, the local deformation has to be increased. One known formula is from Einstein, for the hydro-mechanical reinforcement factor X, he calculated

$$X = 1 + 2.5\Phi \tag{2.14}$$

with the filler volume fraction Φ. In literature, more formulas like this can be found, which take into account quadratic terms due to the particle-particle interactions, Guth and Simha [1936]. One more important part is the bonding of the particle and the filler. In this section, some brief definitions are given. In the following chapters, this phenomenon is described in more detail.

The number of bonded elastomer chain segments per unit volume is denoted by N_B and the total area of active absorption sides from the filler particle per unit volume

by A. The ratio of both dimensions is an important material parameter

$$\kappa = \frac{A}{N_{\mathrm{B}}}.\tag{2.15}$$

If κ increases, the chance of a chain segment finding a filler particle for bonding increases. This results in a decrease of average value of chain elements connecting two filler particles, see Figure 2.4.
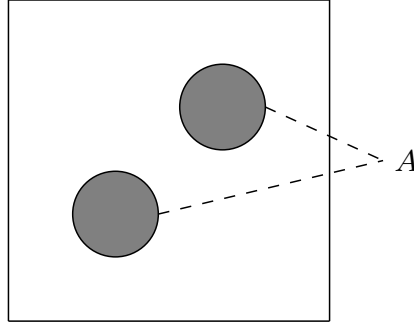
Figure 2.4.: Unit volume for filled elastomer

2.1.5. Temperature Dependent Behaviour
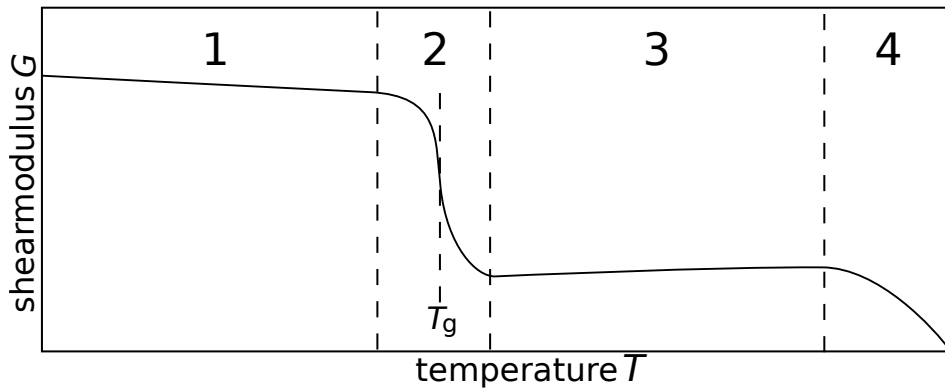
Figure 2.5.: Qualitative curve of temperature dependence of elastomer: region 1) energy elasticity, region 2) glass transition, region 3) entropy elasticity and region 4) chemical decomposition

Elastomer shows different behaviour during the change of temperature, whereby a good description of this temperature dependent behaviour for elastomer and other polymeres can be found in Röthemeyer and Sommer [2013]. The mechanical behaviour can be separated into four different temperature regions, see Figure 2.5.

For low temperatures, elastomer shows an energy elastic behaviour. This temperature is below the glass transition temperature T_{g}, where the chain elements are in a frozen state, hence they cannot move relative to each other.

The second temperature region is named as the glass transition region. This region shows the strongest temperature dependence. In this region, the shear modulus is

decreasing over decades while the temperature is increasing. The inflexion point is named as the glass transition temperature. The elastomer chains transform from the state of sticking together to a state of a moving amorphous network. More details about the ongoing effects can be found in Gibbs and DiMarzio [1958].

The third temperature region is the entropy elastic region. Here, the mechanism described in section 2.1.2 holds. For elastomers, this region is the region of importance. Here, the shear modulus is increasing slightly linear with the increase in the temperature. The chemical decomposition starts when the temperature increases to temperature region four. Further, chemical decomposition appears in the form of melting or chemical reactions with oxygen.

In Table 2.1, the differences between energy and entropy elasticity are shown. It emerges that the mechanical behaviour is somehow shifted for an elastomer during passing the glass transition temperature. For example, the temperature is increasing while stretching an elastomer below the glass transition temperature and above the temperature is decreasing.

Table 2.1.: Characteristics of energy and entropy elasticity

	Entropy elastic	Energy elastic
Example of material	Polymer	Metal, Polymer in glassary state
Stretching	Entropy decreases	Inner energy increases
Change of volume	Almost iso-volumetric	volume change in general
Stretching	Temperature increases	Temperature decreases
Heating	Stretch decreases	Stretch increases
Micromechanics	see section 2.1.2	Energy increases due to attractive forces caused by distance change between the atoms

2.2. Chemistry of Elastomer

In this section, the chemical synthesis of polymers is described, see also Hiemenz and Lodge [2007] and Baerns et al. [2013]. The main three chemical processes are the chain polymerization, addition polymerization and the condensation polymerization. The main scheme for all these process are the same, namely the monomers react with each other and build an elastomer chain.

2.2.1. Chain Polymerization

Chain polymerization is one of three major principles of polymers synthesis. It is characterized by an ongoing addition of mostly unsaturated monomers on the growing chain and no split off chemical by-products. Also, no change of molecular groups takes place inside the reactant. It can be classified by the active center in radical, anionic and cationic coordination valence. Another classification is made by the number of different monomers: for homopolymerization, only one type monomer reacts with each other; for copolymerization, two or more types of monomers react with each other.

The radical chain polymerization can be divided into three steps:

1. Starting reaction: a new active center is formed (free radical)

2. Growth reaction: the macromolecular chain is growing in a chain reaction, ongoing attachment of monomers

3. Termination reaction: the growth of a chain is terminated irreversibly.

During the starting reaction, a monomer reacts with a free radical and the double bonding of the monomer between the two carbon elements is split. The free radical is now bonded with the carbon elements. This leads to a free electron on the second carbon atom, see Figure 2.6.
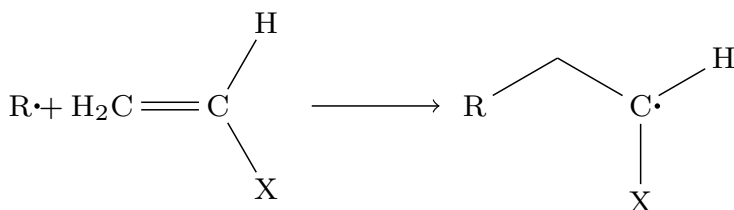
Figure 2.6.: Polymerization starting reaction

During the growth reaction, the second monomer is attached to the chain, see Figure 2.7. In this case, the carbon element splits the double bonding, which leads to another free electron. Now, the typical form of the elastomer chain emerges. The valence angle is a fix value but the rotation angle is random. The number of chain elements is repeatedly increased by the same phenomena.
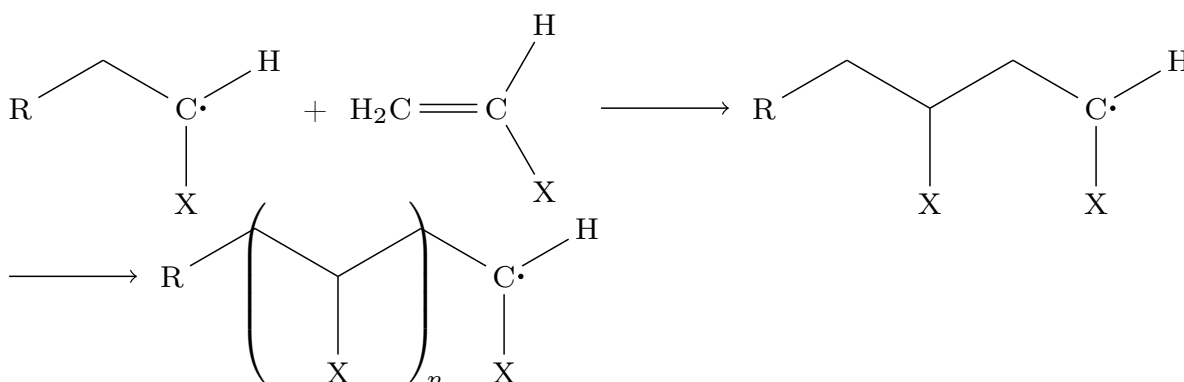
Figure 2.7.: Polymerization growth reaction

The growth of the chain elements can be stopped by the junction of two radicals. The free electrons of two elastomer chains create a junction resulting in one elastomer chain that is no longer growing, see Figure 2.8. Another possible termination reaction is the disproportionation. Here, one hydrogen element from the second carbon atom from the right chain will change its position to the left chain. Now, the carbon atom of the left chain no longer has a free electron, whereas the right chain has two carbon elements with a free electron, followed by sharing of electrons via double bonding. The result is two chains that can no longer grow, see Figure 2.9.

To understand the progress of chain polymerization, two important definitions are made:
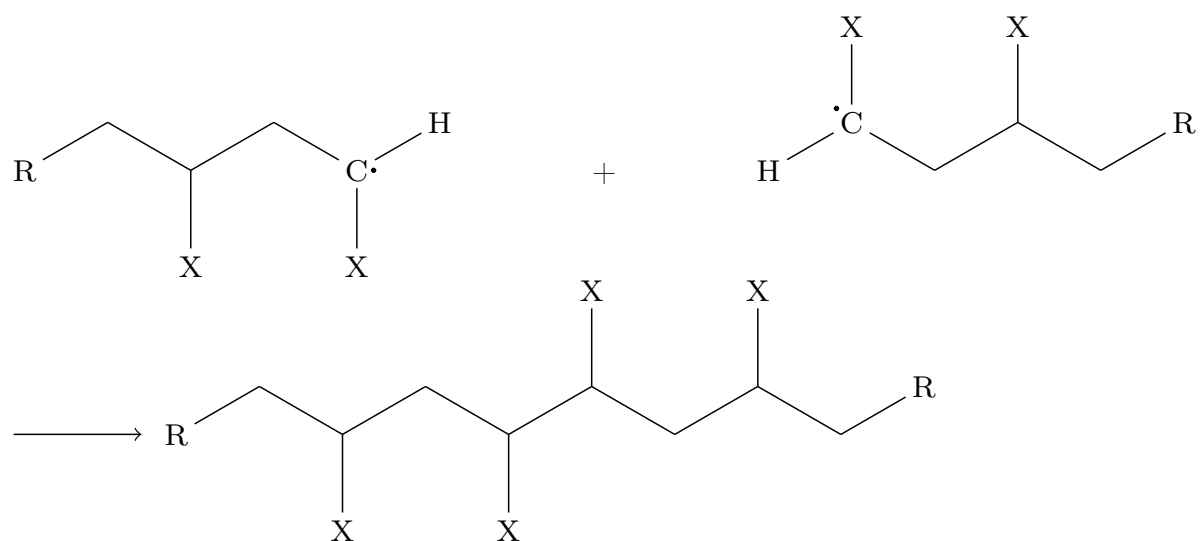
Figure 2.8.: Polymerization termination reaction: junction of two radicals
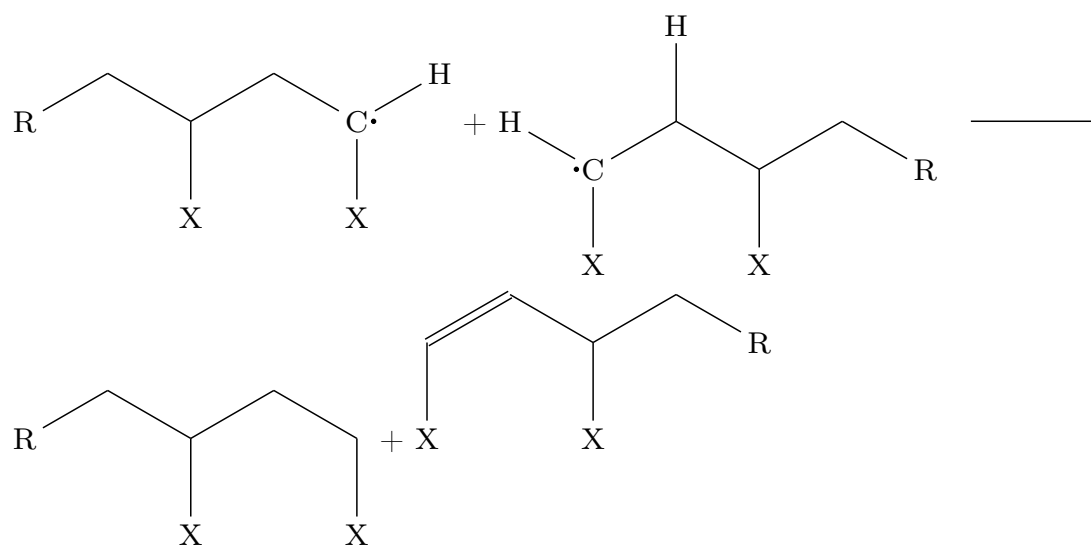
Figure 2.9.: Polymerization termination reaction: disproportionation

- Chemical yield: the percentage of reactants which reacted. For polymer case, the percentage of monomers that are attached to the chains.

- Degree of polymerization: the number of monomers in a polymer chain. However only the average of this value can be measured. The standard deviation is also significant for describing the polymerization.

The process of the radical polymerization is divided into different stages, corresponding to the chemical yield:

For yield less than 0.01%: initiation with a non-stationary progression take place. This state is characterized by a massive nucleation of initial radicals, many primary radicals and few oligarchy radicals. Further, the reaction speed increases rapidly, while the average degree of polymerization remains low.

For yield of 0.01% to 5%: stationary reaction take place. The concentration of monomers is almost constant, given that the yield is low. Besides, the reaction speed is constant.

For yield of 5% to 20%: end of stationary reaction state take place. The reaction speed is decreasing as well as the monomer concentration is decreasing. Finally, the first macromolecules reach their final length and further the first termination reactions take place.

For yield 20% to 60%: gel effect arises, which is also known as Tommsdorff-Norris effect, see also Alger [1996] and O'Neil et al. [1996]. Though, the reaction speed should decrease in this state, however, an acceleration is observed. The polymer chains reach a high degree of polymerization, therefore the diffusion slows down, which results in less termination reactions. In contrast to the polymer chains, the monomers are small enough for diffusion, hence the polymerization is kept alive. The degree of polymerization increases very heavily and the standard deviation increases too.

For yield of 60% to maximum: glass effect arises. Please note, this name should not be mixed with the glass transition described previously. Here, the diffusion of the polymer molecules and the radicals is very slow. Moreover, the remaining polymers have problems to move, which result in continuous decrease of the reaction speed. A chemical yield of 100% is generally not reached, depending on the polymerization procedure. The polymerization in liquids helps in decreasing viscosity and hence it is possible to achieve the higher yield.

For the radical chain, the polymerization radicals build the active center on the growing end of the chain. The starting reaction is initialised by an acid, such as sulphuric acid H_2SO_4, fluoroboric acid HBF_4 or aluminium chloride $AlCl_3$. The acid reacts with the water, which leads to free positive charged hydrogen ions. The starting reaction combines the hydrogen elements to H_2. This leads to change of bonding type from double to single followed by a positive charged carbon element on the right hand side, see Figure 2.10.

The growth reaction is similar to the radical chain polymerization, where the chain elements are continuously added. The termination reaction cannot take place, given that the growing end of the chain elements are both positively charged. However, an elimination reaction can take place, where one proton changes to the new monomer unit. The chain growth ends now and a positive hydrogen ion is ready for a new

$$\text{H}^{\oplus}[\text{BF}_3\text{OH}]^{\ominus} + \text{CH}_2 \!\!=\!\! \underset{X}{\overset{}{\text{C}}} \!\!-\!\! \text{H} \longrightarrow [\text{BF}_3\text{OH}]^{\ominus} + \text{CH}_3 \!\!-\!\! \underset{X}{\overset{\oplus}{\text{C}}} \!\!-\!\! \text{H}$$
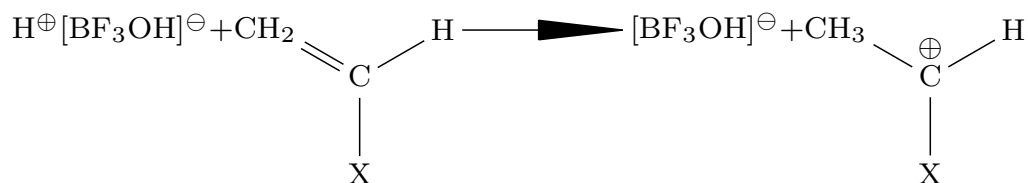
Figure 2.10.: Starting reaction of cationic chain polymerization

$$\text{nHO} - (\text{CH}_2)_4 - \text{OH} + \text{nO} \!\!=\!\! \text{C} \!\!=\!\! \text{N} - (\text{CH}_2)_6 - \text{N} \!\!=\!\! \text{C} \!\!=\!\! \text{O}$$
$$\longrightarrow \ (\text{O} - (\text{CH}_2)_4 - \text{O} - \text{CO} - \text{NH} - (\text{CH}_2)_6 - \text{NH} - \text{CO})\text{n}$$
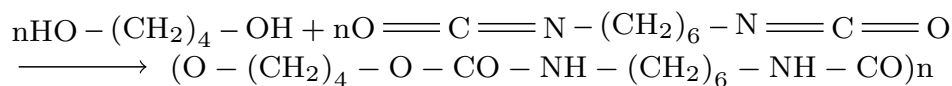
Figure 2.11.: Synthesis of polyurethane

starting reaction. A simple way to stop the polymerization process controlled is to add a lye.

The anisotropic polymerization uses an anion for growing the chain. It is mostly not possible to formulate a growth and termination reaction. This type of polymerization is called living polymerization. For this type of polymerization, the degree of polymerization is close to a linear function of the chemical yield and it is possible to achieve the polymers with almost the same chain length.

2.2.2. Addition Polymer

The addition polymer is a polymer formed by addition reactions. A polymer is formed by the rearrangement of bonds, where no atoms and molecules are lost, however an addition polymer is step-wise formed with molecules of low degree of polymerization. First dimer and trimer are formed, which then are bonded to a polymer of higher degree of polymerization, and so on. As an example, the formation of polyurethane is shown in Figure 2.11.

2.2.3. Condensation Polymer

In condensation polymerization, small molecules are lost when monomers join together. An example of such molecules can be water, carbon dioxide or hydrogen chloride. The forming process is slower than for addition polymers and the degree of polymerization is generally lower. In Figure 2.12, a typical polymer condensation reaction is shown. In this case, one chain produces two water molecules and the functional groups on the end of the chain remain active, hence the short groups can combine together resulting in longer chains. The presence of the shorter polar functional groups on the chains often enhances the chain-chain attractions, such as hydrogen bonding. This leads to crystallisation and higher tensile strength.

2.2.4. Vulcanisation of Polymer

The vulcanisation of polymers is a chemical process for converting polymers into more durable rubber by using high-energy radiation peroxides or sulphur. The first vulcanisation process was invented by Goodyear [1844], in which sulphur was used, see Figure 2.13. The chains are bonded by sulphur brides resulting in an elastic
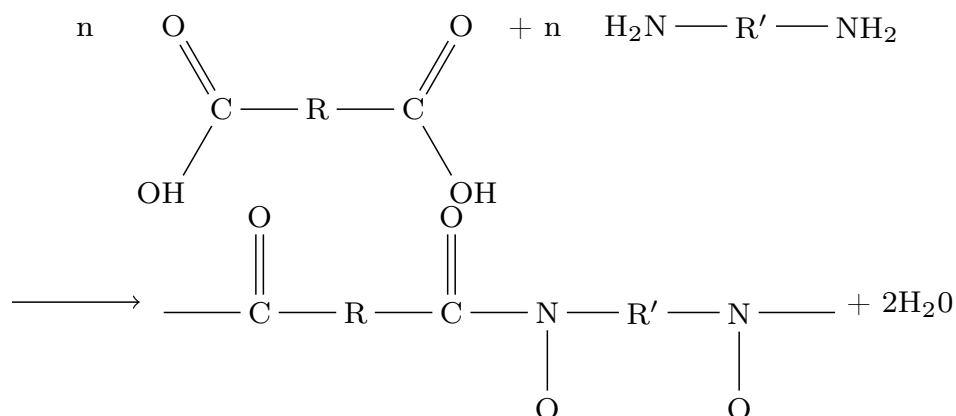
Figure 2.12.: Synthesis of one type of condensation polymer

response, as the chains can no longer move relative to each other. Moreover, the other vulcanisation processes establish chemical bondings between the chains. For sulphur vulcanisation, oxygen embrittlement is a known problem, which means the sulphur bridges are replaced with the oxygen, hence the material response become more stiffer and more brittle, see Blum et al. [1951].
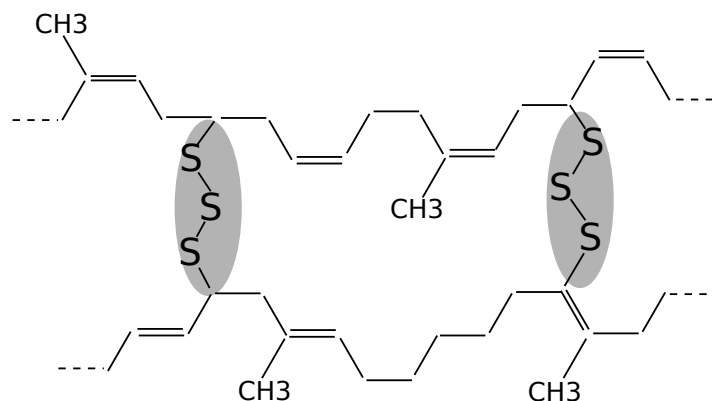
Figure 2.13.: Vulcanisation of elastomer: two chain elements are linked by sulphur bridges (grey areas)

3. Non-linear Continuum Mechanics Background

The continuum mechanics describes the movement of material bodies in space and time. In this chapter, the most important continuum quantities are summarised, in particular, the measurement of stress and strain. These measurements are written in a general way, which results in non-linear relations. In continuum mechanics, the inner assembly of the material is neglected; for example, the atoms. The material is treated as a continuous medium characterized by the certain field quantities like density, strain and velocity. This is referred as the macroscopic view of the material. This chapter provides a brief introduction to understand the viscoelastic damage model for elastomer, which is described in detail in the next chapters. A more detailed description can be found in Holzapfel [2000], Truesdell and Noll [1965], Malvern [1969] and [Marsden and Hughes, 1983].

3.1. Kinematics
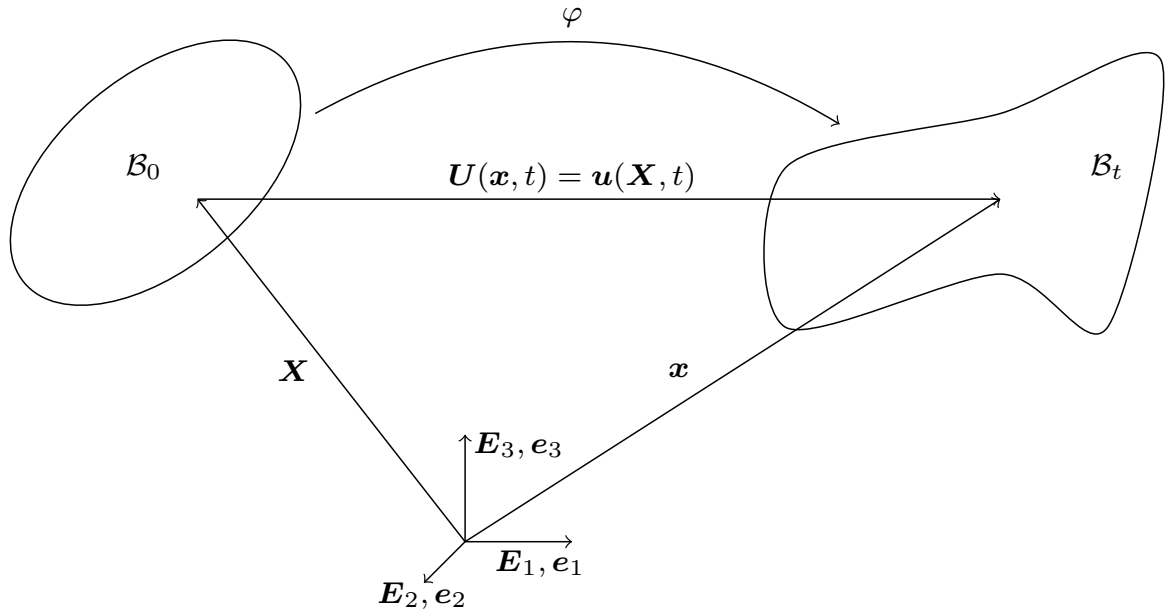
Figure 3.1.: Kinematic relations of a continuum body

The kinematics of a continuous body describes the motion of each given particle for each time without considering the cause of the movement. The reference or initial configuration of the body is denoted by $\mathcal{B}_0$ and the actual or deformed configuration by $\mathcal{B}_t$, see Figure 3.1. In the following, capital letters denote values in reference configuration and lower case letters in deformed configuration. The unit vectors $\boldsymbol{E}_1, \boldsymbol{E}_2, \boldsymbol{E}_3$ and $\boldsymbol{e}_1, \boldsymbol{e}_2, \boldsymbol{e}_3$ span a three-dimensional Eulerian space $\mathbb{R}^3$, and the time t belongs to $\mathbb{R}_+$.

The mapping φ is introduced to describe the deformation and movement in each material point between the reference and the deformed configuration

$$\varphi(\boldsymbol{X}, t): \quad \boldsymbol{X} \mapsto \boldsymbol{x} \quad \forall \boldsymbol{X} \in \mathcal{B}_0. \tag{3.1}$$

The inverse operator φ^{-1} maps each point from the deformed to the current configuration

$$\varphi^{-1}(\boldsymbol{x}, t): \quad \boldsymbol{x} \mapsto \boldsymbol{X} \quad \forall \boldsymbol{x} \in \mathcal{B}_t. \tag{3.2}$$

The motion of the points from reference to current configuration is called displacement field

$$\boldsymbol{U}(\boldsymbol{X}, t) = \boldsymbol{x}(\boldsymbol{X}, t) - \boldsymbol{X} \tag{3.3}$$

in material description (Lagrangian form), where U is a function of reference position $\boldsymbol{X}$ and time, the displacement field can also be written in spatial description (Eulerian form)

$$\boldsymbol{u}(\boldsymbol{x}, t) = \boldsymbol{x} - \boldsymbol{X}(\boldsymbol{x}, t), \tag{3.4}$$

where $\boldsymbol{u}$ is a function of deformed position $\boldsymbol{x}$ and time. The two equations are related by the mapping defined by equation (3.1)

$$\boldsymbol{U}(\boldsymbol{X}, t) = \boldsymbol{U}((\varphi^{-1}(\boldsymbol{x}, t), t)) = \boldsymbol{u}(\boldsymbol{x}, t) \tag{3.5}$$

hence, $\boldsymbol{U}$ and $\boldsymbol{u}$ have the same values but different arguments.

To describe the deformations (strains and rigid body motions) of a continuum body, a mapping of an infinitesimal line element in reference configuration $\mathrm{d}\boldsymbol{X}$ to its corresponding deformed configuration $\mathrm{d}\boldsymbol{x}$ is necessary. Therefore, the deformation gradient $\boldsymbol{F}$ is defined as follows

$$\mathrm{d}\boldsymbol{x} = \boldsymbol{F} \cdot \mathrm{d}\boldsymbol{X} \tag{3.6}$$

with

$$\boldsymbol{F}(\boldsymbol{X}, t) = \frac{\partial \phi(\boldsymbol{X}, t)}{\partial \boldsymbol{X}} = \mathrm{Grad}\boldsymbol{x}(\boldsymbol{X}, t) \tag{3.7}$$

or

$$\boldsymbol{F}^{-1}(\boldsymbol{x}, t) = \frac{\partial \phi^{-1}(\boldsymbol{x}, t)}{\partial \boldsymbol{x}} = \mathrm{grad}\boldsymbol{X}(\boldsymbol{x}, t) \tag{3.8}$$

In general, the deformation gradient is a non-symmetric tensor with nine independent components. As the deformation gradient contains the rigid body motions in particular rotations, which makes it dependent on the reference system and hence, it is not an objective measure for deformation.

The deformation gradient is a two-point tensor that is related to both configurations and provides a linear transformation. Since the transformation has an inverse transformation, its determinant is not equal to zero. The determinant also provides the volume change of an infinitesimal volume element. Therefore, from a physical perspective, the determinant or volume ratio has to be greater than zero

$$\det \boldsymbol{F} = J > 0. \tag{3.9}$$

The transformation of an infinitesimal surface element $\mathrm{d}\boldsymbol{A}$ can be calculated by

$$\mathrm{d}\boldsymbol{a} = J\boldsymbol{F}^{-\mathrm{T}}\mathrm{d}\boldsymbol{A}, \tag{3.10}$$

which is known as Nanson's formula.

To obtain an objective measure for the deformation, strain tensors are introduced. First, the formulas (3.3) and (3.7) are combined to calculate the displacement gradient

$$\boldsymbol{H} = \mathrm{Grad}\boldsymbol{U} = \mathrm{Grad}\boldsymbol{x}(\boldsymbol{X}, t) - \mathrm{Grad}\boldsymbol{X} = \boldsymbol{F} - \boldsymbol{I} \tag{3.11}$$

with the unit tensor

$$\boldsymbol{I} = \begin{bmatrix} 1 & 0 & 0 \\ 0 & 1 & 0 \\ 0 & 0 & 1 \end{bmatrix}. \tag{3.12}$$

Now, a strain measure can be obtained by describing the squared change of length of an infinitesimal line element as follows

$$||\mathrm{d}\boldsymbol{x} \cdot \mathrm{d}\boldsymbol{x}|| - ||\mathrm{d}\boldsymbol{X} \cdot \mathrm{d}\boldsymbol{X}|| = \mathrm{d}\boldsymbol{x} \cdot \mathrm{d}\boldsymbol{x} - \mathrm{d}\boldsymbol{X} \cdot \mathrm{d}\boldsymbol{X} \tag{3.13}$$

$$= \mathrm{d}\boldsymbol{X} \cdot \boldsymbol{F}^{\mathrm{T}} \cdot \boldsymbol{F} \cdot \mathrm{d}\boldsymbol{X} - \mathrm{d}\boldsymbol{X} \cdot \mathrm{d}\boldsymbol{X} \tag{3.14}$$

$$= \mathrm{d}\boldsymbol{X} \cdot \left(\boldsymbol{F}^{\mathrm{T}} \cdot \boldsymbol{F} - 1\right) \cdot \mathrm{d}\boldsymbol{X} \tag{3.15}$$

$$= \mathrm{d}\boldsymbol{X} \cdot 2\boldsymbol{E} \cdot \mathrm{d}\boldsymbol{X} \tag{3.16}$$

with the Green-Lagrange strain tensor

$$\boldsymbol{E} = \frac{1}{2}(\boldsymbol{F}^{\mathrm{T}} \cdot \boldsymbol{F} - 1). \tag{3.17}$$

By using equation (3.11), the Green-Lagrange strain tensor can be reformulated to

$$\boldsymbol{E} = \frac{1}{2}\left(\boldsymbol{H} + \boldsymbol{H}^{\mathrm{T}} + \boldsymbol{H} \cdot \boldsymbol{H}^{\mathrm{T}}\right). \tag{3.18}$$

This tensor is symmetric and contains no longer rotations. This can be easily seen by decomposing the deformation gradient in stretch and in rotation part

$$\boldsymbol{F} = \boldsymbol{R} \cdot \boldsymbol{U} = \boldsymbol{v} \cdot \boldsymbol{R}. \tag{3.19}$$

With the rotation tensor $\boldsymbol{R}$, the right (or material) stretch tensor $\boldsymbol{U}$ and the left (or spatial) stretch tensor $\boldsymbol{v}$. The part of equation (3.18) with the deformation gradient and its inverse leads to $\boldsymbol{F}^{\mathrm{T}} \cdot \boldsymbol{F} = \boldsymbol{U}^{\mathrm{T}} \cdot \boldsymbol{R}^{\mathrm{T}} \cdot \boldsymbol{R} \cdot \boldsymbol{U} = \boldsymbol{U}^{\mathrm{T}} \cdot \boldsymbol{I} \cdot \boldsymbol{U}$. The rotation vanishes and only the stretch part is represented. By neglecting the higher order terms in equation (3.18), the engineering strain tensor

$$\boldsymbol{\varepsilon} = \frac{1}{2}\left(\boldsymbol{H} + \boldsymbol{H}^{\mathrm{T}}\right) \tag{3.20}$$

is defined. Another deformation tensor is the right Cauchy-Green tensor

$$\boldsymbol{C} = \boldsymbol{F}^{T} \cdot \boldsymbol{F}. \tag{3.21}$$

Its representation in the deformed configuration is the left Cauchy-Green deformation tensor

$$\boldsymbol{b} = \boldsymbol{F} \cdot \boldsymbol{F}^T. \tag{3.22}$$

For this thesis, the definition of the stretch vector is very important since it will be used for the micro-mechanical modelling. First, a direction $\boldsymbol{d}$ is defined, now the stretch can be calculated by the use of the deformation gradient

$$\boldsymbol{\lambda}_{\mathrm{d}} = \boldsymbol{F}(\boldsymbol{X}, t) \cdot \boldsymbol{d}. \tag{3.23}$$

The stretch vector is not only dependent on the space and time, but also on the chosen direction $\boldsymbol{d}$, which is pointed out by the subscript $_{\mathrm{d}}$. The stretch ratio is defined by

$$\lambda_{\mathrm{d}} = |\boldsymbol{\lambda}_{\mathrm{d}}|, \tag{3.24}$$

which is a measure for the extension of a unit vector. For extension $\lambda_{\mathrm{d}} > 1$ holds, for compression $0 < \lambda_{\mathrm{d}} < 1$ and for the unstretched state $\lambda_{\mathrm{d}} = 1$.

3.2. Stress Measures

The forces are actions on a part or the entire surface of the body. The internal load of a body can be measured by the stresses. The body is cut at point $\boldsymbol{x}$ by a plane surface. To derive the Cauchy stress vector, the force acting on infinitesimal surface element $\mathrm{d}a$ is related to the force acting on it

$$\boldsymbol{t} = \frac{\mathrm{d}\boldsymbol{f}}{\mathrm{d}a}. \tag{3.25}$$

This measure is not objective, rather it generally depends on the orientation of the cutting plane. The Cauchy-Theorem states that there exists a unique second order tensor $\boldsymbol{\sigma}$ so that

$$\boldsymbol{t}(\boldsymbol{x}, t, \boldsymbol{d}) = \boldsymbol{\sigma}(\boldsymbol{x}, t) \cdot \boldsymbol{d}. \tag{3.26}$$

The Cauchy stress tensor $\boldsymbol{\sigma}$ is an objective measure that does not depend on the orientation of the surface element, furthermore, it is symmetric. By relating the force to an infinitesimal surface element of the initial configuration $\mathrm{d}A$, one can find the Piola-Kirchhoff stress vector

$$\boldsymbol{T} = \frac{\mathrm{d}\boldsymbol{f}}{\mathrm{d}A}. \tag{3.27}$$

Again, applying the Cauchy-Theorem,

$$\boldsymbol{T}(\boldsymbol{X}, t, \boldsymbol{d}) = \boldsymbol{P}(\boldsymbol{X}, t) \cdot \boldsymbol{d}, \tag{3.28}$$

the first Piola-Kirchhoff stress tensor is obtained. This tensor is a non-symmetric two-field tensor like the deformation gradient, which has some drawbacks, especially in computation. Therefore, the second Piola-Kirchhoff stress tensor is introduced

$$\boldsymbol{S} = \boldsymbol{F}^{-1} \cdot \boldsymbol{P} = J\boldsymbol{F}^{-1} \cdot \boldsymbol{\sigma} \cdot \boldsymbol{F}^{-\mathrm{T}}. \tag{3.29}$$

This tensor is entirely related to the initial configuration. The tensor is obtained by performing the pull-back operator $\boldsymbol{F}^{-1}(\bullet)\boldsymbol{F}^{-\mathrm{T}}$ to the Kirchhoff stress tensor which is defined as

$$\boldsymbol{\tau} = J \cdot \boldsymbol{\sigma}. \tag{3.30}$$

3.3. Balance Laws

The balance laws are the fundamental laws that are valid for all the materials. One set of the principles comprises of the four conservation laws: conservation of mass, conservation of linear and angular momentum and the balance of energy. Another principle is the second law of thermodynamics, which is not a conservation principal. It describes in which direction the process goes, e.g. the heat flow takes place from higher to lower temperatures. Therefore, the entropy principle is expressed as an inequality.

3.3.1. Conservation of Mass

The mass of a body is an extensive value. For a material body $\mathcal{B}_t$, the mass

$$m = \int_{\mathcal{B}_0} \rho_0 \mathrm{d}V = \int_{\mathcal{B}_t} \rho \mathrm{d}v \tag{3.31}$$

is calculated by the integral over the extensive value mass density over the entire body. The mass density is denoted as ρ_0 for the initial and as ρ for deformed configuration. In this work, the body is treated as a closed system; therefore, the amount of mass is constant and only energy can cross the boundaries of the system. With the volume ratio the relation

$$\rho_0 = J\rho \tag{3.32}$$

between the densities can be found. Due to the fact that the mass is constant, the change of mass vanishes

$$\frac{\mathrm{d}}{\mathrm{d}t} m = \frac{\mathrm{d}}{\mathrm{d}t} \int_{\mathcal{B}_0} \rho_0 \mathrm{d}V = \int_{\mathcal{B}_0} \frac{\mathrm{d}}{\mathrm{d}t}(\rho J) \mathrm{d}V$$
$$= \int_{\mathcal{B}_0} J(\dot{\rho} + \rho \operatorname{div} \dot{\boldsymbol{x}}) \mathrm{d}V = \int_{\mathcal{B}_t} (\dot{\rho} + \rho \operatorname{div} \dot{\boldsymbol{x}}) \mathrm{d}v = 0. \tag{3.33}$$

This equation is called the integral form of mass conversation. The continuity equation

$$\dot{\rho} + \rho \operatorname{div} \dot{\boldsymbol{x}} = 0 \tag{3.34}$$

is valid at every point of the body. Equation (3.34) is called the local form of mass conservation in spatial description.

3.3.2. Conservation of Linear Momentum

The linear momentum vector is defined as follows

$$\boldsymbol{L} = \int_{\mathcal{B}_0} \rho_0 \dot{\boldsymbol{X}} \mathrm{d}V = \int_{\mathcal{B}_t} \rho \dot{\boldsymbol{x}} \mathrm{d}V. \tag{3.35}$$

Using Newton's second law of motion, whereby the sum of externally applied forces is equal to the change of linear momentum, the law is formulated for a continuum body

$$\frac{\mathrm{d}\boldsymbol{L}}{\mathrm{d}t} = \int_{\mathcal{B}_t} \rho \tilde{\boldsymbol{b}} \mathrm{d}V + \int_{\partial \mathcal{B}_t} \boldsymbol{t} \mathrm{d}a \tag{3.36}$$

with the body force per unit mass $\tilde{\boldsymbol{b}}$ and the surface traction vector $\boldsymbol{t}$. For the fulfilment of equation (3.35), it is necessary and sufficient that the Cauchy theorem holds. By using the divergence theorem, the external force term can be reformulated as follows

$$\int_{\partial \mathcal{B}_t} \boldsymbol{t} \mathrm{d}a = \int_{\partial \mathcal{B}_t} \boldsymbol{\sigma} \cdot \boldsymbol{d} \mathrm{d}a = \int_{\partial \mathcal{B}} \mathrm{div}\, \boldsymbol{\sigma} \cdot \boldsymbol{d} \mathrm{d}v. \tag{3.37}$$

Using equation (3.36) and (3.37), the local form of linear momentum balance is found

$$\mathrm{div}\, \boldsymbol{\sigma} + \tilde{\boldsymbol{b}} = \rho \ddot{\boldsymbol{x}}. \tag{3.38}$$

In statics, the acceleration term vanishes

$$\mathrm{div}\, \boldsymbol{\sigma} + \tilde{\boldsymbol{b}} = 0. \tag{3.39}$$

This equation is referred as Cauchy's equation of equilibrium.

3.3.3. Conservation of Angular Momentum

The angular momentum emerges as a cross product of linear momentum and position vector $\boldsymbol{x}$

$$\boldsymbol{J} = \int_{\partial \mathcal{B}} \boldsymbol{x} \times \rho \dot{\boldsymbol{x}} \mathrm{d}V. \tag{3.40}$$

The reference point can be chosen arbitrary. For simplification, the coordinate origin is considered. Analogous to linear momentum, the time derivative of angular momentum must be equal to externally applied torques

$$\frac{\mathrm{d}\boldsymbol{J}}{\mathrm{d}t} = \int_{\mathcal{B}_t} \boldsymbol{x} \times \rho \tilde{\boldsymbol{b}} \mathrm{d}V + \int_{\partial \mathcal{B}_t} \boldsymbol{x} \times \boldsymbol{t} \mathrm{d}a. \tag{3.41}$$

In static, it can be shown that balance of angular momentum holds if and only if the Cauchy stress tensor is symmetric $\boldsymbol{\sigma} = \boldsymbol{\sigma}^{\mathrm{T}}$.

3.3.4. Conservation of Energy

The balance of energy is well known as the first law of thermodynamics, which states that the change of inner energy $\mathcal{U}$ and kinetic energy $\mathcal{K}$ equals the power of external forces $\mathcal{W}$ plus the rate of thermal work $\mathcal{Q}$

$$\dot{\mathcal{U}} + \dot{\mathcal{K}} = \mathcal{W} + \mathcal{Q}. \tag{3.42}$$

With the deformed configuration, the single parts are calculated as follows:

$$\mathcal{U} = \int_{\mathcal{B}_t} \rho u \mathrm{d}v \tag{3.43}$$

$$\mathcal{K} = \int_{\mathcal{B}_t} \frac{1}{2} \rho \dot{\boldsymbol{x}} \cdot \dot{\boldsymbol{x}} \mathrm{d}v \tag{3.44}$$

$$\mathcal{W} = \int_{\mathcal{B}_t} \rho \tilde{\boldsymbol{b}} \cdot \dot{\boldsymbol{x}} \mathrm{d}v + \int_{\partial \mathcal{B}_t} \boldsymbol{t} \cdot \dot{\boldsymbol{x}} \mathrm{d}a \tag{3.45}$$

$$\mathcal{Q} = \int_{\mathcal{B}_t} \rho r \mathrm{d}v - \int_{\partial \mathcal{B}_t} \boldsymbol{q} \cdot \boldsymbol{d} \mathrm{d}a \tag{3.46}$$

with the specific inner energy u, the specific inner heat source r and the heat flux over the boundaries $\boldsymbol{q}$. All the equations together lead to the integral form of energy balance

$$\frac{\mathrm{d}}{\mathrm{d}t} \int_{\mathcal{B}_t} \rho \left(u + \frac{1}{2}\rho \dot{\boldsymbol{x}} \cdot \dot{\boldsymbol{x}} \right) \mathrm{d}v = \int_{\mathcal{B}_t} \rho \left(\tilde{\boldsymbol{b}} \cdot \dot{\boldsymbol{x}} \mathrm{d}v + r \right) \mathrm{d}a + \int_{\partial \mathcal{B}_t} (\boldsymbol{t} \cdot \dot{\boldsymbol{x}} - \boldsymbol{q} \cdot \boldsymbol{d}) \, \mathrm{d}a. \quad (3.47)$$

To avoid the boundary integral, the Cauchy-Theorem followed by partial integration is applied

$$\int_{\mathcal{B}_t} \rho \left(\dot{u} + \frac{1}{2}\rho \dot{\boldsymbol{x}} \cdot \ddot{\boldsymbol{x}} \right) \mathrm{d}v = \int_{\mathcal{B}_t} \left[\rho \left(\tilde{\boldsymbol{b}} \cdot \dot{\boldsymbol{x}} \mathrm{d}v + r \right) + \operatorname{div} (\dot{\boldsymbol{x}} \cdot \boldsymbol{\sigma} - \boldsymbol{q}) \right] \mathrm{d}a \quad (3.48)$$

solving the divergence term and using the fact that the linear momentum should vanish at every point, the conservation of energy is reduced to

$$\rho \dot{u} = \operatorname{grad}\dot{\boldsymbol{x}} \cdot \cdot \boldsymbol{\sigma} + \rho \cdot r - \operatorname{div}\boldsymbol{q}. \quad (3.49)$$

3.3.5. Entropy Inequality Principle

While the first law of thermodynamics describes the energy transfer of a thermodynamic process, the second law describes the direction of energy transfer. In section 2.1.2 entropy was introduced as a measure of microscopic disorder. For the continuum mechanics, the entropy is measured per unit volume η in the reference configuration. The entropy of a body is denoted as

$$\mathcal{S} = \int_{\mathcal{B}} \eta \mathrm{d}V = \int_{\mathcal{B}_t} J \eta \mathrm{d}v. \quad (3.50)$$

The second law of thermodynamics states that the change of entropy is always greater or equal than the heat generation plus the heat inward flux over the boundaries divided by the thermodynamic temperature

$$\frac{\mathrm{d}\mathcal{S}}{\mathrm{d}t} \geq \int_{\mathcal{B}} \frac{1}{T}\rho r \mathrm{d}v + \int_{\partial \mathcal{B}_t} \frac{1}{T}\boldsymbol{q} \cdot \boldsymbol{d} \mathrm{d}a. \quad (3.51)$$

In analogy to energy balance, the boundary integral is converted to a volume integral

$$\int_{\partial \mathcal{B}_t} \frac{1}{T}\boldsymbol{q} \cdot \boldsymbol{d} \mathrm{d}a = \int_{\mathcal{B}} \operatorname{div}\left(\frac{1}{T}\boldsymbol{q} \right) \mathrm{d}v = \int_{\mathcal{B}} \frac{1}{T}\operatorname{div}\boldsymbol{q} - \frac{1}{T^2}\boldsymbol{q}\operatorname{grad}T \mathrm{d}v. \quad (3.52)$$

The local form follows to

$$T\rho\dot{\eta} \geq \rho r - \operatorname{div}\boldsymbol{q} + \frac{1}{T}\boldsymbol{q}\operatorname{grad}T. \quad (3.53)$$

With the Helmholtz Free Energy

$$\varphi = u - Ts \quad (3.54)$$

and the energy balance equation, the Clausius-Duhem equation

$$-\rho(\dot{\varphi} + s\dot{T}) + \operatorname{grad}\dot{\boldsymbol{x}} \cdot \cdot \boldsymbol{\sigma} - \frac{1}{T}\operatorname{grad}T \geq 0 \quad (3.55)$$

can be found. For isothermal processes, the Clausius-Duhem equation is equal to dissipated energy

$$\mathcal{D} = \operatorname{grad}\dot{\boldsymbol{x}} \cdot \cdot \boldsymbol{\sigma} - \rho\dot{\varphi} \geq 0. \quad (3.56)$$

3.4. Constitutive Theory

In the previous sections, the kinematic relations and the balance principles were discussed, which are valid for any material. However, there is a lack of equations, for the description of velocities and movements of the material. These equations, known as constitutive equations or material model, should provide a relation between the stress and the strain for a mechanical system. For thermomechanical systems, there is also a relation between the temperature and the heat flux, although only isothermal processes are considered in this thesis.

The material model can be somewhat arbitrary, although it has to fulfil the thermodynamic laws. For the constitutive description, the displacement vector $\boldsymbol{u}$ is normally chosen as the independent variable. The thermodynamic state of material can be described by the following equations

$$\psi = \psi(\boldsymbol{F}) \tag{3.57}$$

$$\eta = \eta(\boldsymbol{F}) \tag{3.58}$$

$$\boldsymbol{\sigma} = \boldsymbol{\sigma}(\boldsymbol{F}). \tag{3.59}$$

The free energy, the entropy and the Cauchy stress are the dependent variables. To find some restrictions for the material law, the material derivative of free energy function

$$\dot{\psi} = \frac{\partial \psi}{\partial \boldsymbol{F}} \cdot \cdot \dot{\boldsymbol{F}} \tag{3.60}$$

is considered. Substituting equation (3.60) into the Clausius-Duhem equation for isothermal process (3.56) yields

$$\operatorname{grad}\dot{\boldsymbol{x}} \cdot \cdot \boldsymbol{\sigma} - \rho \frac{\partial \psi}{\partial \boldsymbol{F}} \cdot \cdot \dot{\boldsymbol{F}} \geq 0. \tag{3.61}$$

Using equations (3.6) and (3.6), the equation above can be reformulated to

$$\left(\sigma - \rho \frac{\partial \psi}{\partial \boldsymbol{F}} \right) \dot{\boldsymbol{F}} \geq 0. \tag{3.62}$$

The time derivative of the deformation gradient is arbitrary, therefore, the equation can only be fulfilled if the expression in the brackets vanishes. This leads to the following equation

$$\boldsymbol{\sigma} = \rho \frac{\partial \psi}{\partial \boldsymbol{F}} \cdot \cdot \dot{\boldsymbol{F}}. \tag{3.63}$$

3.4.1. Concept of Internal Variables

The materials used in engineering often show inelastic behaviour. The inelastic effects can include damage, plasticity or creep. The concept described in the previous section proves non-adequate for describing such effects, as they consider simple elastic effects, which is not dependent on the loading history. To overcome this problem the concept of internal variables has been developed by Coleman and Gurtin [1967],

Lubliner [1969], Haupt [1985]. The Helmholtz Free Energy function depends on the deformation gradient and a set of inner variables

$$\psi = \psi(F, \xi_1, \ldots, \xi_m). \tag{3.64}$$

The internal variables can generally be tensor valued, although for this thesis only scalar variables are used. Analogous to the pure elastic constitutive theory, the material time derivative

$$\dot{\psi} = \frac{\partial \psi}{\partial \boldsymbol{F}} \cdot\cdot \dot{\boldsymbol{F}} + \sum_{\alpha=1}^{m} \frac{\partial \psi}{\partial \xi_\alpha} \cdot\cdot \dot{\xi}_\alpha \tag{3.65}$$

is considered. The internal dissipation can be calculated to

$$\mathcal{D} = \left(\boldsymbol{P} - \rho \frac{\partial \psi}{\partial \boldsymbol{F}} \right) \dot{\boldsymbol{F}} - \sum_{\alpha=1}^{m} \frac{\partial \psi}{\partial \xi_\alpha} \cdot\cdot \dot{\xi}_\alpha \geq 0. \tag{3.66}$$

Applying the Coleman-Noll procedure, the internal variables have to be dissipative

$$-\sum_{\alpha=1}^{m} \frac{\partial \psi}{\partial \xi_\alpha} \cdot\cdot \dot{\xi}_\alpha \geq 0. \tag{3.67}$$

The internal variables require the additional equations to describe the evolution of the internal variables. These equations are restricted to satisfy the equation (3.67) and they generally depend on the deformation gradient and the internal variables itself ξ_α,

$$\dot{\xi}_\alpha = \boldsymbol{E}_\alpha(\boldsymbol{F}, \xi_1, \ldots, \xi_m). \tag{3.68}$$

The evolution function is mostly dependent on stress or strain, whereby they are called stress or strain-like internal variables. For an equilibrium state, it is required that the evolution function is equal to zero.

4. Review of Material Models for Elastomers

This chapter summarises the existing material models for filled and unfilled elastomer. This kind of material models have to deal with large strain and incompressibility. The first part will provide a brief overview of the hyperelastic material model and the analytical homogenization techniques as a first approach to describe the effect of filler reinforcement. Subsequently, simple damage models are presented to describe the Mullins effect. At the end, a brief introduction of visco-elastic material models is given.

4.1. Elastic Material Models

For elastic behaviour of elastomers, a broad class of material models exist. In this overview, only isothermal models are considered (for temperature depended models see Holzapfel and Simo [1996], Reese and Govindjee [1997], Lion [1997] Reese [2003] and Suwannachit and Nackenhorst [2013]). This category of material models is called hyperelastic, since their stress strain relationship is derived from a strain energy density function, see Ogden [1984]. The hyperelastic models are derived from the equation (3.57). The first phenomenological models were developed, such as the Yeoh- or Mooney-Rivlin model. Later developed models were motivated by the micromechanics of the material, for example, the extended tube model by Heinrich and Kaliske [1997]. Moreover, models directly derived from chain statistics can be found in literature, e.g. Miehe et al. [2004].

For elastomers, it is known that the behaviour in shear and compression is entirely different. The compressive modulus is about 50 times higher than the shear modulus, which leads to a Poisson ratio of approximately $\nu = 0.49$. Elastomer is almost incompressible, whereby a special case of incompressibility is characterized by a $\nu = 0.5$. For a proper constitutive formulation, the free energy function is split into a volumetric and a deviatoric part

$$\psi = \psi(J) + \psi(\overline{\boldsymbol{F}}) \tag{4.1}$$

without any loss of generality. The deviatoric part of the deformation gradient $\overline{\boldsymbol{F}}$ is calculated by a multiplicative volumetric deviatoric split

$$\boldsymbol{F} = J^{\frac{1}{3}} \overline{\boldsymbol{F}}. \tag{4.2}$$

In the following, the deviatoric part is denoted with an overline. A simple example for the volumetric part of the free energy function is

$$\psi(J) = \frac{\kappa}{2} \left(\frac{J^2 - 1}{2} - \ln J \right), \tag{4.3}$$

with the bulk modulus κ.

For the deviatoric part, the principal invariants are defined first. The use of invariants ensures an objective material model, because a rotation of the coordinate system has

no effect on the invariants. Using equation (4.2), the deviatoric part of left and right Cauchy-Green stretch tensor are obtained

$$\overline{\boldsymbol{b}} = J^{-\frac{1}{3}} \boldsymbol{F} \cdot \left(J^{-\frac{1}{3}} \boldsymbol{F} \right)^{\mathrm{T}} = J^{-\frac{2}{3}} \boldsymbol{F} \cdot \boldsymbol{F}^{\mathrm{T}} \tag{4.4}$$

$$\overline{\boldsymbol{C}} = J^{-\frac{1}{3}} \boldsymbol{F}^{\mathrm{T}} \cdot \left(J^{-\frac{1}{3}} \boldsymbol{F} \right) = J^{-\frac{2}{3}} \boldsymbol{F}^{\mathrm{T}} \cdot \boldsymbol{F}. \tag{4.5}$$

Now, the three principal invariants can be calculated with the principal stretches λ_1, λ_2 and λ_3 to

$$I_{\overline{\boldsymbol{b}}} = I_{\overline{\boldsymbol{C}}} = \lambda_1^2 + \lambda_2^2 + \lambda_3^2 \tag{4.6}$$

$$II_{\overline{\boldsymbol{b}}} = II_{\overline{\boldsymbol{C}}} = \lambda_1^2 \lambda_2^2 + \lambda_2^2 \lambda_3^2 + \lambda_1^2 \lambda_3^2 \tag{4.7}$$

$$III_{\overline{\boldsymbol{b}}} = III_{\overline{\boldsymbol{C}}} = \lambda_1^2 \lambda_2^2 \lambda_3^2 \tag{4.8}$$

The simplest hyper-elastic material is the Neo-Hooke material model

$$\psi_{\mathrm{NH}} = \frac{\mu}{2} \left(I_{\overline{\boldsymbol{b}}} - 3 \right), \tag{4.9}$$

it is micro-mechanically motivated by the Gaussian Chain theory, see section 2.1.2. This model is similar to Neo-Hooke Law, which was originally proposed by Rivlin 1948. Since it has only one term, it can only describe a part of the elastomer stress strain curve in a sufficient way.

To obtain the stress tensor, the derivative of the free energy function with respect to the left Cauchy-Green tensor

$$\overline{\boldsymbol{\tau}} = 2 \frac{\partial \psi(\overline{\boldsymbol{b}})}{\partial \overline{\boldsymbol{b}}} \overline{\boldsymbol{b}} \tag{4.10}$$

has to be calculated. The Neo-Hooke model leads to the Kirchhoff stress tensor

$$\overline{\boldsymbol{\tau}}_{\mathrm{NH}} = \frac{\mu}{2} \mathrm{dev}(\overline{\boldsymbol{b}}), \tag{4.11}$$

with the definition of the deviator $\mathrm{dev}(\bullet) = \bullet - \frac{1}{3}\mathrm{tr}(\bullet)\boldsymbol{I}$. The deviator should not be mixed with the isocoric part. For the deviator, the relation $\mathrm{tr}(\mathrm{dev}\bullet) = 0$ holds, which ensures a stress free initial condition for the following strain relations.

A more general model is the Yeoh model

$$\psi_{\mathrm{Y}} = C_1 \left(I_{\overline{\boldsymbol{b}}} - 3 \right) + C_2 \left(I_{\overline{\boldsymbol{b}}} - 3 \right)^2 + C_3 \left(I_{\overline{\boldsymbol{b}}} - 3 \right)^3 \tag{4.12}$$

with the material parameters C_1, C_2 and C_3. It considers higher order terms, which improves the capability to model more general material behaviour, e.g. the upturn known for elastomer when the chains reach their final extensibility. Again, using formula (4.10), the stress is calculated as

$$\overline{\boldsymbol{\tau}}_{\mathrm{Y}} = \left[2C_1 + 4C_2 \left(I_{\overline{\boldsymbol{b}}} - 3 \right) + 6C_3 \left(I_{\overline{\boldsymbol{b}}} - 3 \right)^2 \right] \mathrm{dev}(\overline{\boldsymbol{b}}). \tag{4.13}$$

The Mooney-Rivlin model

$$\psi_{\mathrm{MR}} = C_1 \left(I_{\overline{\boldsymbol{b}}} - 3 \right) + C_2 \left(II_{\overline{\boldsymbol{b}}} - 3 \right) \tag{4.14}$$

also considers the second invariant. The corresponding stress tensor leads to

$$\overline{\boldsymbol{\tau}}_{\mathrm{MR}} = 2\mathrm{dev}\left((C_1 + C_2 I_{\overline{\boldsymbol{b}}})\overline{\boldsymbol{b}} + C_2\overline{\boldsymbol{b}}^2\right). \tag{4.15}$$

All three models can be seen as special case of general polynomial hyperelastic model

$$\psi_{\mathrm{P}} = \sum_{i,j=0}^{n} C_{ij}\left(I_{\overline{\boldsymbol{b}}} - 3\right)^i \left(II_{\overline{\boldsymbol{b}}} - 3\right)^j \tag{4.16}$$

by Rivlin and Saunders [1951a]. With the material parameter C_{ij} and $C_{00} = 0$ to ensure energy free state in initial configuration

$$\psi_{\mathrm{P}}(\overline{\boldsymbol{b}} = \boldsymbol{I}) = 0. \tag{4.17}$$

Another type of hyperelastic material models are the models in terms of principal stretches, whereby the Ogden material is a well known material model, see Ogden [1973].

A model considering the finite limiting chain extensibility was presented by Gent [1996], which uses the natural logarithm for the free energy function

$$\psi_{\mathrm{G}} = -\frac{\mu J_{\mathrm{m}}}{2}\ln\left(1 - \frac{I_{\overline{\boldsymbol{b}}} - 3}{J_{\mathrm{m}}}\right) \tag{4.18}$$

with the extensibility limit J_{m}, as a material parameter. Depending on this parameter, the first invariant is limited to $I_{\overline{\boldsymbol{b}}} \leq J_{\mathrm{m}} + 3$. For limiting case of J_{m} reaching infinity, the model coincidents to the Neo-Hooke material model, which can be shown by the use of a Taylor series expression, see Gent [1996]. The corresponding stress emerges as

$$\overline{\boldsymbol{\tau}}_{\mathrm{G}} = \frac{\mu J_{\mathrm{m}}}{J_{\mathrm{m}} - I_{\overline{\boldsymbol{b}}} + 3}\mathrm{dev}\left(\overline{\boldsymbol{b}}\right). \tag{4.19}$$

In Figure 4.1, the stress strain curves for the most important hyperelastic material models are shown. All material models have a singular behaviour for compression to stretch, being equal to zero. The Neo-Hooke and Mooney-Rivlin material models show a linear behaviour for high strain, whereas the Yeoh material model shows an upturn for high strain. The Gent material model also shows an upturn, but introduces a singularity for strains that reach the limit of $I_{\overline{\boldsymbol{b}}} = J_{\mathrm{m}} + 3$.

All such models have to be fitted to material tests, since most of their material parameters have no physical meaning. In Marlow [2003], a first invariant material model is proposed, which require no parameter fitting to experimental data. The free energy function can be directly derived by the integration of the stress strain curve in a uniaxial tension test, which means the derivative is the measured stress strain curve. The measurement points are exactly represented in the material model, although this model also has no parameters with physical meaning.

An example for a micromechanical motivated model is the tube model. Heinrich and Kaliske [1997] and Kaliske and Heinrich [1999] used a molecular statistical modelling
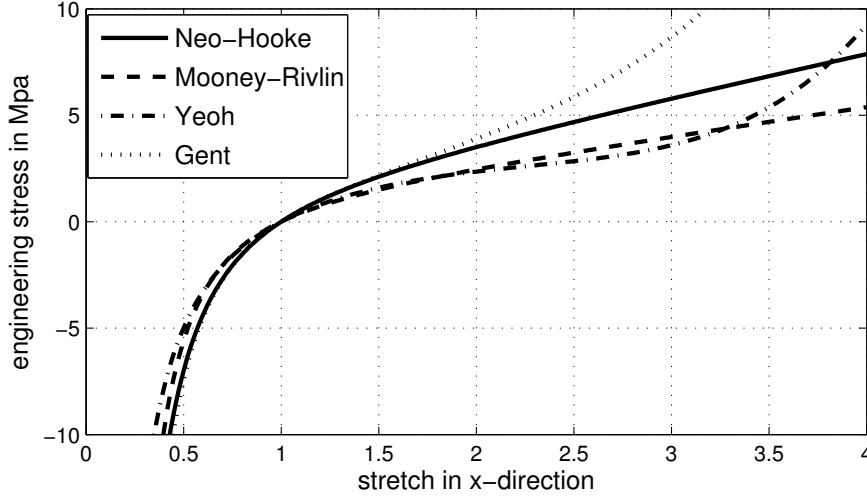
Figure 4.1.: Comparison of hyperelastic material models for uniaxial tension.

approach, which turn out

$$\psi_{\mathrm{T}} = \psi_{\mathrm{chem}} + \psi_{\mathrm{topo}} \tag{4.20}$$

$$= \frac{G_{\mathrm{c}}}{2} \left(\frac{(1 - \delta^2)(I_{\overline{\boldsymbol{b}}} - 3)}{1 - \delta^2(I_{\overline{\boldsymbol{b}}} - 3)} + \ln \left[1 - \delta^2 (I_{\overline{\boldsymbol{b}}} - 3)) \right] \right) + \frac{2G_{\mathrm{e}}}{\beta^2} \sum_{i=1}^{3} \left(\overline{\lambda}_i^{\beta} - 1 \right), \tag{4.21}$$

with the deviatoric part of the principal stretches $\overline{\lambda}_{1,2,3}$. The deviatoric free energy function is decomposed into two parts. The first part corresponds to the chemical bounds of the chains, while the second part represents the additional stiffness due to the topological restraints. G_{c} and G_{e} denote the elastic shear modulus for chemical and topological part, respectively. The parameter δ accounts for the maximum extensibility of the chains. The fitting parameter β can be set to one for long chains. This model could be used for the micro-mechanical description for the elastic part. However, two reasons are against this: first, it uses some non-physical parameters; and second, it will be complicated to extend this model for anisotropic damage and viscous effects. For this reason, a model suggested by Miehe et al. [2004] will be used later on, see section 5.3.

4.1.1. Analytical Homogenization Methods for Filled Elastomers

Filled elastomer is a two-phase material, one phase is the elastomer chains and the other phase involves the filler particles. The properties of the elastomer chains are known from testing and statistical mechanics. The filler particles are much stiffer and often treated as rigid for homogenization.

The exact microstructure is normally not known and if it is known from electron microscopy, it is not applicable to model the microstructure for engineering application. Therefore, analytical homogenization techniques provide a powerful framework, see Hill [1963], Hashin [1962], Kröner [1977]. For elastomers, these techniques will be used to describe the elastic response. To describe the Mullins effect, it is not applicable, because this effect is resulted from the interface of chains and filler particle.

For homogenization, a representative volume element (RVE) is necessary. It is defined as a volume with sufficient number of inclusions. It has to be statistically uniform from a macroscopic perspective. For the application of the RVE as a sufficient average, the material body of interest has to be much larger than the RVE.

For the RVE, the volume average $< \bullet >$ is defined as follows

$$< \bullet >= \frac{1}{V} \int \bullet \mathrm{d}V, \tag{4.22}$$

while $\bullet$ represents an arbitrary quantity, e.g. the stress or strain. A fundamental condition in micromechanics is the Hill-Condition, see [Hill, 1963], stating that the macroscopic power or rate of strain energy $< \boldsymbol{P} > \cdot \cdot < \dot{\boldsymbol{F}} >$ equals the mean value of microscopic power $< \boldsymbol{P} \cdot \cdot \dot{\boldsymbol{F}} >$

$$< \boldsymbol{P} > \cdot \cdot < \dot{\boldsymbol{F}} >=< \boldsymbol{P} \cdot \cdot \dot{\boldsymbol{F}} > . \tag{4.23}$$

For the quantification of the reinforcement, the filler volume fraction

$$\Phi = \frac{V_{\text{filler}}}{V_{\text{ges}}} \quad \in (0, 1) \tag{4.24}$$

with the volume of RVE V_{ges} and the corresponding filler volume V_{filler} is introduced. Without any knowledge of the shape of filler reinforcement, Young's modulus is bounded by Reuss [1929] (lower bound) and Voigt [1889] (upper bound), see Figure 4.2. These bounds can be seen as springs in parallel and springs in series. A more restrictive bound was introduced by Hashin [1962]. All the other analytical homogenization rules lie in between these bounds, at least in their range of applicability, e. g. Guth and Simha [1936] and the famous formula by Einstein [1906]. The self-consistent rule from Budiansky takes into account the higher order terms, for this reason, the reinforcement factor is higher for higher filler concentrations. The bounds hold the consistency condition, which means for $\Phi = 0$, the normalised Young' s modulus is one and for $\Phi = 1$, it equals the ratio of Young's modulus. Some homogenization rules violate the second condition, although remain applicable for filler volume fraction less than 0.3, which are related to technical application.

A recent homogenization rule comes from Rault et al. [2006]. This study is dedicated to elastomer materials. This mixing rule is chosen for two reasons: first, this rule is derived from the micromechanics of elastomers; and second, it is validated with a broad range of test data. The rule is defined by the following equation

$$X = \frac{1}{1 - \Phi^y} \tag{4.25}$$

with $y = 1/3$ for spherical inclusions. For the derivation of this rule, the filler particles are assumed to be rigid. If a specimen is stretched from the length L_0 to L, the average stretch is λ and the elongation equals $\delta L = L_O - L$. The stretch between the particles must be higher than the overall average stretch to compensate the stiff filler particle.

The distance between the filler particles is assumed to be L_0^*. With this definition, the elongation between two filler particles is calculated as

$$\delta L^* = (1 - \lambda^*)L_0^* \tag{4.26}$$
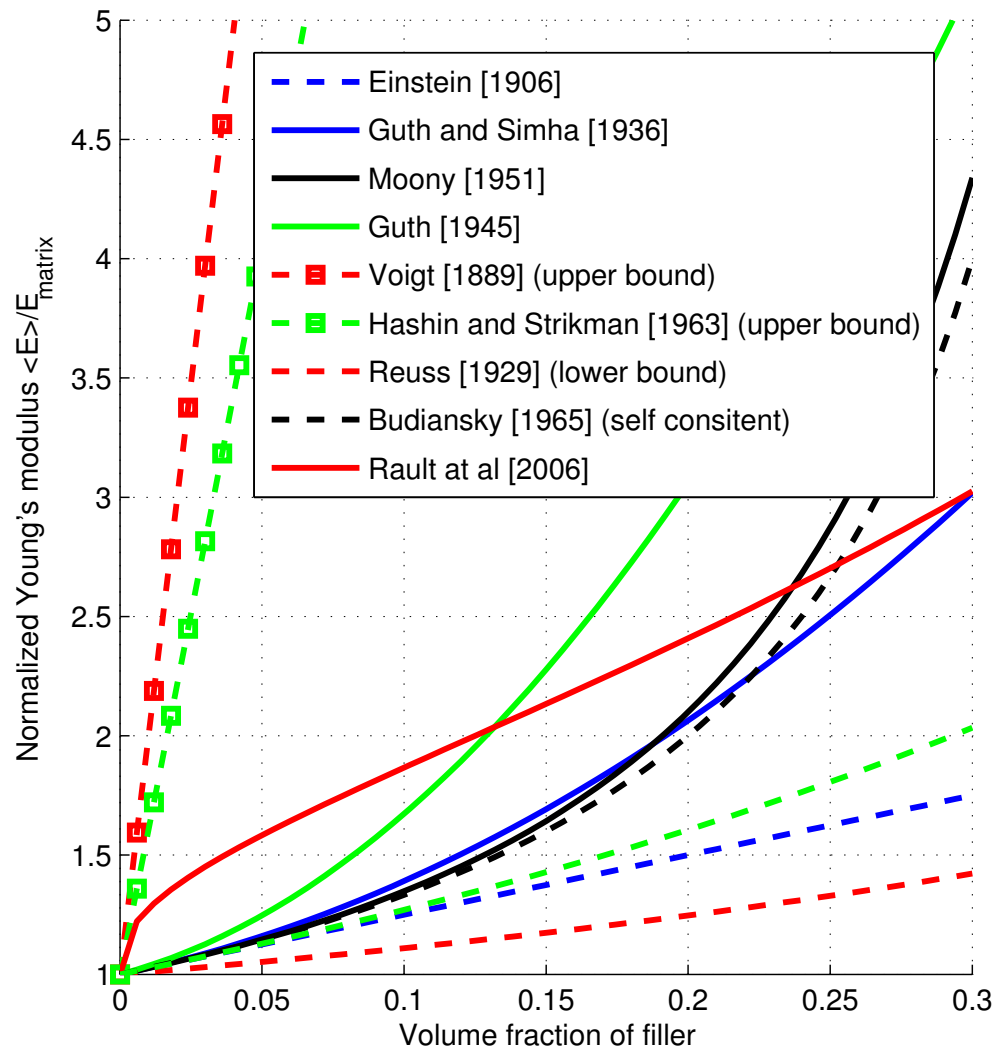
Figure 4.2.: Overview of analytical homogenization methods, filler reinforcement for material with ratio Young-Modulus for the phases of 100

and on average for the specimen

$$\delta L = (1 - \lambda)L_0 \tag{4.27}$$

Equation (4.26) and (4.27) are linked by the filler volume fraction and the geometry of filler particles as follows

$$L_0 = (1 - \Omega^y)L_0^*. \tag{4.28}$$

Combining all three equations leads to

$$\lambda^* = \frac{\lambda - \Omega^y}{1 - \Omega^y}. \tag{4.29}$$

Finally, the derivative of equation (4.29) with respect to the stretch λ leads to (4.25).

4.2. Damage Models
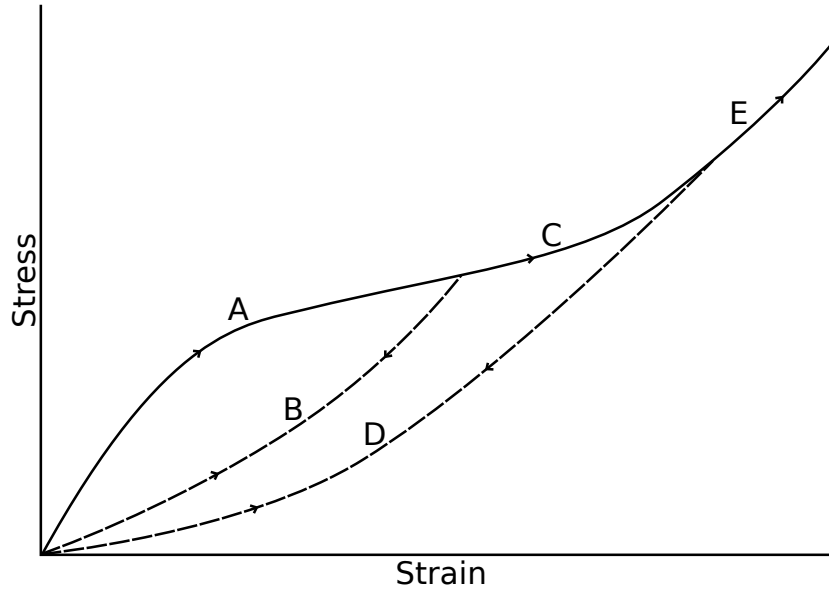
Figure 4.3.: Typical stress strain curve for isotropic Mullins effect without rate dependent effects

A damage model is used for the description of the so called Mullins effect. Therefore, an internal variable is introduced, see section 3.4.1. In Figure 4.3, a typical stress strain curve of the Mullins effect is shown. First, a virgin sample is loaded (line A) to a certain strain. In case of an isotropic Mullins effect, unloading at a certain point of the stretch follows the line B, which ends at the origin. Accordingly, this means that no residual stress occurs while releasing the stress to zero, further reloading will follow the same line as unloading until the stretch reaches the virgin loading curve. Between the curves A and B, a strong hysteresis can appear. This area between the curves is the energy dissipation. Further loading will be reached again at the virgin loading curve C, which is not influenced by the loading history. Unloading from a higher stretch (line D) leads to a lower stiffness than unloading from a lower stretch (line B).

From the typical Mullins effect curves, it can be seen that the damage depends only on the maximum of strain in loading history. Only the virgin loading is dissipative, while unloading and reloading are reversible.

The continuum damage theory is applied to describe this kind of effect. This theory prescinds from the damage in the micro-level and postulates a homogenized damage parameter D. This leads to a free energy function of the form

$$\psi = \psi(\boldsymbol{F}, D) = (1 - D)\psi_0(\boldsymbol{F}), \tag{4.30}$$

the damage parameter can be seen as a reduction parameter and is treated as an internal variable. To obtain the stress, the derivative of (4.30) with respect to time, i.e.

$$\dot{\psi} = (1 - D)\frac{\partial \psi_0}{\partial \boldsymbol{F}} \cdot \cdot \dot{\boldsymbol{F}} - \psi_0 \dot{D}, \tag{4.31}$$

is performed by use of chain rule. With equation (3.66), the internal dissipation is calculated as

$$\mathcal{D} = \left(\boldsymbol{P} - (1 - D)\frac{\partial \psi_0}{\partial \boldsymbol{F}} \right) \cdot \cdot \dot{\boldsymbol{F}} + \psi_0 \dot{D} \geq 0. \tag{4.32}$$

As the deformation gradient is arbitrary, hence the first part of the above equation has to vanish to fulfil this criterion. This leads to the following equation

$$\mathcal{D} = f\dot{D} \geq 0, \tag{4.33}$$

with the thermodynamic force $f = \Psi_0(\boldsymbol{F})$. Equation (4.33) shows that damage is a dissipative process. By using equation (4.30), it can be seen that the thermodynamic force f is related to the internal variable D as follows

$$f = \psi_0(\boldsymbol{F}) = -\frac{\partial \psi}{\partial D}. \tag{4.34}$$

As result of equation (4.34), the process of damage can be controlled by the effective strain energy function ψ_0 rather than the internal variable.

The above equations construct a framework for describing the damage in a general way. For the phenomenological constitutive description of damage, the evolution equation is missing. One example of the damage evolution according to Holzapfel [2000] is

$$D = D(\alpha) = D_\infty \left[1 - \exp\left(-\frac{\alpha}{\alpha_{\text{ref}}} \right) \right]. \tag{4.35}$$

with the maximum damage $D_\infty \in [0, 1]$, which is usually less than one to avoid an ill-conditioned equation system in the finite element calculation and the damage saturation parameter α_{ref}.

The damage variable α has to be determined from the history of the effective free energy function until the current time. For the Mullins effect, the damage is assumed to be discontinuous, which means that damage only occurs during virgin loading. This can be expressed by using the maximum of effective free energy function in time t

$$\alpha_D(t) = \max_{[0,t]} \psi_0. \tag{4.36}$$

For modelling the continuous damage (damage occurs in loading and in unloading) the maximum can be replaced by the integral over time

$$\alpha_C(t) = \int_0^t \psi_0 \mathrm{d}t \tag{4.37}$$

For the determination of the damage variable, stress tensors (stress introduced damage) or strain tensors (strain introduced damage) also can be used.

Another class of damage models predicts the damage initiation criteria. The material is reversible until a certain stress level is reached, in analogy to plasticity, see Lemaitre and Desmorat [2005].

The concept of pseudo elasticity can also be used as a simple approach. For loading, a hyperelastic material model is used. At each point of unloading, the weakened material model is initiated, see Ogden and Roxburgh [1999].

Recently, there are models available to describe the anisotropic Mullins effect in a phenomenological way, by using a set of internal variables, see Itskov et al. [2010].

4.3. Visco-Elastic Models

The first models in the field of viscosity are simple one-dimensional rheological models. These models comprise of springs and dampers. Two well-known models are the Kelvin model, which is a parallel connection of springs and dampers, and the Maxwell model, which is a connection in series.

In material testing, the relaxation test and the creep test are carried out. For the relaxation test, the specimen is stretched immediately to a certain value and then the stretch is held constant. It emerges that the stress jumps to a higher level and will decrease over time. In a creep test, the stress is increased to a certain level and is held constant. The stretch is increasing at constant stress until it saturates. For elastomers, the characteristic time for creep is much higher than for the relaxation test.

The Kelvin element is able to model the creep test, whereby the stress in the damper decrease by time and the stretch increases until the stress in spring equals the external stress. The relation test cannot be modelled by the Kelvin element because the damper precludes an immediate stretch jump. For the Maxwell element, it is vice versa, the relaxation test can be modelled, but the creep test will turn out an infinity stretch, because the damper increases the stretch in a constant rate at a constant stress.

Both Kelvin and the Maxwell models are inadequate to model the visco-elastic behaviour. To overcome this problem, a three-parameter model is introduced. It is a parallel connection of Maxwell element with a spring. The three parameters are the Young's modulus in equilibrium state E_∞, the Young's modulus for non-equilibrium state E and the damper constant η. This model shows the correct behaviour in both tests. In relaxation test, the initial stiffens is $E_\infty + E$, it will relaxate the stiffness of E. In creep test the strain is limited by parallel spring E_∞.

For elastomers, it is known that it has different time constant and stiffness for different loading speeds. Therefore, the three-parameter model is generalised by adding i spring

damper modules in parallel, see Figure 4.4. The stress is calculated by the summation of all the elements

$$\sigma_{11} = E_\infty \epsilon + \sum_i E_i(\epsilon - \alpha_v i),\tag{4.38}$$

with a set of internal variables α_i, which store the relaxation state of each spring damper element. This model is especially useful for small strains. The material parameter can be fitted by using optimisation tools to a standard harmonic excitation test without knowing what is going on inside the material.

A three-dimension model can be found in Simo [1987] and Simo and Hughes [2000]. The model is presented in the case of a small strain, with the assumption that only the deviatoric part has an influence on the viscous response. Also, the stress can be expressed in an elegant way with the use of convolution integral

$$\overline{\sigma}(t) = \int_\infty^t g(t-s)\frac{\mathrm{d}}{\mathrm{d}s}\left[\mathrm{dev}\left(\frac{\partial\overline{\psi}}{\overline{\epsilon}}\right)\right]\mathrm{d}t.\tag{4.39}$$

This formula is also known as fading memory integral, because the inputs will loose their effect with time. The shortening $g(t)$ describes the normalised relaxation function

$$g(t) = \gamma_\infty + \sum_i \gamma_i \exp\left(\frac{t}{\tau_i}\right)\tag{4.40}$$

and the normalised elastic modulus as material parameters

$$\gamma_i = \frac{E_i}{E_0}\tag{4.41}$$

$$\gamma_\infty = \frac{E_\infty}{E_0}.\tag{4.42}$$

For consistency

$$\sum_i \gamma_i + \gamma_\infty = 1\tag{4.43}$$

has to be satisfied.

In analogy to the generalised relaxation element, a finite-strain three-dimensional visco-elastic model was proposed by Simo [1987]. The viscous effects are modelled with a set of internal variables for each spring damper element. An uncoupled free energy density function is proposed. The first part considers the equilibrium part, the second part comprises the non-equilibrium energy of the viscous effects. The decoupling of deviatoric and volumetric response is motivated by the hyperelastic material models, as shown in section 4.1. For the viscous part, it is only dependent on the deviatoric components. This is mainly motivated by two reasons: first, the volumetric deformation is small in comparison with the deviatoric one; and second, no sliding of chains takes place, during compression. This material is energy elastic due to the change of atomic distance. For the finite-strain model, the free energy density function is formulated as follows

$$\Psi(\boldsymbol{C}, \boldsymbol{\alpha}_v) = \Psi(J) + \Psi(\overline{\boldsymbol{C}}) - \sum_i \frac{1}{2}\overline{\boldsymbol{C}}\cdot\cdot\alpha_v^i + \theta\left(\sum_i \alpha_v^i\right)\tag{4.44}$$
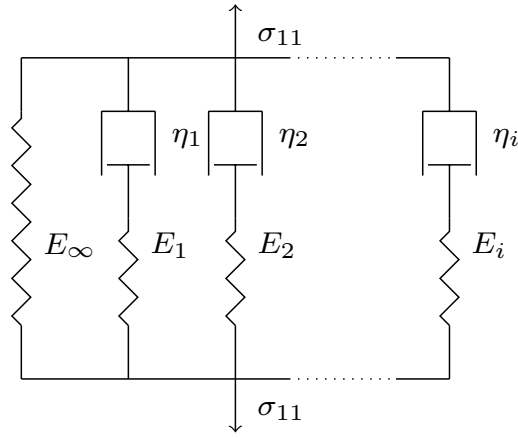
Figure 4.4.: Generalised relaxation model with i spring damper modules in parallel

with the set of internal variables α_v^i.

A thermoviscoelastic approach can be found in Suwannachit and Nackenhorst [2013]. It uses internal heating due to viscous effects and temperature dependent material behaviour. This model is used in stationary rolling contact in an Arbitrary Lagrangian Eulerian framework. The temperature and the inelastic history is propagated through a fixed mesh with a Time Discontinuous Galerkin method.

A two scale model for non-linear viscoelasticity was published by Tang et al. [2012]. It introduce an additional degree of freedom for the free chain network theory presented in Treloar [1975]. A statistical approach for visco-plastic material behaviour can be found in Martinez et al. [2011].

5. Micromechanically Motivated Material Model

A micromechanically motivated material model for elastomer is presented in this chapter. The chapter starts with the description of the micro plane model applied in this thesis. Subsequently, the specific constitutive equations for elastic, anisotropic Mullins-type damage and viscous parts will be developed.

5.1. Network Decomposition Concept

The model is based upon the network decomposition concept, which is widely used to describe the microstructure of particle-filled elastomer, see e.g. Klueppel [2003] and Tang et al. [2012].

The network decomposition concept is operating on the length scale of elastomer chains and filler particles, whereby the structure of an elastomer chain has been described in section 2.1. There are three different phases in filled elastomers, which are decomposed according to Figure 5.1. The first phase is the chain-chain network, which is responsible for the elastic stiffness. This phase is stretched during the deforming of the specimen, while there is no change in network topology. The second phase is the chain-filler network, which is responsible for the Mullins effect. The third phase is associated with the free chains, which are responsible for the viscous behaviour. It is assumed that there is no interaction between the chain-chain and chain-filler network. For the free chains, an unilateral interaction with the chain-chain network is assumed. The chain-chain network acts as an obstacle for the free chains. With

elastomer nano scale   chain-chain network   free chains   chain-filler network
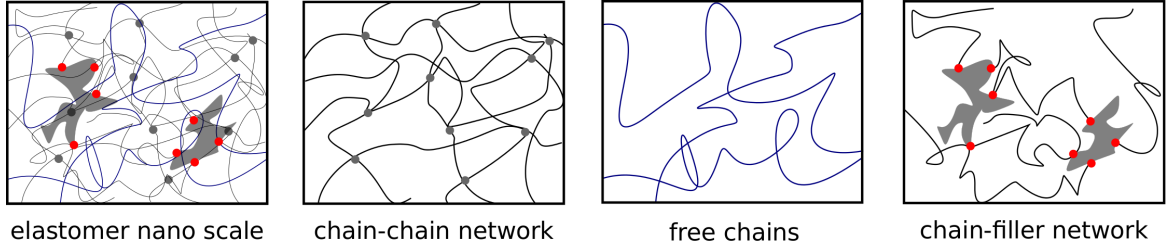
Figure 5.1.: Illustration of the network decomposition concept, grey curves: connected chains, grey dots: connection points, blue curves: free chains, red dots: chain-filler bonding, grey areas: filler particle

this assumption, the free energy of an elastomer ψ can be written as the sum of free energy of the phases, whereby the total free energy can be expressed as

$$\psi = \psi_{\mathrm{cc}} + \psi_{\mathrm{cf}} + \psi_{\mathrm{fc}}, \tag{5.1}$$

with the free energy of the chain-chain network ψ_{cc}, chain-filler network ψ_{cf} and free chain network ψ_{fc}. In the following section, the free energy function is described, in particular, for the different types of network by using the statistical approaches for the chain and filler distribution and alignment.

5.2. Micro Plane Model

The idea to describe the material plasticity in several micro planes dates back to Taylor [1938]. In fact, the micro plane model is not limited to plasticity, rather it is applicable for material modelling in general.

In computational mechanics, the micro plane model was first successfully applied for the concrete materials by Bazant and Oh [1985]. For concrete, it is known that the failure stress in compression is much higher than in stretch. This phenomenon is explained by microstructure. In compression, small cracks will close and transmit forces, while in tension, the cracks will open and propagate. This leads to a decrease of the effective area, where tension stress will be transmitted. It appears obvious that the cracks will open and proceed depending on the stress state, which leads to a strain introduced anisotropy. Doubtless, the anisotropic damage cannot be described by a free function (4.30).

The idea of the micro plane modelling introduces a stress strain relation at multiple micro planes, where a one-dimensional constitutive equation depending on the stretch in the micro plane normal direction of $\boldsymbol{d}$ has to be formulated at each micro plane.

In order to obtain a three-dimensional material model, the integral over the unit sphere S

$$\boldsymbol{\tau} = \int \bullet \frac{1}{4\pi} \boldsymbol{d} \times \boldsymbol{d} \, \mathrm{d}S \tag{5.2}$$

has to be evaluated. By $\bullet$, the material equation in direction $\boldsymbol{d}$ is expressed. This integral can only be evaluated analytically for the simple material equations. In general, it has to evaluated numerically. In the next section, a numerical efficient integration scheme is presented.

5.2.1. Numerical Integration at the Surface of a Unit Sphere

The finite element implementation of the micro plane concept requires an efficient and accurate numerical integration over the surface of a unit sphere. A simple approach is to perform the integration over a rectangular domain in the direction of the spherical angular coordinates. However, this approach is inefficient, since the integration points are crowded on the poles of the sphere, see Bazant and Oh [1986]. In order to find a Gauss like integration rule, the integration points have to be distributed as equally as possible. The use of platonic solids has been suggested by Albrecht and Collatz [1958], although this approach is limited to maximum of 20 integration points over the unit sphere, because no regular polyhedron exists with more than 20 surfaces, as proven by Euclid around 300 BC. With the 20-point integration formula, only polynomials upto 5th order can be integrated exactly.

A more efficient approach has been published by Bazant and Oh [1986], using the material symmetry, so the integration has to be performed on a half sphere. With some optimality criteria, they found the so-called 21×2 integration schema, which is accurate up to the order of 9, see appendix A.1. In Figure 5.2, the location of the optimal integration points can be seen. Geometrically, this schema can be seen as the interpolation of an octahedron. The additional integration points are located on lines, that bisect the border of the 1/8 unit sphere. The 1/8 part of the unit sphere

corresponds to one face of an octahedron, which is known to be optimal. The inner points are located by minimization of agglomeration of integration points. Putting all eight faces of the octahedron together and removing the redundant points, the unit sphere is approximated by 42 optimal integration points. By using the symmetry of the points, the 21×2 integration schema evolves.

The numerical integration of equation (5.2) can now be carried out by using the simple formula

$$\boldsymbol{\tau} = \sum_i \bullet w_i \boldsymbol{d}_i \times \boldsymbol{d}_i. \tag{5.3}$$

The integration weights w_i and the corresponding directions $\boldsymbol{d}_i$ can be found in appendix A.1.
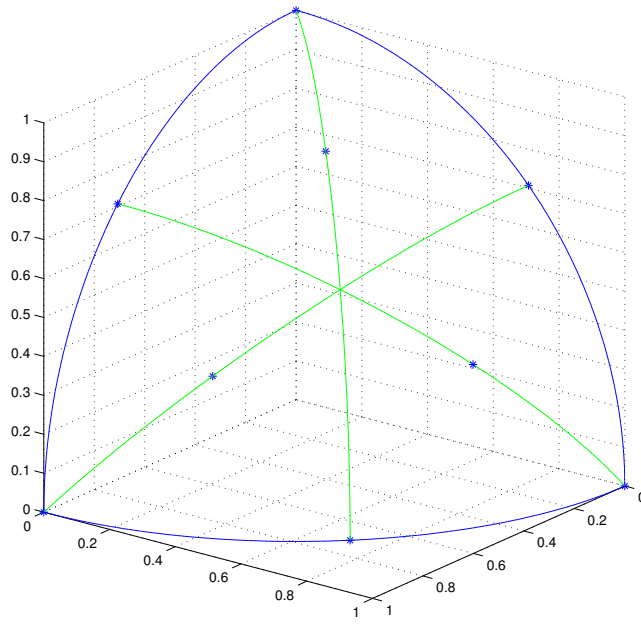

Figure 5.2.: Distribution of the integration points for 21×2 integration schema on $1/8$ of a unit sphere

5.3. Elastic Part of Material Model

The elastic part of the material model is based upon the suggestions from Miehe et al. [2004], describing the micromechanics of the chain-chain network.

5.3.1. Material Tangent

In this section, the material tangent for large strain conditions under almost incompressible behaviour is derived, see Miehe [1994] and Miehe [1996]. A hyperelastic material model from the type of equation (4.1) is used. In particular, the free energy function

$$\psi_{\mathrm{cc}}(J, \boldsymbol{g}, \overline{\boldsymbol{F}}) = U_{\mathrm{cc}}(J) + \overline{\psi}_{\mathrm{cc}}(\boldsymbol{g}, \overline{\boldsymbol{F}}) \tag{5.4}$$

has a volumetric part $U_{\mathrm{cc}}(J)$ and a deviatoric part $\overline{\psi}_{\mathrm{cc}}(\boldsymbol{g}, \overline{\boldsymbol{F}})$. The deviatoric part depends on a metric tensor $\boldsymbol{g}$, for a Cartesian coordinate system, the metric tensor is the unit tensor I defined in equation (3.12).

The first step is to derive the Kirchhoff stress tensor and the material tangent from equation (5.4). Starting with the volumetric part, the deviatoric Kirchhoff stress

$$\tau = 2\frac{\partial U_{\mathrm{cc}}(J)}{\partial \boldsymbol{b}} \cdot \boldsymbol{b} \tag{5.5}$$

is defined as the directional derivative of free energy function with respect to the left Cauchy-Green tensor $\boldsymbol{b}$. In some references, the Cauchy-Green tensor is called the Finger deformation tensor. Using chain rule equation for (5.5) and $\frac{\partial J}{\partial \boldsymbol{b}} = \frac{1}{2}J\boldsymbol{b}^{-1}$ emerges as

$$\tau = 2\frac{\partial U_{\mathrm{cc}}(J)}{\partial J}\frac{\partial J}{\partial \boldsymbol{b}} \cdot \boldsymbol{b} \tag{5.6}$$

$$= JU_{\mathrm{cc}}'(J)\boldsymbol{g}^{-1}. \tag{5.7}$$

Finally, with the abbreviation $p = JU_{\mathrm{cc}}'(J)$, the volumetric part of the Kirchhoff stress follows to

$$\tau = p\boldsymbol{g}^{-1}. \tag{5.8}$$

The material tangent is calculated by the second directional derivative of volumetric free energy function

$$\mathbb{C} = 4\boldsymbol{b} \cdot \frac{\partial^2 U_{\mathrm{cc}}(J)}{\partial \boldsymbol{b}^2} \cdot \boldsymbol{b}. \tag{5.9}$$

The first derivative is known from the derivation of the stress tensor, therefore, the second derivative leads to

$$\frac{\partial^2 U_{\mathrm{cc}}(J)}{\partial \boldsymbol{b}^2} = \frac{\partial \frac{1}{2}J\boldsymbol{b}^{-1}U_{\mathrm{cc}}'(J)}{\partial \boldsymbol{b}}. \tag{5.10}$$

Again, this equation is derived by using chain rule and $\frac{\partial \boldsymbol{b}^{-1}}{\partial \boldsymbol{b}} = -\boldsymbol{b}^{-1} \cdot \mathbb{I} \cdot \boldsymbol{b}^{-1}$,

$$\frac{\partial^2 U_{\mathrm{cc}}(J)}{\partial \boldsymbol{b}^2} = \frac{1}{4}\left[Jb^{-1}U_{\mathrm{cc}}'(J)\boldsymbol{b}^{-1} - Jb^{-1} \cdot \mathbb{I} \cdot \boldsymbol{b}^{-1}U_{\mathrm{cc}}'(J) + J^2\boldsymbol{b}^{-1}U_{\mathrm{cc}}''(J)\boldsymbol{b}^{-1}\right]. \tag{5.11}$$

With the abbreviation $k = J^2 U''_{\mathrm{cc}}(J)$, hence equation (5.11) simplifies to

$$\frac{\partial^2 U_{\mathrm{cc}}(J)}{\partial \boldsymbol{b}^2} = \frac{1}{4} \boldsymbol{b}^{-1} \left[(p+k)\boldsymbol{g}^{-1} \otimes \boldsymbol{g}^{-1} - 2\mathbb{I}p \right] \boldsymbol{b}^{-1}. \tag{5.12}$$

Finally, insertion of equation (5.12) into (5.9) leads to the volumetric part of the material tangent

$$\mathbb{C} = (p+k)\boldsymbol{g}^{-1} \otimes \boldsymbol{g}^{-1} - 2\mathbb{I}p. \tag{5.13}$$

The next step is to derive the deviatoric parts of Kirchhoff stress tensor and material tangent. The derivative of deviatoric part of the left Cauchy-Green tensor with respect to the left Cauchy-Green itself is calculated by

$$\frac{\partial \overline{\boldsymbol{b}}}{\partial \boldsymbol{b}} = J^{-2/3} (\mathbb{I} - \frac{1}{3}\boldsymbol{b}^{-1} \otimes \boldsymbol{b}). \tag{5.14}$$

The deviatoric stress is defined as

$$\overline{\tau} = 2\boldsymbol{b} \frac{\partial \overline{\psi}_{\mathrm{cc}}(\boldsymbol{g}, \overline{\boldsymbol{F}})}{\partial \boldsymbol{b}}. \tag{5.15}$$

Using equations (5.14) and (5.15), the stress is calculated with the definition of the projection tensor $\mathbb{P} = \mathbb{I} - \frac{1}{3}\boldsymbol{g}^{-1} \otimes \boldsymbol{g}^{-1}$ to

$$\overline{\tau} = 2\boldsymbol{b} \left(J^{-2/3}\mathbb{I} - \frac{1}{3}\boldsymbol{b}^{-1} \otimes \overline{\boldsymbol{b}} \right) \cdot \cdot \frac{\partial \overline{\psi}_{\mathrm{cc}}(\boldsymbol{g}, \overline{\boldsymbol{F}})}{\partial \overline{\boldsymbol{b}}} \tag{5.16}$$

$$= 2\mathbb{P} \cdot \cdot \left(\overline{\boldsymbol{b}} \frac{\partial \overline{\psi}_{\mathrm{cc}}(\boldsymbol{g}, \overline{\boldsymbol{F}})}{\partial \overline{\boldsymbol{b}}} \right). \tag{5.17}$$

The second derivative of the deviatoric part of the free energy with respect to the left Cauchy-Green tensor is calculated in analogy to the volumetric part. Using the results from the stress tensor, this leads to

$$\frac{\partial^2 \overline{\psi}_{\mathrm{cc}}}{\partial \boldsymbol{b}^2} = \frac{\partial \left[\left(J^{-2/3}\mathbb{I} - \frac{1}{3}\boldsymbol{b}^{-1} \otimes \overline{\boldsymbol{b}} \right) \cdot \cdot \frac{\partial \overline{\psi}_{\mathrm{cc}}(\boldsymbol{g}, \overline{\boldsymbol{F}})}{\partial \overline{\boldsymbol{b}}} \right]}{\partial \boldsymbol{b}}. \tag{5.18}$$

With the use of chain rule, the second derivative of the free energy can be derived

$$\frac{\partial^2 \overline{\psi}_{\mathrm{cc}}}{\partial \boldsymbol{b}^2} = \boldsymbol{b}^{-1} \left[\mathbb{P} \cdot \cdot \left(\overline{\boldsymbol{b}} \frac{\partial^2 \overline{\psi}_{\mathrm{cc}}}{\partial \overline{\boldsymbol{b}}^2} \overline{\boldsymbol{b}} \right) \cdot \cdot \mathbb{P} + \frac{1}{3}\mathrm{tr}\left(\frac{\partial \overline{\psi}_{\mathrm{cc}}}{\partial \overline{\boldsymbol{b}}} \right) \left(\mathbb{I} + \frac{1}{3}\boldsymbol{g}^{-1} \otimes \boldsymbol{g}^{-1} \right) \right.$$
$$\left. - \frac{1}{3}[\overline{\boldsymbol{b}} \left(\frac{\partial \overline{\psi}_{\mathrm{cc}}}{\partial \overline{\boldsymbol{b}}} \right) \otimes \boldsymbol{g}^{-1} + \boldsymbol{g}^{-1} \otimes \left(\frac{\partial \overline{\psi}_{\mathrm{cc}}}{\partial \overline{\boldsymbol{b}}} \right) \overline{\boldsymbol{b}}] \right] \boldsymbol{b}^{-1}. \tag{5.19}$$

With the definitions $\overline{\mathbb{C}} = 4\overline{\boldsymbol{b}} \frac{\partial^2 \overline{\psi}_{\mathrm{cc}}}{\partial \boldsymbol{b}^2} \overline{\boldsymbol{b}}$ and $\overline{\tau} = 2\overline{\boldsymbol{b}} \frac{\partial \overline{\psi}_{\mathrm{cc}}}{\partial \overline{\boldsymbol{b}}}$, the deviatoric part of the material tangent is obtained

$$\mathbb{C}_{\mathrm{cc}} = \mathbb{P} \cdot \cdot \overline{\mathbb{C}} \cdot \cdot \mathbb{P} + \frac{2}{3}\overline{\tau} \cdot \cdot \boldsymbol{g}^{-1} \left(\mathbb{I} + \frac{1}{3}\boldsymbol{g}^{-1} \otimes \boldsymbol{g}^{-1} \right) - \frac{2}{3} \left(\overline{\tau} \otimes \boldsymbol{g}^{-1} + \boldsymbol{g}^{-1} \otimes \overline{\tau} \right). \tag{5.20}$$

Combining equation (5.13) and (5.20) leads to the general material tangent

$$\mathbb{C}_{\mathrm{cc}} = (p+k)\boldsymbol{g}^{-1} \otimes \boldsymbol{g}^{-1} - 2\mathbb{I}p$$
$$+ \mathbb{P} \cdot \cdot \left(\overline{\mathbb{C}} + \frac{2}{3}\overline{\tau} \cdot \cdot \boldsymbol{g}^{-1} \left(\mathbb{I} + \frac{1}{3}\boldsymbol{g}^{-1} \otimes \boldsymbol{g}^{-1} \right) - \frac{2}{3}\left(\overline{\tau} \otimes \boldsymbol{g}^{-1} + \boldsymbol{g}^{-1} \otimes \overline{\tau} \right) \right) \cdot \cdot \mathbb{P}$$
$$(5.21)$$

with the application of the projection property $\mathbb{P} = \mathbb{P} \cdot \cdot \mathbb{P}$. This projection property states that multiple projection leads to the same result as applying the projection once, see also Itskov [2007].

5.3.2. Non-Gaussian Statistic for Chain Entropy

In section 2.1.2 the derivation of the entropy of a single elastomer chain has been shown. A Gaussian statistic was used, which is limited to small deformation. Now, as elastomer undergoes large deformation, a non Gaussian statistic is used in this section. It describes the behaviour correctly for large deformation theory.

A model based upon the Largevin function was introduced by Kuhn and Grün [1942] and James and Guth [1943]. They found a probability density in analogy to equation (2.5) of the form

$$p_f(\lambda) = p_o \exp\left[-N\left(\lambda_r \mathcal{L}^{-1}(\lambda_r) + \ln\left(\frac{\mathcal{L}^{-1}(\lambda_r)}{\sinh \mathcal{L}^{-1}(\lambda_r)} \right) \right) \right], \qquad (5.22)$$

with the normalised constant p_0 and the definition of relative stretch

$$\lambda_r = \frac{r}{L} = \frac{\lambda}{\sqrt{n}} \quad \in [0, 1), \qquad (5.23)$$

where $L = nl$ denotes the contour length and $\mathcal{L}^{-1}$ is the inverse of the well known Langevin function

$$\mathcal{L}(x) = \coth x - \frac{1}{x}. \qquad (5.24)$$

Applying the procedure as described in section 2.1.2, the free energy of a single elastomer chain is

$$\psi_C(\lambda) = nk_{\mathrm{B}}T \exp\left[-N\left(\lambda_r \mathcal{L}^{-1}(\lambda_r) + \ln\left(\frac{\mathcal{L}^{-1}(\lambda_r)}{\sinh \mathcal{L}^{-1}(\lambda_r)} \right) \right) \right] + \psi_0, \qquad (5.25)$$

with the constant ψ_0. Applying the first derivative with respect to the stretch λ to the free energy function gives the force acting on a free chain. According to Treloar [1954], the chain force is calculated as

$$F_C = k_{\mathrm{B}}T\sqrt{n}\mathcal{L}^{-1}(\lambda_r). \qquad (5.26)$$

The force is a non-linear function of the stretch and has asymptotic behaviour at the limited end to end distance of a chain. The extensibility limit is reached at $\lambda_r \to 1$ or $\lambda \to \sqrt{n}$.

Since there is no analytical function inverse of the Langevin function, an approximation is necessary. One idea is to construct an invertible Taylor series approximation

for the Langevin function, although this leads to either long polynomial functions or even poor approximation. A simple and precise approximation of the inverse Langevin function is the Padê approximation, i. e.

$$\mathcal{L}^{-1}(\lambda_r) \approx \lambda_r \frac{(3 - \lambda_r^2)}{(1 - \lambda_r^2)}. \tag{5.27}$$

In Figure 5.3, the normalised stress for Gaussian and Langevinian statistics is compared. The first term of the Taylor series of the Langevin function proves to represent the Gaussian statistics. Consequently, for small strain, both functions match well.
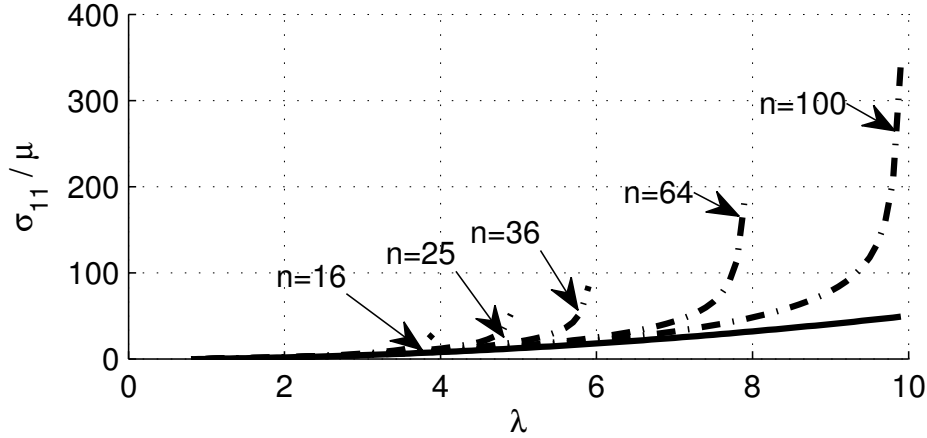

Figure 5.3.: Normalised stress for Gaussian (solid line) and Langevinian (dashed lines) statistics for different chain length n

5.3.3. Stress and Material Tangent for Affine Network Model

First, the deviatoric part of stretch in direction d and its absolute value are defined

$$\overline{\boldsymbol{\lambda}}_{\mathrm{d}} = \overline{\boldsymbol{F}} \cdot \boldsymbol{d}, \tag{5.28}$$

$$\overline{\lambda}_{\mathrm{d}} = |\overline{\boldsymbol{\lambda}}_{\mathrm{d}}|. \tag{5.29}$$

To visualise the concept of stretches in different directions, some typical stretch states are shown in Figure 5.4, assuming a preserved volume. The uniaxial stretch is well known from common material testing machines. If the specimen is stretched to twice its length in one direction, the stretch in both perpendicular directions is $1/\sqrt{2}$. In equibiaxial tests, the specimen is stretched in two directions with the same stretch, consequently, its contraction in perpendicular direction is $1/4$. This test is quite similar to uniaxial stretch, because it yields familiar Mohr's circles. In pure shear or stripbiaxial extension (definition according to Holzapfel [2000]), the specimen is stretched in one direction and compressed in the second direction to $1/2$. Consequently, the stretch equals one, in the third direction. For the corresponding experimental set-up, the reader is referred to Rivlin and Saunders [1951b].

The stress is defined as the derivative of the free energy function with respect to the metric

$$\overline{\tau} = 2\boldsymbol{b} \frac{\partial \overline{\psi}_{\mathrm{cc}}(\boldsymbol{g}, \overline{\boldsymbol{F}})}{\partial \boldsymbol{g}}. \tag{5.30}$$

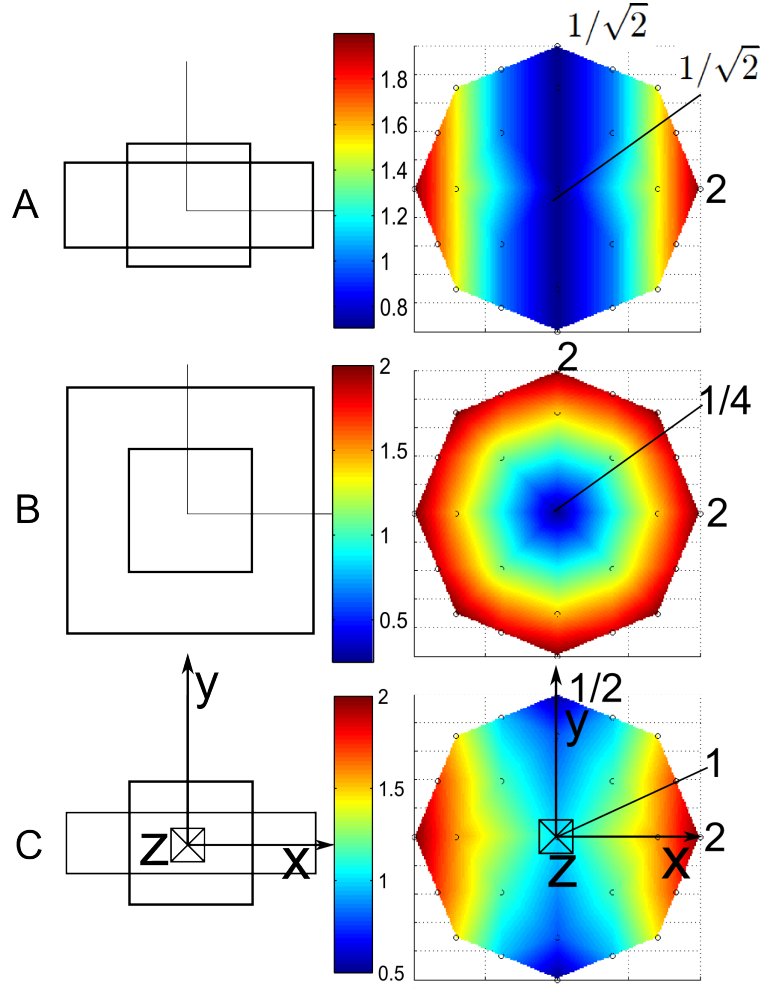**Figure 5.4.:** Visualisation of typical stretch states on one half of a unit sphere, the numbers describe the stretch in the corresponding direction. The compression stretches ($\overline{\boldsymbol{\lambda}}_d < 1$) are marked in dark blue, while elongation stretches ($\overline{\boldsymbol{\lambda}}_d > 1$) are red. A) uniaxial stretch, B) equibiaxial stretch and C) pure shear or stripbiaxial extension

Inserting equations (5.23) and (5.27) into (5.26) leads to

$$F_c = \frac{\partial \psi_c(\lambda)}{\partial \lambda} = k_\mathrm{B} T \lambda \frac{3n - \lambda^2}{n - \lambda^2}, \tag{5.31}$$

which represents a computable form of the free energy function of a single chain in dependence of the stretch λ. Applying chain rule and the derivative of stretch with respect to the metric $\frac{\partial \lambda}{\partial \boldsymbol{g}} = \lambda^{-1} \overline{\boldsymbol{\lambda}}_\mathrm{d} \otimes \overline{\boldsymbol{\lambda}}_\mathrm{d}$, the stress is obtained as

$$\overline{\tau} = \frac{1}{2} \frac{\partial \overline{\psi}_\mathrm{cc}(\boldsymbol{g}, \overline{\boldsymbol{F}})}{\partial \lambda} \frac{\partial \lambda}{\partial \boldsymbol{g}} = N_{cc} k_\mathrm{B} T \left\langle \frac{3n - \lambda^2}{n - \lambda^2} \overline{\boldsymbol{\lambda}}_\mathrm{d} \otimes \overline{\boldsymbol{\lambda}}_\mathrm{d} \right\rangle. \tag{5.32}$$

N_cc is the number of chains in the chain-chain network per unit volume. The brackets $\langle \bullet \rangle$ symbolise averaging over the unit sphere.

The next step is to derive the material tangent. This is achieved by chain rule, where $\frac{\partial \overline{\boldsymbol{\lambda}}_\mathrm{d} \otimes \overline{\boldsymbol{\lambda}}_\mathrm{d}}{\partial \boldsymbol{g}} = 0$. With the definition

$$\overline{\mathbb{C}} = 4 \frac{\partial^2 \overline{\psi}_\mathrm{cc}(\boldsymbol{g}, \overline{\boldsymbol{F}})}{\partial \boldsymbol{g}^2} \tag{5.33}$$

the material tangent follows to

$$\overline{\mathbb{C}} = N_\mathrm{cc} k_\mathrm{B} T \left\langle \left(\frac{\lambda^4 - 3n^2}{(n - \lambda^2)^2} - \frac{3n - \lambda^2}{n - \lambda^2} \right) \overline{\lambda}_\mathrm{d}^{-2} \overline{\boldsymbol{\lambda}}_\mathrm{d} \otimes \overline{\boldsymbol{\lambda}}_\mathrm{d} \otimes \overline{\boldsymbol{\lambda}}_\mathrm{d} \otimes \overline{\boldsymbol{\lambda}}_\mathrm{d} \right\rangle. \tag{5.34}$$

Finally, the averaging has to be performed by using numerical integration with the weights w_i, i. e.

$$\overline{\tau} = N_\mathrm{cc} k_\mathrm{B} T \sum_i \frac{3n - \lambda^2}{n - \lambda^2} \overline{\boldsymbol{\lambda}}_\mathrm{d} \otimes \overline{\boldsymbol{\lambda}}_\mathrm{d} w_i \tag{5.35}$$

$$\overline{\mathbb{C}} = N_\mathrm{cc} k_\mathrm{B} T \sum_i \left(\frac{\lambda^4 - 3n^2}{(n - \lambda^2)^2} - \frac{3n - \lambda^2}{n - \lambda^2} \right) \overline{\lambda}_\mathrm{d}^{-2} \overline{\boldsymbol{\lambda}}_\mathrm{d} \otimes \overline{\boldsymbol{\lambda}}_\mathrm{d} \otimes \overline{\boldsymbol{\lambda}}_\mathrm{d} \otimes \overline{\boldsymbol{\lambda}}_\mathrm{d} w_i. \tag{5.36}$$

Equations (5.35) and (5.36) are computable representation for the deviatoric stress and the material tangent.

5.4. Anisotropic-Mullins Type Damage Model

The damage in filled elastomers has attracted the research interest since long time. From the experimental results, it is known that the strain softening strongly depends on the filler concentration. The softening in unfilled elastomer appears to be negligible, while for elastomers with high filler concentration, the softening becomes increasingly intense, Mullins [1969]. In Harwood et al. [1965], possible reasons for the damage are discussed, e.g. debonding of chains from filler particles, the recreation of cross-links and chain breakage.

Based upon the theory of chain debonding, Govindjee and Simo [1991] introduced a micromechanically motivated model, whereby they derived an equation for the chain distribution between the filler particles. With this distribution function, the damage state of the material can be calculated by debonding of the chains due to network

stretch. This model shows good results, although it is unable to describe the strain introduced anisotropy and permanent set. In Göktepe and Miehe [2005], a model was presented, that takes anisotropic damage into account, although the damage function is of phenomenological type and not directly derived from micromechanics. Dargazany and Itskov [2009] presented a micro-mechanical based model including anisotropy. Due to the mathematical structure of this model, an efficient finite element implementation is not straightforward. Motivated by this, a fully micro-mechanical based damage model suitable for an efficient FE implementation will be derived below.

5.4.1. Statistical Distribution of Chains between Filler Particles

The anisotropic damage model is based upon the transient network theory, which means the network is evolving during deformation. This evolution takes place in the chain-filler network, see Figure 5.5. During stretching, some chains reach their fully stretched length and debond from the filler particles. This leads to a decrease of material stiffness.
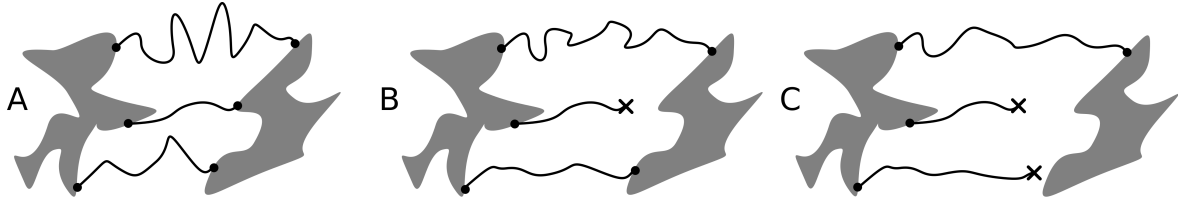

Figure 5.5.: Development of filler particle network during stretching, A) unstreched state, B) stretched state first chain debonding and C) second chain debonding

To provide a physical description of the transient network model, a statistical description for the connection of two filler particles is necessary. According to Govindjee and Simo [1991], the probability for the bondage of the n-th chain element to a filler can be described as

$$P(n, z(\bar{r})) = \frac{1}{4} \kappa \sqrt{\frac{24}{\pi n}} \exp\left(\frac{z^2}{n} - \frac{1}{2} \kappa \sqrt{\frac{24}{\pi}} \left(\sqrt{\pi} z \left[\operatorname{erf}\left(\frac{z}{\sqrt{n}}\right) - \operatorname{erf}(z)\right]\right.\right.$$
$$\left.\left. + \sqrt{n} \exp\left(\frac{-z^2}{n}\right) - \exp\left(-z^2\right)\right)\right), \quad (5.37)$$

with the abbreviation

$$z = \sqrt{\frac{3}{2}} \bar{r}. \tag{5.38}$$

The material parameter κ (see equation (2.15)) is the quotient of available and used absorption area. In Figure 5.6, the probability density function is plotted. The probability is zero until the fully stretched chain is long enough to bridge the distance $\bar{r}$ between two aggregate surfaces. In Figure 5.7, the absorption points or chain bonding points are illustrated, whereby each absorption point can only be used once. If the nearest absorption is already allocated by another chain, the number of chain elements has to increase to find a free absorption point. Depending on κ, a maximum is reached
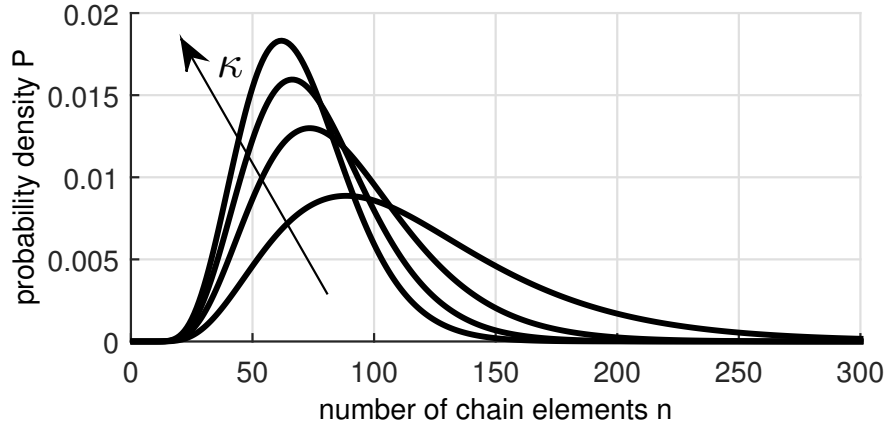
Figure 5.6.: Probability distribution for the connection of n-th chain element to a filler particle according to Govindjee and Simo [1991]. With $\bar{r} = 10$, and $\kappa = \{1, 2, 3, 4\}$, the curve become flatter with decreasing κ.

for different numbers of chain elements. For a high number of κ, the maximum is reached at a low chain length since there are many free absorption points. If κ decreases, the probability of finding a free absorption point close to the beginning of the chain decreases. Accordingly, the maximum of probability density will be reached at higher number of chain elements and further the curves will become flatter.
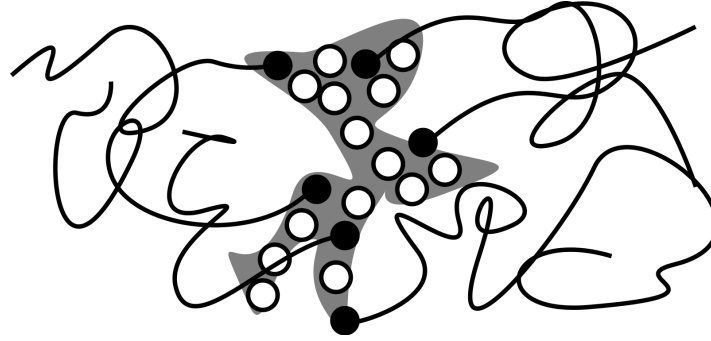
Figure 5.7.: Illustration of free (white) and allocated (black) absorption points for chain-filler bonding.

5.4.2. Microscopic Free Energy Function for Mullins Effect

The anisotropic damage model illustrated here is based upon the same framework as introduced for the elastic material law, as the material micromechanis is integrated over the unit sphere. For treatment of the damage, it is enhanced with internal variables and a non-affine micro stretch assumption. Hence, the correction factors suggested by Treloar [1975] are used to find the end to end distance of an elastomer chain:

$$\tilde{a} = \frac{1}{\cos(\theta/2)\sqrt{\alpha}}, \tag{5.39}$$

$$\tilde{b} = \cos^2(\theta/2)\sqrt{\alpha}, \tag{5.40}$$

with the valence angle $\theta = 109.5$ and the common assumption $\alpha = 1$, see Flory [1989]. The end to end distance of a fully stretched chain can be calculated with use of Treloar correction factors and microstretch χ to

$$r_{\mathrm{f}} = \frac{\chi \overline{r}_0}{\tilde{a} \tilde{b}}. \tag{5.41}$$

This is about one-half of the contour length of the corresponding elastomer chain. The microstrech is calculated by the macrostretch λ multiplied by the reinforcement factor X

$$\chi = X\lambda \tag{5.42}$$

The next step is to provide a criterion for the initiation of the chain debondage. It is known that the chain strength is much higher than the chain-filler bonds, see Bueche [1960]. Once the chain is detached, the chain remains irreversibly detached. The debonding force is denoted as F_{u}. This force is attained when the chain is close to its fully stretched length. The criteria, when the chain starts to debond can be written as

$$n_{\mathrm{l}} = \frac{\nu \chi \overline{r}_0}{\tilde{a} \tilde{b}}, \tag{5.43}$$

with the sliding ratio $\nu > 1$. The debonding corresponds to the minimal available chain length n_{l} between two filler particles. In van der Linden et al. [1994] and Huber and Vilgis [1998], the influence of the chain factors were investigated, ascertaining that the chain length has no influence, whereas the surface topology has a strong influence. Therefore, the sliding parameter is treated as a material parameter for all chains that are connecting to filler particles. The additional free energy of the chain-filler network can be described by

$$\tilde{\psi}_{cf} = \int_{n_{\mathrm{l}}}^{n_{\mathrm{u}}} \psi_c(\lambda, n) \mathcal{C} P(n) \mathrm{d}\, n, \tag{5.44}$$

with the correction factor $\mathcal{C}$, which is discussed later. The minimal chain length is related to the actual stretch by the sliding factor and can be treated as an internal variable. The minimal chain length is dependent on the material history, in particular the maximum stretch in a certain direction. The maximal chain length n_{u} is similar to a cut off radius in molecular dynamics. This assumption is applicable when a greater cut off radius has no significant influence. The most influence term of equation (5.44) have chain lengths close to the minimal chain length because the force is close to infinity. For large chains, the probability function $P(n)$ tends to zero. Another reason for neglecting large chain is because finite volume between two filler particles makes it geometrically impossible to place long chains. In Figure 5.8, it can be seen that a detachment of a chain do not inevitably leads to a complete loss of entropic stiffness. A multiple attached chain can activate another bonding. Overall, this leads to a constant number of chain elements. The $P(n)$ has to be corrected in case of activation of new bonds. By considering the assumption that the number of active chain elements remains constant, the correction factor is expressed as follows

$$\mathcal{C} = \frac{\int_{n_{\mathrm{l}}(1)}^{n_{\mathrm{u}}} P(n) n \,\mathrm{d}n}{\int_{n_{\mathrm{l}}(\chi)}^{n_{\mathrm{u}}} P(n) n \,\mathrm{d}n}. \tag{5.45}$$
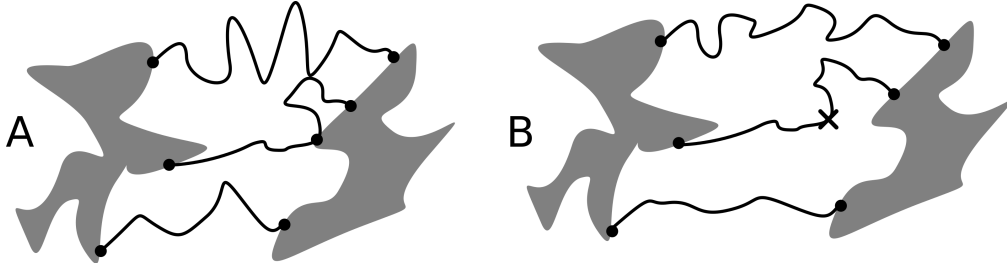
Figure 5.8.: Development of filler particle network during stretching, A) unstretched state and B) stretched state chain debonding with activation of another bonding

5.4.3. Material Tangent with Approximate Probability Function

The probability density function (5.37) is far too complicated for analytical integration over the number of chain elements, since it contains the error function. The computational cost for a numerical integration is too high, because the calculation has to be made a for each Gauss point in each iteration of a finite element calculation. Another complication is that the probability density function has to be multiplied with the force acting on the elastomer chains in dependence of its relative length. Because of these reason, a simple function has to be found to approximate the relevant part of the probability density function in an appropriate way. The use of the Gauss function leads to the problem after multiplication of the chain force. The solution of the integral requires multiple integration by parts. The first integral of exponential function can be found to the error function, although for the second time, there is no longer an analytical expression.

A Taylor series expansion of the function avoids such kind of problems, since it can be derived and integrated without problems. The remaining question is the order of the Taylor expression. To answer this question, different degrees of polynomial function are tested, whereby it emerges that the best correlation can be found for fourth order polynomial expression. The second order has an acceptable accuracy, while the third order has almost the same result as the second order. The fourth order approximation require too much computational cost after integration. Hence, the second order polynomial is chosen, see Figure 5.9. Later, it will be shown that the model with this approximation can very well represent the test results.

Table 5.1.: Coefficients and R-square for different polynomial approximation orders

order	R-square	p_1	p_2	p_3	p_4	p_5
2	0.95198	-1.05E-2	1.34E-3	-0.02598	-	-
3	0.95287	-1.68E-5	-7.45E-3	0.00118	-0.02335	-
4	0.99810	5.88E-6	-1.43E-3	0.0001112	-0.002907	0.02445

In Table 5.1, the results of the curve fitting are shown. R-square is a measure of the quality for the used approximation. It is defined as follows

$$\text{R-square} = 1 - \frac{\sum_i (f(x)_i - g_i)^2}{\sum_i (f(x)_i - \overline{f(x)})^2}, \tag{5.46}$$
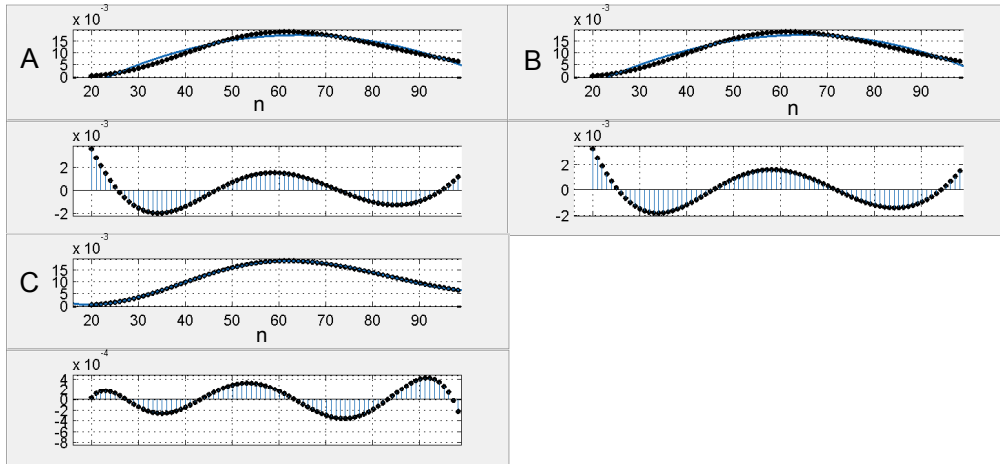
Figure 5.9.: Chain length in chain elements n as a function of the probability density. Fitting of probability density function with polynomial function and the corresponding residual: A) second order, B) third order and C) fourth order

with the function values $f(x)_i$, the approximated function values g_i and the mean function value over the approximation interval $\overline{f(x)}$. Normally, R-square of 0.95 is required, beside the maximum R-square of 1 can be achieved in case of perfect fitting. Therefore, the second order model is reasonably good compromise between computational cost and accuracy.

In general, the polynomial approximation of order o has the following form

$$P(n) = \sum_{i=1}^{o+1} p_i n^{o-i+1}. \tag{5.47}$$

For the special case of order of two, the probability density function is approximated by

$$P(n) = p_1 n^2 + p_2 n + p_3 \tag{5.48}$$

with the coefficients p_1, p_2, p_3. The coefficients are not physical material parameters, but are dependent on κ, which has a physical representation in elastomer micromechanics. Therefore, they are interpreted as intermediate or pseudo parameters, which are calculated before the FE-calculation.

The approximated probability density function is multiplied with the chain force and the correction factor. Since the correction factor only depends on the minimal available chain length, it can be placed before the integral, whereas the remaining part of the function has to be integrated over the chain length n. The force in one direction caused from the chain-filler interaction is calculated as

$$\tau_D = k_B TC \int_{n_l}^{n_u} F_C P(n) \mathrm{d}n \tag{5.49}$$

$$\tau_{D1} = \int_{n_l}^{n_u} \frac{\overline{r}}{\tilde{a}\tilde{b}n} \frac{3 - \left(\frac{\overline{r}}{\tilde{a}\tilde{b}n}\right)^2}{1 - \left(\frac{\overline{r}}{\tilde{a}\tilde{b}n}\right)^2} (p_1 n^2 + p_2 n + p_3) \mathrm{d}n \tag{5.50}$$

$$\tau_D = k_B TC \tau_{D1}. \tag{5.51}$$

The integral part τ_{D1} of equation (5.50) has to be evaluated to calculate the macro stress. After integrating over the chain length and the using the bounds, τ_{D1} can be written as

$$
\tau_{D1} = \frac{r\overbrace{[\ln(r + n_\mathrm{u}\tilde{a}\tilde{b}) - \ln(r + n_\mathrm{l}\tilde{a}\tilde{b})]}^{u_1}\overbrace{(p_3\tilde{a}\tilde{b}^2 - p_2\tilde{a}\tilde{b}r + p_1 r^2)}^{u_2}}{\tilde{a}\tilde{b}^3}
$$

$$
+ \frac{r\overbrace{[\ln(n_\mathrm{u}\tilde{a}\tilde{b} - r) - \ln(n_\mathrm{l}\tilde{a}\tilde{b} - r)]}^{u_3}\overbrace{(p_3\tilde{a}\tilde{b}^2 + p_2\tilde{a}\tilde{b}r + p_1 r^2)}^{u_4}}{\tilde{a}\tilde{b}^3}
$$

$$
+ \overbrace{\frac{3[n_\mathrm{u} - n_\mathrm{l}]p_2 r}{\tilde{a}\tilde{b}} + \frac{3[n_\mathrm{u}^2 - n_\mathrm{l}^2]p_1 r}{2\tilde{a}\tilde{b}} + \frac{p_3 r[\ln(n_\mathrm{u}) - \ln(n_\mathrm{l})]}{\tilde{a}\tilde{b}}}^{u_5} . \tag{5.52}
$$

The resulting micro force is split into parts to perform the derivative with respect to λ and the minimal available chain length n_l. Using the chain rule, the derivative is first calculated with respect to $\bar{r}$. Here the correction factor for reactivation of bondings is not taken into account, since it does not directly depend on λ. The derivatives are solved as follows

$$
\frac{\partial u_1}{\partial r} = \frac{1}{r + n_\mathrm{u}\tilde{a}\tilde{b}} - \frac{1}{r + n_\mathrm{l}\tilde{a}\tilde{b}} \tag{5.53}
$$

$$
\frac{\partial u_2}{\partial r} = -p_2\tilde{a}\tilde{b} - 2p_1 r \tag{5.54}
$$

$$
\frac{\partial u_3}{\partial r} = -\frac{1}{n_\mathrm{u}\tilde{a}\tilde{b} - r} + \frac{1}{n_\mathrm{l}\tilde{a}\tilde{b} - r} \tag{5.55}
$$

$$
\frac{\partial u_4}{\partial r} = p_2\tilde{a}\tilde{b} - 2p_1 r \tag{5.56}
$$

$$
\frac{\partial u_5}{\partial r} = \frac{3[n_\mathrm{u} - n_\mathrm{l}]p_2}{\tilde{a}\tilde{b}} + \frac{3[n_\mathrm{u}^2 - n_\mathrm{l}^2]p_1}{2\tilde{a}\tilde{b}} + \frac{p_3[\log(n_\mathrm{u}) - \log(n_\mathrm{l})]}{\tilde{a}\tilde{b}} \tag{5.57}
$$

with the abbreviations

$$
u_6 = u_1 u_2 + r\frac{\partial u_1}{\partial r}u_2 + r u_1\frac{\partial u_2}{\partial r} \tag{5.58}
$$

$$
u_7 = u_3 u_4 + r\frac{\partial u_3}{\partial r}u_4 + r u_3\frac{\partial u_4}{\partial r} \tag{5.59}
$$

the following derivative is obtained

$$
\frac{\partial \tau_D}{\partial r} = u_6 + u_7 + \frac{\partial u_5}{\partial r} \tag{5.60}
$$

and furthermore

$$
\frac{\partial n_\mathrm{l}}{\partial \lambda} = \frac{1}{1 - C^y}\frac{n_\mathrm{u}\bar{r}_0}{ab} \tag{5.61}
$$

$$
\frac{\partial r}{\partial \lambda} = \frac{\bar{r}_0}{1 - C^y} . \tag{5.62}
$$

Equation (5.60) describes the change of micro force with respect to the distance between two filler particles. The change of the lower integration bound with respect

to the stretch is described by (5.61). In equation (5.62), the distance between two filler particles is related to the stretch, depending on the filler volume fraction C.

A major part of the material tangent are the derivatives described above. Therefore, it has to be distinguished between the two given cases. In the first case, n_l remains constant, which means that the damage is not evolving. In the second case, the maximal stretch is reached. Further the debonding of elastomer chain takes place and the damage is evolving. To distinguish these two cases, the damage switch s_D is introduced as follows

$$s_D = \begin{cases} 1, & \text{if } \dot{n}_\mathrm{l} > 0 \\ 0, & \text{if } \dot{n}_\mathrm{l} = 0 \end{cases}. \tag{5.63}$$

For a positive change rate of minimal chain length between two filler particles $\dot{n}_\mathrm{l} > 0$, whereby the damage is evolving in the computed direction, the derivative with respect to n_l has to be evaluated. For $\dot{n}_\mathrm{l} = 0$, there is no need to calculate the derivative. Finally, the consistent tangent for one integration point in the unit sphere leads to

$$c_D = \frac{\mathrm{d}\tau_D}{\mathrm{d}\lambda} = \frac{\partial \tau_D(\lambda, n_\mathrm{l}(\lambda))}{\partial \lambda} + s_D \frac{\partial \tau_D(\lambda, n_\mathrm{l}(\lambda))}{\partial n_\mathrm{l}(\lambda)} \frac{\partial n_\mathrm{l}(\lambda)}{\partial \lambda} \tag{5.64}$$

$$c_D = \frac{\partial \tau_D(r(\lambda), n_\mathrm{l}(\lambda))}{\partial r} \frac{\partial r(\lambda)}{\partial \lambda} + s_D \frac{\partial \tau_D(r(\lambda), n_\mathrm{l}(\lambda))}{\partial n_\mathrm{l}(\lambda)} \frac{\partial n_\mathrm{l}(\lambda)}{\partial \lambda}, \tag{5.65}$$

with the derivative of tension with respect to the minimal available chain length

$$\frac{\partial \tau_{D1}}{\partial n_\mathrm{l}} = -\frac{r(p_3 \tilde{a} \tilde{b}^2 - p_2 \tilde{a} \tilde{b} r + p_1 r^2)}{\tilde{a} \tilde{b}^2 (r + n_\mathrm{l} \tilde{a} \tilde{b})} - \frac{r(p_3 \tilde{a} \tilde{b}^2 + p_2 \tilde{a} \tilde{b} r + p_1 r^2)}{\tilde{a} \tilde{b}^2 (n_\mathrm{l} \tilde{a} \tilde{b} - r)} - \frac{3 p_2 r}{\tilde{a} \tilde{b}} - \frac{3 n_\mathrm{l} p_1 r}{\tilde{a} \tilde{b}} - \frac{p_3 r}{\tilde{a} \tilde{b} n_\mathrm{l}} \tag{5.66}$$

and derivative of the correction factor for the reactivation of debonded chains with respect to n_l

$$\frac{\partial \mathcal{C}}{\partial n_\mathrm{l}} = -\frac{\int_{n_\mathrm{l}(1)}^{\max} P(n) n \, \mathrm{d}n (-p_1 n_\mathrm{l}^3 - p_2 n_\mathrm{l}^2 - p_3 n_\mathrm{l})}{\left(\int_{n_\mathrm{l}(\lambda)}^{\max} P(n) n \, \mathrm{d}n \right)^2} \tag{5.67}$$

$$\frac{\partial \tau_D}{\partial n_\mathrm{l}} = \mathcal{C} \frac{\partial \tau_{D1}}{\partial n_\mathrm{l}} + \frac{\partial \mathcal{C}}{\partial n_\mathrm{l}} \tau_{D1}. \tag{5.68}$$

In analogy to the elastic part of the material tangent, the macro stress tensor integrating over the unit sphere yields

$$\overline{\boldsymbol{\tau_D}} = N_\mathrm{cf} k_\mathrm{B} T \sum_i \tau_D \overline{\lambda}^{-1} \overline{\boldsymbol{\lambda}}_\mathrm{d} \otimes \overline{\boldsymbol{\lambda}}_\mathrm{d} w^i \tag{5.69}$$

with the number of chain elements per unit volume N_cf that are connecting two filler particles. Hence the material tensor is calculated as

$$\overline{\mathbb{C}_D} = N_\mathrm{cf} k_\mathrm{B} T \sum_i (c_D - \tau_D \overline{\lambda}^{-1}) \overline{\lambda}^{-2} \overline{\boldsymbol{\lambda}}_\mathrm{d} \otimes \overline{\boldsymbol{\lambda}}_\mathrm{d} \otimes \overline{\boldsymbol{\lambda}}_\mathrm{d} \otimes \overline{\boldsymbol{\lambda}}_\mathrm{d} w^i. \tag{5.70}$$

Due to the use of product rule, the material tensor comprises of the micro tangent c_D and the micro stress tensor τ_D, which is in analogy to the elastic material tensor.

5.5. Viscous Part of Material Model

In this section, the viscous part of elastomer is derived from its microstructure. Based on a micro-mechanical tube model, a computable form of the material tangent will be presented.

5.5.1. Micro-mechanical Motivation of Elastomer Viscosity

A review of elastomer viscosity can be found in Doi and Edwards [1986]. The main idea of describing the viscous effects is to focus on the behaviour of free moving chains. In this case, free means that the chains are neither connected to other chains nor to the filler particles. However, their confirmation is not really free because it is constrained due to the other chains, whereby the chain is aligned in a kind of virtual tube, see Figure 5.10. If it is assumed that the other chains are frozen, the chains marked as dots form up obstacles for the chains within the tube. As the deformation of the elastomer specimen changes, the entropy of free moving chains is also affected. If the specimen is stretched in a particular direction, elastomer chains related to this direction are also stretched.
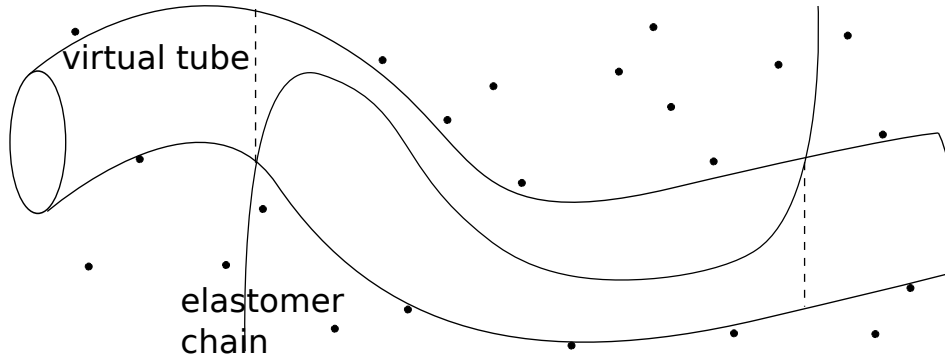

Figure 5.10.: The elastomer chain is aligned in a virtual tube which is bounded by the chains surrounding the free elastomer chain (black dots). The part of the chain, inside the tube, is marked by two dashed lines

Here, the concept of the statistics for chain entropy can be used. Hence, the entropy of the stretched free chains decreases, as in elastomer elasticity. This means that the stretched chains are no longer in a thermodynamic preferred state. In the case of elasticity, force on a chain is in static equilibrium with the connected chains and fillers. For the free chains, there are no reaction forces at the chains ends, which implies that the chain is able to return to its thermodynamic preferred state. This results in a diffusion process for the free chain. For the description of this diffusion process, the probability of chain remaining in the original tube is required. It is assumed that the chain has the length L. For the parametrisation of this length, the variable s is introduced. The probability that a part of the chain remains in the tube segment at time t is denoted as $P_T(s,t)$. Its average over the chain length L is calculated as

$$\langle P_T \rangle = \int_0^L P_T(s,t)\,\mathrm{d}s. \tag{5.71}$$

According to Doi and Edwards [1986], the relaxation time for free elastomer chains can be described, starting with the probability that describes the movement of the

chains. Using the Rouse model, see Rouse [1953], the probability $P_M(\zeta, t, s)$, that the chain moves the distance ζ, while the ends do not reach the end of the tube at time $t = 0$ is described by the following equation of motion

$$m_c \ddot{P}_M + f \dot{P}_M - \frac{3 k_B T}{\tilde{a}} P_M = F(s, t), \tag{5.72}$$

with the mass of the chain m_c, the normalised bread friction factor f and the thermal noise function $F(s, t)$. This equation can be solved by neglecting the inertia term. After some mathematical steps, a one-dimensional diffusion equation is obtained as

$$\frac{\partial P_M}{\partial t} = D_c \frac{\partial^2 P_M}{\partial \zeta^2}, \tag{5.73}$$

following the condition

$$P_M(\zeta, t, s) = 1 \quad \text{for} \quad s \geq 0 \leq 1. \tag{5.74}$$

The solution of (5.73) with respect to the initial condition can be calculated by the infinite sum as

$$P_M(\zeta, t, s) = \sum_{p=1}^{\infty} \frac{2}{L} \sin\left(\frac{p\pi s}{L}\right) \sin\left(\frac{p\pi(s - \zeta)}{L}\right) \exp\left(\frac{-p^2 t}{\tau_d}\right) \tag{5.75}$$

with the time constant

$$\tau_d = \frac{L^2}{D_c \pi}. \tag{5.76}$$

To find a probability function that only depends on time, the function will be integrated over the remaining part of chain inside the tube. The remaining tube element can be located between $s - L$ and s, the integration over ζ yields

$$P_T(s, t) = \int_{s-L}^{s} P_M(\zeta, t, s) = \sum_{p;\text{odd}} \frac{4}{p\pi} \sin\left(\frac{p\pi s}{L}\right) \exp\left(\frac{-p^2 t}{\tau_d}\right). \tag{5.77}$$

As can be seen in equation (5.77), the summation has to be only carried out for the odd numbers of $p = 1, 3, 5, \ldots$. Now, the dynamics of the chains can be described by the correlation between initial time $t = 0$ and actual time t. Therefore, a time correlation function $\langle \boldsymbol{P}(0) \cdot \boldsymbol{P}(t) \rangle$ is defined with the following definitions

$$\boldsymbol{P}(0) = A_0 C + CD + DB_0 \tag{5.78}$$
$$\boldsymbol{P}(t) = A_t C + CD + DB_t. \tag{5.79}$$

For the definition of the particular distance between the points in initial and current configuration, see Figure 5.11. There is no correlation between the vectors $A_t C$ and DB_t with $\boldsymbol{P}(0)$, therefore the time correlation function has the following form

$$\langle \boldsymbol{P}(0) \cdot \boldsymbol{P}(t) \rangle = \langle CD^2 \rangle = \tilde{a} \langle P_T \rangle \tag{5.80}$$

which is the contour length of the remaining chain. Using equation (5.71) leads to

$$\langle \boldsymbol{P}(0) \cdot \boldsymbol{P}(t) \rangle = L \tilde{a} P_T(t) = n \tilde{b}^2 P_T(t) \tag{5.81}$$
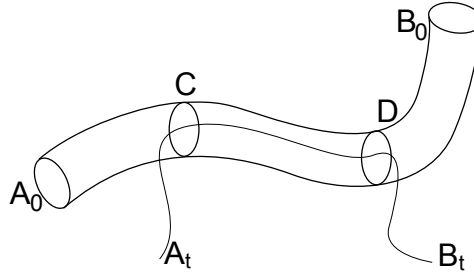
Figure 5.11.: Correlation of original tube with the tube at time t

with

$$P_T(t) = \frac{1}{L} \int_0^L P_T(s,t)\mathrm{d}s = \sum_{p;\text{odd}} \frac{8}{p^2\pi^2} \exp\left(\frac{-p^2 t}{\tau_d}\right) . \qquad (5.82)$$

Finally, the time correlation function is calculated as

$$\langle P(t) \cdot P(0) \rangle = n\tilde{b}^2 \sum_{p;\text{odd}} \frac{8}{p^2\pi^2} \exp\left(\frac{-p^2 t}{\tau_d}\right) \qquad (5.83)$$

with the longest relaxation time defined as

$$\tau_d = \frac{fn^3\tilde{b}^4}{\pi k_\mathrm{B} T}, \qquad (5.84)$$

where f defines the normalised bead friction power. The bead friction power describes the energy dissipation due to frictional contact between free chains and chain-chain network. The relaxation time strongly depends on the chain length. Since the elastomer contains different length of the free chains, an integration over the different chain lengths was suggested by Martinez et al. [2011] and Tang et al. [2012]. From micro-mechanical perspective, this approach is the most accurate, however there are two major problems: first, there is no micro-mechanical distribution function for the free chains described in literature, rather a generic function has to be assumed, and second, the numerical cost is much too high for practical finite element usage. The simplest approach is to use one fixed chain length in analogy to the elastic part of the model, although this approach is unable to deal with different damping behaviour at different excitations speeds.

Existing material models with a phenomenological approach use at least three different time constants, see e. g. Miehe and Göktepe [2005]. The idea for a micro-mechanical motivated model is to find three characteristic chain lengths for the free chain network, see Figure 5.12. The smallest chain length n_{fc1} relates to small branches on the end of elastomer chains, see also McLeish and Larson [1998]. The chains, bonded to filler particles at only one side belong to the class of middle chain length n_{fc2}. while the chains that are not bonded, build the class of long chain length n_{fc3}.

The next step is to find the additional stress caused by the free chains. For a single chain, the free energy in dependence of its stretch state is known from Gaussian or Langevinian chain theory. In this case, the Gaussian statistic is suitable for two reasons: first, the viscous behaviour is important in load cases, where normally the

ultimate extensibility of chains is not reached (e.g. cyclic loading) and second, the chains that are close to the finite extensibility are almost straight, so they cannot transmit forces to the chain-chain network.

5.6. Numerical Implementation

For the numerical implementation, the framework proposed by Miehe and Göktepe [2005] is used. Each increment in the solution procedure is interpreted as a time step. Time steps are assumed to be quasi static, which means the inertia terms are neglected. The free energy function is constructed with strain-like internal variables for one direction as follows

$$\psi_f = \psi_f(\overline{\lambda}_{\mathrm{d}}, \epsilon_a) \quad \text{and} \quad \epsilon_a(0) = 0 \tag{5.85}$$

with the set of internal variables ϵ_a. This set of internal variables contains the internal variables for the three chain lengths. The free energy function is assumed as follows

$$\psi_f = \frac{1}{2} \sum_a \mu_a (\ln \overline{\lambda}_{\mathrm{d}} - \epsilon_a)^2. \tag{5.86}$$

The dissipation on the microscale can be expressed as

$$\mathcal{D}_{\mathrm{micro}} = \sum_a \beta_a \dot{\epsilon}_a \geq= 0 \tag{5.87}$$

with the micro force

$$\beta_a = \frac{\partial \psi_f}{\partial \epsilon_a} = \mu_a (\ln(\overline{\lambda}_{\mathrm{d}}) - \epsilon_a). \tag{5.88}$$

For the internal variables, evolution equations are necessary. Due to the change of the internal variable, the free energy change equals the dissipated energy

$$\frac{\partial \psi_f}{\partial \epsilon_a} + \frac{\partial \phi_a}{\partial \dot{\epsilon}_a} = 0 \tag{5.89}$$

with the dissipation function

$$\phi_a = \frac{1}{\tau_a} \dot{\epsilon}_a{}^2. \tag{5.90}$$

To ensure the thermodynamic consistency, equation (5.90) has to be convex, the function will be convex for $\tau_a > 0$. This means that the relaxation times have to be positive, which is physically consistent.

The insertion of equations (5.86) and (5.90) in (5.89) gives the evolution equation for the micro forces

$$\dot{\beta}_a + \frac{1}{\tau_a} \beta_a = \mu_a \frac{\mathrm{d}}{\mathrm{d}t} (\ln \overline{\lambda}_{\mathrm{d}}) \quad \text{with} \quad \beta_a(0) = 0. \tag{5.91}$$

The shear stiffnesses and relaxation times can be calculated from equation (5.83) as

$$\mu_a(n,p) = N(n)k_\mathrm{B}T \sum_{p;\text{odd}} \frac{8n\tilde{b}^2}{p^2\pi^2} \tag{5.92}$$

$$\tau_a(n,p) = \frac{n^3\tilde{b}^4}{p^2\pi k_\mathrm{B}T} \tag{5.93}$$

with the number of chain elements per unit volume $N(n)$ for the specific chain length. For the overstress the derivative of the free energy function with respect to the microstretch

$$\beta(n) = \frac{\mathrm{d}\psi_f}{\mathrm{d}\overline{\lambda}_\mathrm{d}} \sum_a \mu_a(\ln(\overline{\lambda}_\mathrm{d}) - \epsilon_a)\frac{1}{\overline{\lambda}_\mathrm{d}} = \frac{1}{\overline{\lambda}_\mathrm{d}} \sum_a \beta_a, \tag{5.94}$$

is calculated. The derivative of overstress with respect to microstretch leads to the micro tangent

$$c(n) = \frac{\mathrm{d}\beta_n}{\mathrm{d}\overline{\lambda}_\mathrm{d}} = \frac{1}{\overline{\lambda}_\mathrm{d}^2} \sum_a \beta_a + \frac{1}{\overline{\lambda}_\mathrm{d}} \sum_a \mu_a. \tag{5.95}$$

In analogy to elasticity, macroscopic overstress

$$\overline{\tau}^v = k_\mathrm{B}T \sum_i \left[\sum_n N(n)\beta_n\overline{\lambda}_\mathrm{d}^{-1}\mathbf{1}\overline{\boldsymbol{\lambda}}_\mathrm{d} \otimes \overline{\boldsymbol{\lambda}}_\mathrm{d}\right] w_i \tag{5.96}$$

and material tangent

$$\overline{\mathbb{C}}^v = k_\mathrm{B}T \sum_i \left[\sum_n N(n)\left(c(n) - \beta_n\overline{\lambda}_\mathrm{d}^{-1}\mathbf{1}\right)\overline{\lambda}_\mathrm{d}^{-1}\overline{\boldsymbol{\lambda}}_\mathrm{d} \otimes \overline{\boldsymbol{\lambda}}_\mathrm{d} \otimes \overline{\boldsymbol{\lambda}}_\mathrm{d} \otimes \overline{\boldsymbol{\lambda}}_\mathrm{d}\right] w_i \tag{5.97}$$
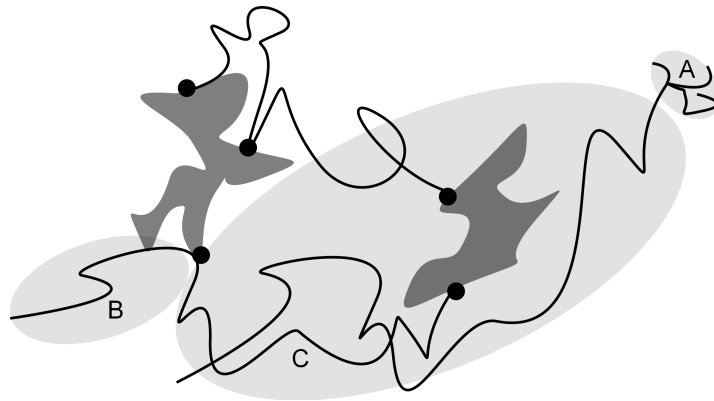
can be calculated.

Figure 5.12.: Visualisation of three different chain length for elastomer diffusion: A) short chains, branches of chains, middle length chains, B) middle length chains, chains attached on filler particle and C) long, uncrosslinked chains

5.6.1. Update Step for Internal Variables

The microforces have to be integrated over the time. For each load step, a time step $\Delta t = t^{m+1} - t^m$ is associated. Replacing the stretch time derivative in equation (5.91) leads to

$$\frac{\beta_a}{\Delta t} + \frac{1}{\tau_a}\beta_a = \frac{\mu_a}{\Delta t}\left(\ln \frac{\overline{\lambda}_d^{m+1}}{\overline{\lambda}_d^m}\right) \quad \text{with} \quad \beta_a(0) = 0. \tag{5.98}$$

Now, the implicit Euler update step is calculated as

$$\beta_a^{n+1} = \Delta t\left[-\frac{1}{\tau_a}\beta_a^{n+1} + \frac{\mu_a}{\Delta t}\left(\ln \frac{\overline{\lambda}_d^{m+1}}{\overline{\lambda}_d^m}\right)\right] \quad \text{with} \quad \beta_a(0) = 0 \tag{5.99}$$

by using the values at the time $n+1$. Finally, equation (5.99) can be solved explicitly

$$\beta_a^{n+1} = \frac{\tau_a \mu_a}{\tau_a + \Delta t}\left(\ln \frac{\overline{\lambda}_d^{m+1}}{\overline{\lambda}_d^m}\right) \quad \text{with} \quad \beta_a(0) = 0. \tag{5.100}$$

6. Finite Element Method

In this chapter, the finite element method (FEM) is described. The FEM is a general framework to solve the partial differential equations numerically. In this work, a finite element description for filler-reinforced elastomer is developed. Therefore, the basics of non-linear FEM are outlined. Furthermore, the numerical implementation of the micro-sphere model in FEM framework is shown. For further details concerning the mathematical background and the implementation of the FEM for non-linear problems, the reader can refer to Bathe [2006], Zienkiewicz et al. [2005], Bonet and Wood [2008] and Wriggers [2008].

6.1. Weak Form of Equilibrium

In chapter 3, equations for kinematics, conservation of linear and angular momentum were highlighted. On combining these equations with the constitutive equation, presented in chapter 5, leads to a system of coupled partial differential equations. This initial boundary value problem contains two kinds of non-linearities: first, the constitutive law is non-linear; and second, the geometry is non-linear since it undergoes large deformations. The static mechanical boundary value problem can be written in an elegant way by expressing the equilibrium over the body $\mathcal{B}_t$ and the boundary $\partial \mathcal{B}_t$ at the current time t. Neglecting the body forces, the equilibrium leads to

$$\operatorname{div} \boldsymbol{\sigma} = 0 \quad \text{in} \quad \mathcal{B}_t \tag{6.1}$$

$$\boldsymbol{t} = \bar{\boldsymbol{t}} \quad \text{on} \quad \partial_{\boldsymbol{t}} \mathcal{B}_t \tag{6.2}$$

$$\boldsymbol{u} = \overline{\boldsymbol{u}} \quad \text{on} \quad \partial_{\boldsymbol{u}} \mathcal{B}_t. \tag{6.3}$$

The boundary conditions are separated into a displacement boundary $\partial_{\boldsymbol{u}} \mathcal{B}_t$ or Dirichlet boundary with the enforced displacement $\overline{\boldsymbol{u}}$ and the traction or von Neumann boundary with the traction vector $\boldsymbol{t}$. For the boundary condition, the following conditions hold

$$\partial_{\boldsymbol{u}} \mathcal{B}_t \bigcup \partial_{\boldsymbol{t}} \mathcal{B}_t = \partial \mathcal{B}_t \quad \text{and} \quad \partial_{\boldsymbol{u}} \mathcal{B}_t \bigcap \partial_{\boldsymbol{t}} \mathcal{B}_t = \varnothing. \tag{6.4}$$

The first condition states that the boundary sets are disjunct, while the second condition implies that if no displacement is predescribed, a traction vector is applied including the special case of no traction force.

For a finite element solution of the boundary value problem, a variational is used. Hence, equation (6.1) is multiplied with a weighting function $\boldsymbol{\eta}$. This is also known as virtual displacement or test function. It is arbitrary and vanishes on the displacement boundary $\boldsymbol{\eta} = 0 \quad \text{on} \quad \partial_{\boldsymbol{u}} \mathcal{B}_t$. Finally, the integration over the domain leads to the variational form

$$\int_{\mathcal{B}_t} \operatorname{div} \boldsymbol{\sigma} \cdot \boldsymbol{\eta} \, \mathrm{d}v = 0. \tag{6.5}$$

Using the divergence theorem leads to

$$\mathcal{G} = \int_{\mathcal{B}} \boldsymbol{P} \cdot\cdot \operatorname{grad}\boldsymbol{\eta}\, \mathrm{d}V - \int_{\partial_t \mathcal{B}} \boldsymbol{T} \cdot \boldsymbol{\eta}\, \mathrm{d}A = 0. \tag{6.6}$$

Since the test function is zero on the displacement boundary, the corresponding integral vanishes. Given that the Cauchy stress tensor is symmetric, the gradient of the test function can be replaced by its symmetric part $\bigtriangledown^S \boldsymbol{\eta} = \frac{1}{2}\left(\operatorname{grad}\boldsymbol{\eta} + \operatorname{grad}^{\mathrm{T}}\boldsymbol{\eta}\right)$, which leads to

$$\mathcal{G} = \int_{\mathcal{B}_t} \boldsymbol{\sigma} \cdot\cdot \bigtriangledown^S \boldsymbol{\eta}\, \mathrm{d}v - \int_{\partial_t \mathcal{B}_t} \boldsymbol{t} \cdot \boldsymbol{\eta}\, \mathrm{d}a = 0. \tag{6.7}$$

The weak formulation requires that the balance of linear momentum is satisfied not at all points, but in the integral average over the whole domain. For the weak form, no potential is assumed, therefore, the weak form can be used in general types of problems, such as damage, friction, plasticity and so on. Due to the partial integration, the derivative of the Cauchy stress tensor vanishes. This offers the advantage that no second derivative of the displacement is necessary for the finite element formulation.

6.2. Linearisation

The problems in continuum mechanics essentially prompt three different types of non-linearities, namely geometrical, physical or material non-linearities and nonlinarities due to boundary conditions, such as contact. Elastomers are known for large deformations, non-linear stress strain behaviour and hysteresis, therefore geometrical and material non-linearities have to be taken into account.

For the solution of the non-linear equations, different solution schemes are available. The Newton method is most commonly used, because it guarantees quadratic convergence as long as the initial solution lies in the convergence radius. As a first step, equation (6.7) is linearised with the use of Taylor series expansion at the approximate solution $\boldsymbol{u}$. Usually the load is applied incrementally, which implies for new load step, the converged solution of the last load step can be used. For the first load step, the reference configuration is used. The linearisation follows as

$$D\mathcal{G}(\boldsymbol{u}, \Delta\boldsymbol{u}) = \mathcal{G}(\boldsymbol{u}) + \Delta\mathcal{G}(\boldsymbol{u}, \Delta\boldsymbol{u}) + \mathcal{O}(\varepsilon^2) = 0, \tag{6.8}$$

with the increment given by

$$\Delta\mathcal{G}(\boldsymbol{u}, \Delta\boldsymbol{u}) = \frac{\mathrm{d}}{\mathrm{d}\varepsilon}\, \mathcal{G}(\boldsymbol{u} + \varepsilon\boldsymbol{u})|_{\varepsilon=0} = \frac{\partial\mathcal{G}}{\partial\boldsymbol{u}}\Delta\boldsymbol{u}. \tag{6.9}$$

For this expression, a generalisation of directional derivative to functional spaces is used, which is called the Gateaux derivative. Here ε denotes the direction and $\Delta\boldsymbol{u}$ the displacement increment.

Starting with equation (6.7), the Gateaux derivative in direction of $\Delta\boldsymbol{u}$ is calculated as

$$\frac{\partial\mathcal{G}(\varphi, \boldsymbol{\eta})}{\partial\boldsymbol{u}}\Delta\boldsymbol{u} = \int_{\mathcal{B}} D\boldsymbol{P} \cdot\cdot \operatorname{grad}\boldsymbol{\eta}\, \mathrm{d}V. \tag{6.10}$$

The force is assumed to be independent of the deformation. By using $\boldsymbol{P} = \boldsymbol{F} \cdot \boldsymbol{S}$, the linearisation of the first Piola-Kirchhoff stress tensor leads to

$$\frac{\partial \mathcal{G}(\varphi, \boldsymbol{\eta})}{\partial \boldsymbol{u}} \Delta \boldsymbol{u} = \int_{\mathcal{B}} (\text{Grad}\Delta \boldsymbol{u} \cdot\cdot \boldsymbol{S} + \boldsymbol{F} \cdot\cdot [D\boldsymbol{S} \cdot \Delta \boldsymbol{u}]) \cdot\cdot \text{Grad}\boldsymbol{\eta} \, dV. \tag{6.11}$$

With the linearisation of the second Piola-Kirchhoff stress tensor

$$D\boldsymbol{S} \cdot \Delta \boldsymbol{u} = \mathbb{C}^i \cdot\cdot [\Delta \boldsymbol{E}], \tag{6.12}$$

where $\mathbb{C}^i$ is the elasticity tensor belonging to the initial configuration and $\Delta \boldsymbol{E}$ is the linearisation of the Green-Lagrange strain tensor

$$\Delta \boldsymbol{E} = \frac{1}{2} \left(\boldsymbol{F}^T \cdot\cdot \text{Grad}\Delta \boldsymbol{u} + \text{Grad}^T \Delta \boldsymbol{u} \cdot\cdot \boldsymbol{F} \right) \tag{6.13}$$

the linearisation follows to

$$\frac{\partial \mathcal{G}(\varphi, \boldsymbol{\eta})}{\partial \boldsymbol{u}} \Delta \boldsymbol{u} = \int_{\mathcal{B}} \left(\text{Grad}\Delta \boldsymbol{u} \boldsymbol{S} + \boldsymbol{F} \mathbb{C}^i [\Delta \boldsymbol{E}] \right) \cdot \text{Grad}\boldsymbol{\eta} \, dV. \tag{6.14}$$

Now, using the symmetry of $\mathbb{C}^i$, equation (6.14) can be transformed as

$$\frac{\partial \mathcal{G}(\varphi, \boldsymbol{\eta})}{\partial \boldsymbol{u}} \Delta \boldsymbol{u} = \int_{\mathcal{B}} \left(\text{Grad}\Delta \boldsymbol{u} \boldsymbol{S} \cdot \text{Grad}\boldsymbol{\eta} + \delta \boldsymbol{E} \mathbb{C}^i [\Delta \boldsymbol{E}] \right) \, dV. \tag{6.15}$$

Above derived equations have two terms: the first term corresponds to the geometrical stiffness and the second term corresponds to material stiffness. In the material stiffness $\delta \boldsymbol{E} = \frac{1}{2} \left(\boldsymbol{F}^T \text{Grad}\boldsymbol{\eta} + \text{Grad}^T \boldsymbol{\eta} \boldsymbol{F} \right)$ symbolises the first variation of the Green-Lagrange strain tensor. All variables have to be updated for each iteration of the calculation.

The linearisation in current configuration can be derived by a push forward of equation (6.15)

$$\frac{\partial \mathcal{G}(\varphi, \boldsymbol{\eta})}{\partial \boldsymbol{u}} \Delta \boldsymbol{u} = \int_{\mathcal{B}_t} \left(\text{grad}\Delta \boldsymbol{u} \boldsymbol{\sigma} \cdot \text{grad}\boldsymbol{\eta} + \nabla^s \boldsymbol{\eta} \mathbb{C}^i [\nabla^s \Delta \boldsymbol{u}] \right) \, dv, \tag{6.16}$$

for details see Wriggers [2008]. The symbol ∇^s is the symmetric gradient in current conformation. The formula derived in equation (6.16) called is the updated Lagrangian formulation in literature, as all deformation states have to be updated in each iteration. The linearised relations are used for the finite element discretisation in the next section.

6.3. Discretisation

The variational description, stated in equation (6.7), requires that the problem is fulfilled for every test functions satisfying the displacement boundary conditions, although the basic problem lies in the fact that the number of possible test functions is infinity. In order to reduce the number of test functions, the body in initial conformation is divided into n_d discrete elements. The geometry

$$\mathcal{B} \approx \mathcal{B}^h = \bigcup_{d=1}^{n_d} \Omega_d \tag{6.17}$$
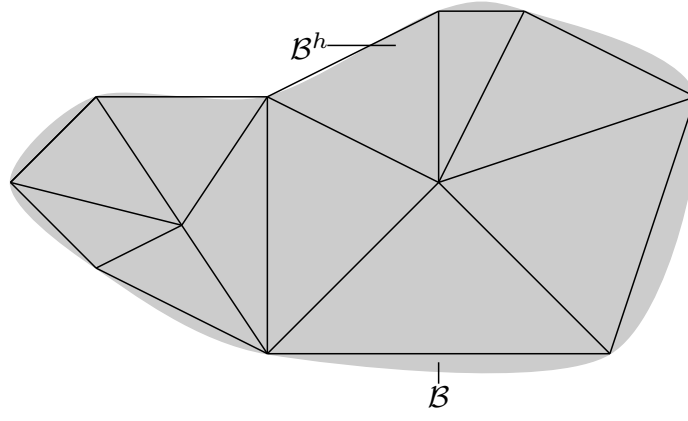
Figure 6.1.: Discretion of the domain $\mathcal{B}$ with 2-dimensional triangular elements leads
to the approximated $\mathcal{B}_h$

is approximated by non-overlapping subdomains or elements Ω_d, which are only connected by the nodes. In this case, the elements form a conforming mesh. In general, the domains $\mathcal{B}$ and $\mathcal{B}^h$ are not the same, as can be seen in Figure 6.1.

Following the standard FEM procedure and use of linear shape functions, the discrete form of boundary value problem (6.1) can be stated as

$$\mathbf{K}_{\mathrm{T}} = \int_{\mathcal{B}_t} \left(\mathrm{grad}\Delta\boldsymbol{u}\boldsymbol{\sigma} \cdot \mathrm{grad}\boldsymbol{\eta} + \bigtriangledown^s\boldsymbol{\eta}\mathbb{C}^i\left[\bigtriangledown^s\Delta\boldsymbol{u}\right] \right) \mathrm{d}v$$

$$\approx \bigcup_{d=1}^{n_{el}} \sum_{i=1}^{n_{\mathrm{gp}}} \left(\mathbf{N}_x^{\mathrm{T}} \cdot \sigma \cdot \mathbf{N}_x + \mathbf{B}^{\mathrm{T}} \cdot \cdot\mathbb{C} \cdot \cdot \mathbf{B} \right) \det \boldsymbol{J}_i w g_i, \quad (6.18)$$

using the Jacoby matrix $\boldsymbol{J}$. Also, two additional matrices have to be calculated. The first matrix is the derivative of test function $\mathbf{N}_x$, with respect to global coordinates and with use of inverse Jacobian and second matrix is the $\mathbf{B}$-matrix. The $\mathbf{B}$-matrix builds the symmetric gradient of test functions and makes it compatible with material tensor. In this case, using linear brick elements and Voigt notation, the dimension of $\mathbf{B}$ is 24×6. The right hand side of equation (6.18) is called the global tangential stiffness matrix $\mathbf{K}_{\mathrm{T}}$.

As a last step, the internal forces are approximated as follows

$$\mathbf{F}_{\mathrm{int}} = \int_{\mathcal{B}_t} \bigtriangledown^s\boldsymbol{\eta}\dot{S}\mathrm{d}v \approx \bigcup_{d=1}^{n_{el}} \sum_{i=1}^{n_{\mathrm{gp}}} \mathbf{B}^{\mathrm{T}} \cdot \boldsymbol{S} \det \boldsymbol{J}_i w g_i. \tag{6.19}$$

6.4. Implementation of Dyadic Product of Stretch Vectors

To calculate the stiffens matrix, an implementation for dyadic product of the stretch vectors d_i is necessary. For stress vectors, two times and for material tensors, four times dyadic product is used. The implementation is done in Voigt notation to save the computational time. The two times dyadic product emerges as 3×3 matrix as follows

$$\boldsymbol{L} = \overline{\boldsymbol{\lambda}}_{\mathrm{d}} \otimes \overline{\boldsymbol{\lambda}}_{\mathrm{d}}. \tag{6.20}$$

This matrix is converted to Voigt notation as follows

$$\boldsymbol{L}_v = \begin{pmatrix} \boldsymbol{L}(1,1) \\ \boldsymbol{L}(2,2) \\ \boldsymbol{L}(3,3) \\ \boldsymbol{L}(2,3) \\ \boldsymbol{L}(1,3) \\ \boldsymbol{L}(1,2) \end{pmatrix}. \tag{6.21}$$

The four times dyadic product

$$\mathbb{L}_v = \boldsymbol{L}_v \otimes \boldsymbol{L}_v \tag{6.22}$$

is calculated with the dyadic product of the two times dyadic product in Voigt notation $\boldsymbol{L}_v$. This emerges as a 6×6 matrix, which is the Voigt representation of a fourth order tensor.

6.5. Solution Algorithm

In this section, the overall solution algorithm is presented, see algorithm 1. The iterative Newton-Raphson scheme is used, in addition, the boundary conditions are applied step-wise to ensure the convergence and to reduce the error in viscous part of solution. Inside the loop over all the Gauss points, the loop over all directions of the unit integration schema is nested. In this loop, the elastic, damage and viscous overstress are calculated using the stretch $\overline{\lambda}_{\mathrm{d}}$. The internal variables will be updated, if they evolve. Multiplication with the dyadic product of stretch vector will emerge as the material tangent and stress vectors.

Algorithm 1 Numerical solution

1: calculate pseudo material parameter p_1, p_2, p_3
2: initialise minimal chain length n_l at each Gauss Point
3: initialise set of internal variable for overstress $\beta(n)$ at each Gauss Point
4: $\boldsymbol{u}_0 = \boldsymbol{0}$
5: **for** load steps or pseudo time step Δt **do**
6:     **while** norm of displacement increment $> \epsilon$ **do**
7:         **for** loop over all elements n_d **do**
8:             **for** loop over all Gauss points n_gp **do**
9:                 **for** loop over all direction $\boldsymbol{d}_i$ over the unit sphere **do**
10:                     calculate stretch vector $\overline{\boldsymbol{\lambda}}_\mathrm{d} = \overline{\boldsymbol{F}} \cdot \boldsymbol{d}$
11:                     calculate stretch $\overline{\lambda}_\mathrm{d} = |\overline{\boldsymbol{\lambda}}_\mathrm{d}|$
12:                     calculate elastic part
13:                     **if** damage is evolving **then**
                            calculate derivative of τ_D with respect to n_l
14:                     **end if**
15:                     calculate viscous overstress
16:                     build part material tangent and stress vector in $\boldsymbol{d}_i$ using $\boldsymbol{L}_v$ and $\mathbb{L}_v$
17:                 **end for**
18:             **end for**
19:             sum element stiffness and residual
20:         **end for**
21:         build $\mathbf{K}_\mathrm{T}, \mathbf{F}_\mathrm{int}, \mathbf{F}_\mathrm{ext}$
22:         solve linearised equation system $\mathbf{K}_\mathrm{T} \Delta \boldsymbol{u}_{k+1} = \mathbf{F}_\mathrm{ext} - \mathbf{F}_\mathrm{ext}$
23:         Newton-Raphson Iteration $\boldsymbol{u}_k = \boldsymbol{u}_k + \Delta \boldsymbol{u}_{k+1}$
24:     **end while**
25:     **if** damage evolved **then**
26:         update of internal variable n_l
27:     **end if**
28:     update of internal variables for viscous overstress $\beta(n)$
29: **end for**

---

7. Numerical Studies

In this chapter, the modelling capabilities of the introduced material model are shown. In parameter studies, the damage and viscous effects of the material model are highlighted.

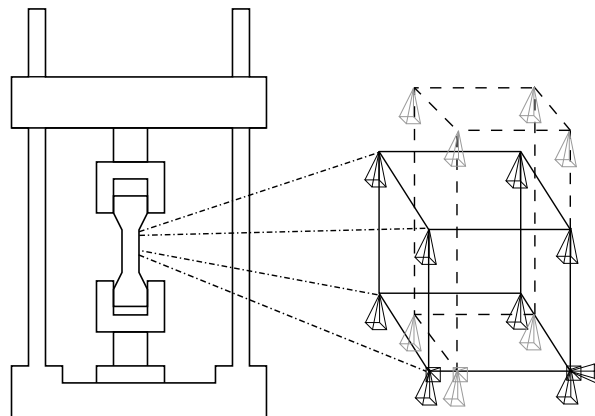## 7.1. Anisotropic Mullins-Type Damage Model

Figure 7.1.: Specimen in a tensile testing machine and corresponding uniaxial load case with boundary conditions for finite element calculation, dashed line shows the deformed element

7.1.1. Parameter Study

For the parameter study, the load case of uniaxial loading is used, which corresponds to tests that can be carried out on a simple tensile testing machine. To apply this load case in a finite element simulation, a single eight-node brick element is necessary, see Figure 7.1. The bottom of the element is fixed in the stretch direction. To avoid rigid body translation on the button plane, one node is fixed in all three degrees of freedom. Moreover, to avoid rotation, another node on the button plane has to be constrained with an additional constraint. This constraint has to be chosen in a way that the rotation is blocked, although the contraction perpendicular to the load direction remains unaffected. On the top of the element, displacement boundary conditions are applied. During stretching, the specimen contracts and a homogeneous strain field is obtained.

Using the described finite element test case, the parameter study is carried out. Subsequently, the results will be compared to uniaxial test data from literature. The anisotropic Mullins-type damage model depends on eight physical material parameters, including two parameters for the elastic response. The material parameters are summarised in Table 7.1.

Table 7.1.: Material parameters for the anisotropic Mullins-type damage model

parameter	description
χ	filler volume fraction
n	chain length of chain-chain network in chain elements
$\bar{r}$	minimal distance between two aggregate surfaces
κ	quotient of available and used absorption area
T	thermodynamic temperature
ν	sliding factor
N_{cc}	number of chains per unit volume in chain-chain network
N_{cf}	number of chains per unit volume in chain-filler network
p_1, p_2, p_3	intermediate parameter, correlated to $\bar{r}$ and κ

The thermodynamic temperature has the same linear influence on the elastic and damage part of the model, since it only acts as a scaling factor. Therefore, the thermodynamic temperature is kept constant at a room temperature of $T = 293.15\,\mathrm{K}$.

In the virtual test, the specimen is first stretched to $\lambda = 1.375$ before the stretch is released to $\lambda = 1.0$. In the next cycle, the stretch is increased to $\lambda = 1.75$ and again released to $\lambda = 1.0$. Since there are no viscous effects considered, the unloading in first cycle falls together with the reloading in the second circle in the range of $\lambda = 1.0$ to $\lambda = 1.375$. In contrast to an isotropic damage model, a residual stretch is observed for each curve without considering plasticity. The stretching in only one direction leads to an anisotropic decrease of the material properties, which is described by internal variables placed on the unit sphere. The material parameters perpendicular to loading direction will remain constant during loading. Therefore, the stress-free state will change to a deformed conformation, because the material is damaged in one direction.

The parameter study starts with the number of chains per unit volume in the chain chain network N_{cc}, see Figure 7.2. An increase of N_{cc} leads to an increase of stiffness, although the hysteresis remains the same. While increasing the number of chains per unit volume N_{cf} in chain-filler network, both stiffness and hysteresis appear increased. This is reasonable since more chains in chains-filler network lead to a higher stiffness, while also more chains detach, which leads to more pronounced hysteresis.

The number of chain elements per chain in the chain-chain network only has minor influence in these studies, since the stretch is quite moderate such that the non-linear terms of the Langevin function are not significant. A lower number of chain elements leads to increased stiffness at high stretches.

The sliding factor ν holds significant influence, whereby a smaller sliding factor leads to increased stiffness and hysteresis, because the chains are stretched close to their extensibility limit. The unloading curve is slightly decreased since more chains are detached.

An increased quotient of the available and used absorption area leads to a gain of stiffness and hysteresis. For high κ values, the distribution of chain length between two filler particle is more dense, see Figure 5.6. Reducing the minimal distance between two aggregate surfaces leads to a significant increase of stiffness at small

stretch, however, for higher stretch, the slope of curve becomes smaller since the peak in the distribution function is passed.

The parameter study is completed with the filler volume fraction. By increasing the filler volume fraction χ, the stiffness is slightly increased during virgin loading and remains almost the same for unloading. From the experimental results, a much stronger dependence of hysteresis on the filler volume fraction is expected. However, the increase of filler volume leads to an increase of active chains in chain-filler network, because more chains can be bonded with the filler particle. Consequently, more chains will detach during stretching resulting in a significant increase of hysteresis.

7.1.2. Comparison with Experimental Data

To validate the anisotropic Mullins-type damage model, special test data is necessary. In Dargazany and Itskov [2009], test data for cyclic loading in two orthogonal directions are provided. The material test to obtain such kind of data requires a special cross shaped specimen, see Figure 7.3, which can be clamped on the grey areas either in x or y direction. To minimize the effect of the unused direction on the measurement area, the clamping strips are multiple slitted. If the specimen is stretched in one direction, the slits will open in the perpendicular direction and an almost homogeneous strain field develops. For more information regarding multi axial loading in material testing, the reader is refereed to Pawelski [2001].

The specimen is first stretched in x direction to $\lambda = 1.15$ and subsequently stress is released. For the next loading cycle, the stretch is increased to $\lambda = 1.3$ and the stretch is released again. The stretch is increased in steps of 0.15 to $\lambda = 1.75$. In a second step, the same specimen is clamped in y direction and the same test is carried out again.

For the identification procedure, some parameters are fixed. The tested material has a filler volume fraction of 0.2, therefore it is fixed to this value. Moreover, the number of chain length in the chain-chain network is fixed to 100, since there is almost no influence, as discussed before. All other parameters are allowed to variate in bounds, which are used in the previous parameter study, see section 7.1.1. A least square fitting is performed to fit the model to the test data of the virgin specimen. The results of fitting are plotted in Figure 7.4. For the virgin specimen, a very good agreement of the model prediction with the experimental data is found.

In Table 7.2, the fitted material parameters are summarised. Using the same set of material parameters, the pre-stressed material is simulated. Moreover, a good agreement with the test data can be found for the pre-stressed specimen. A slight over-prediction of primary loading in the range of $\lambda = 1.4$ to $\lambda = 1.75$ can be seen. The stress level in the pre-stressed curve is significantly lower than the virgin curve, due to two reasons: first, the material is damaged by virgin loading also in directions that have contributions in y direction; and second, the residual strain in x leads to a stretch less than one in y direction, although in measurement, it is treated as one. This results in a decreased maximum stretch and ultimately a lower stress.

A small peak on the pre-stressed curve at the maximum stretch shows that the curve will reach its virgin shape for higher strains. From this point, the influence of loading in x direction is almost vanished, because the chains that are active were not detached in primary loading.
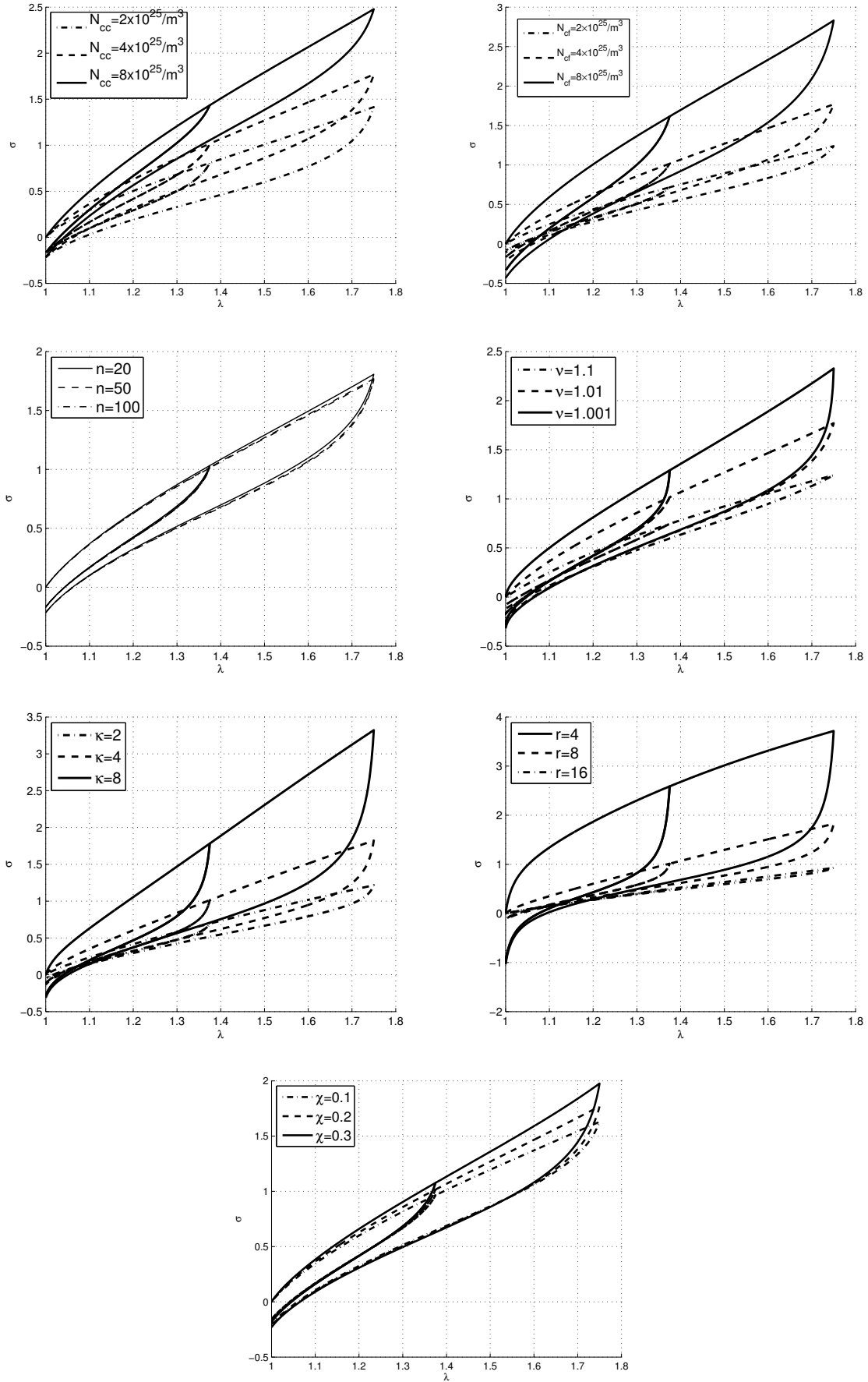
Figure 7.2.: Results of parameter study damage, in each plot one parameter is variated, the remaining parameter are set to $\chi = 0.2$, $N_{cc} = 4 \times 10^{25}\,1/\text{m}^3$, $N_{cf} = 4 \times 10^{25}\,1/\text{m}^3$, $n = 50$, $\nu = 1.01$, $\kappa = 4$ and $\bar{r} = 8$.
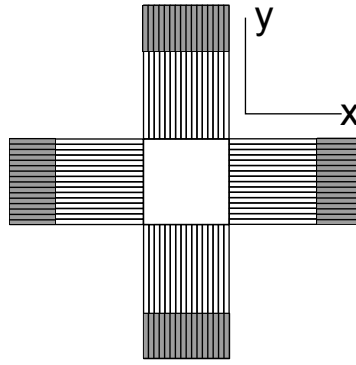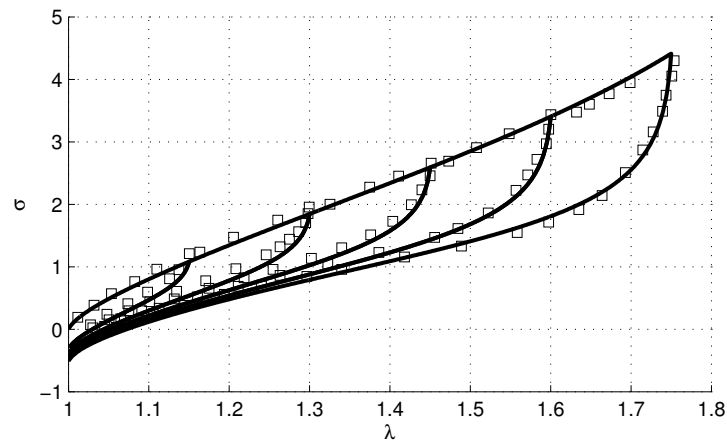
Figure 7.3.: Cross shaped specimen

Virgin specimen (stretch in x direction)
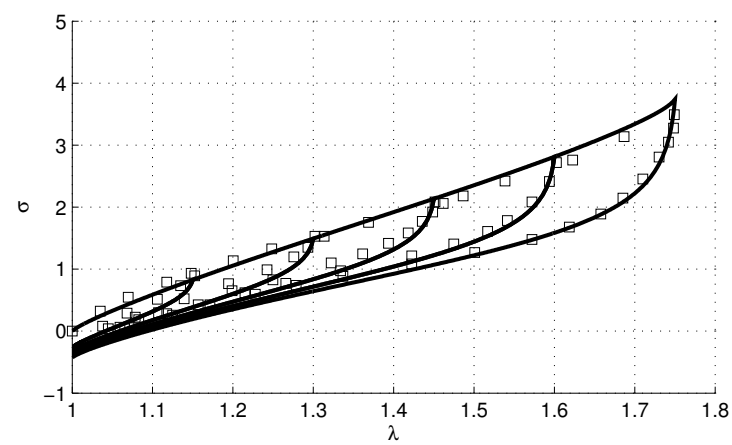

Pre-stressed specimen (stretch in y direction)

Figure 7.4.: Fitting of anisotropic damage model, solid lines model prediction, squares experimental data (from Dargazany and Itskov [2009])

Table 7.2.: Material parameter for the fitted model

$\bar{r}$	κ	ν	N_{cc}	N_{cf}
8.216	4.098	1.0025	$6.01 \times 10^{25}\ 1/\mathrm{m}^3$	$7.30 \times 10^{25}\ 1/\mathrm{m}^3$

κ	p_1	p_2	p_3	
0.2	-1.183×10^{-2}	1.262×10^{-3}	-0.02598	

7.1.3. Loading in Three Directions

In this numerical study, the specimen is stretched in three perpendicular directions. In the first loading cycle, the stretch is oriented in x direction, see Figure 7.5, which leads to residual stresses in x directions. The specimen is now stretched in a second cycle in y direction and in third cycle in z direction. The stretch magnitude is kept the same with $\lambda = 1.75$. In the fourth cycle, the stretch is again in the x direction. The residual stress vanished because the specimen is now equally damaged in all three directions.
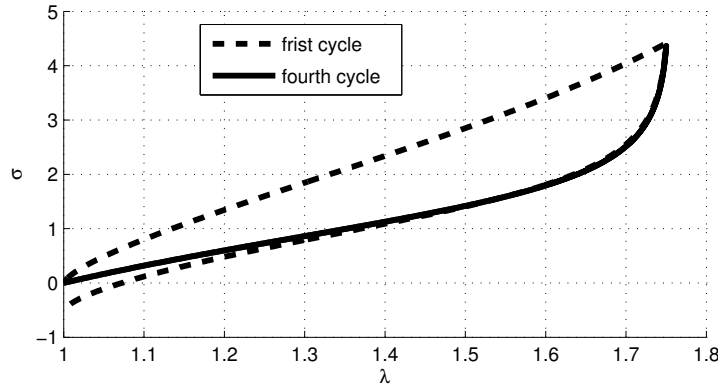
Figure 7.5.: Stress σ_{11}, first and fourth loading cycle

7.1.4. Shear Test

In this section, a shear test is simulated. A $50\,\mathrm{mm} \times 50\,\mathrm{mm} \times 20\,\mathrm{mm}$ rubber block is modelled by using 400 elements with an element edge length of $5\,\mathrm{mm}$. The block is fixed at the bottom and displaced at the top $20\,\mathrm{mm}$ in x-direction, see Figure 7.6.

For the visualisation of damage the average is taken, since the damage has 21 components. The damage is measured in the minimum available chain length, whereby the average is computed as

$$< n_L >= \sum_i n_{Li} w_i, \tag{7.1}$$

with the minimal chain length in the i-th direction n_{Li}. The stress is averaged by von Mises rule. The stress field has its maximum in the acute angle corners. The minimum can be found at the borders of the block between the corners. The damage field has his maximum in the same region as the stress field. The minimum can be

found in the obtuse angle corners. A concentration can be found in the line between the obtuse angle corners, where the maximum shear occurs.
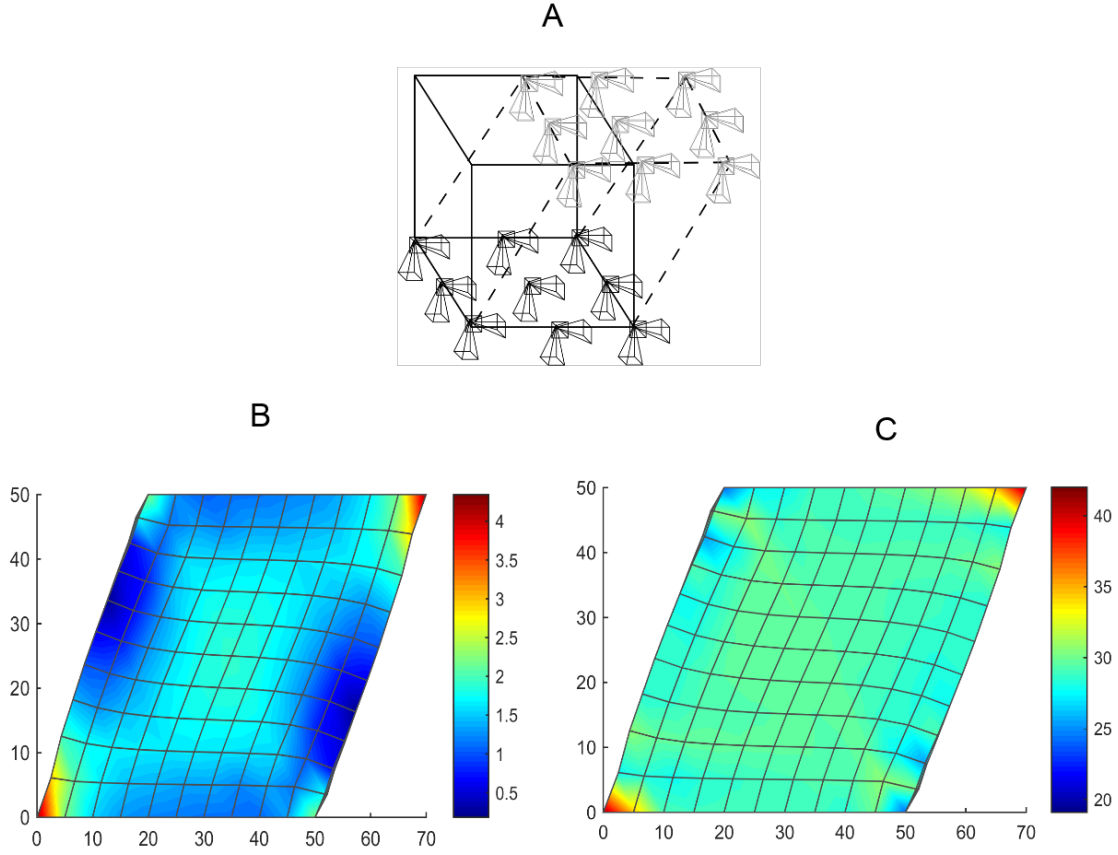
A

B

C

Figure 7.6.: FE-shear test: A) Boundary conditions, B) Von Mises stress field in MPa and C) Average damage field in minimal available chain length

7.2. Viscous Response

In this section, the viscous response of the material is investigated. The material response is time-dependent, whereby a timestep Δt is associated with each loadstep. The mass and inertia effects are neglected, therefore the calculation is called quasi static.

7.2.1. Parameter Study

To investigate the influence of material parameters on the viscous response, a parameter study is performed. The load case is uniaxial loading, in analogy to the parameter study for anisotropic damage. The material parameters for the viscous material behaviour are summarised in Table 7.3. The parameter study is performed with the loading speed of $\dot{\lambda} = 1\,\mathrm{s}^{-1}$, until the maximum stretch of $\lambda = 1.5$ is reached. Three complete cycles from $\lambda = 1.0$ to $\lambda = 1.5$ are simulated.

As expected, the basic form of the curve is quite similar to the anisotropic damage loading curves. During primary loading, the damage takes place, however for unloading and reloading, a difference from pure anisotropic damage can be seen. The unloading and reloading curves are not coincident as for reloading higher stress occurs than in unloading. A hysteresis loop is formed in cyclic loading, whereby the area inside the loop correlates to the dissipation due to viscosity.

In Figure 7.7, the results of the parameter study are presented, showing that a higher bead friction factor leads to stiffening of the material. For a bread friction factor f (internal friction of chains) of 10^{-25} J/m^3, it can be seen that due to the impact of primary loading more than three loading cycles are necessary to obtain a stationary hysteresis curve.

The number of chain elements per unit volume has also an influence on the viscous response. For N_{fc1}, the impact on the curves is very low because the corresponding relaxation time is small in comparison to the loading speed. For N_{fc2}, the effect of a dynamic stiffening can be seen, whereby a higher value leads to an increased stiffness and a larger hysteresis. The same effect can be seen even more pronounced for N_{fc3}. An increase of the number of chain elements per elastomer chain shows qualitatively the same result as increasing the number of elastomer chains per unit volume.

Table 7.3.: Material parameters for the viscous material behaviour

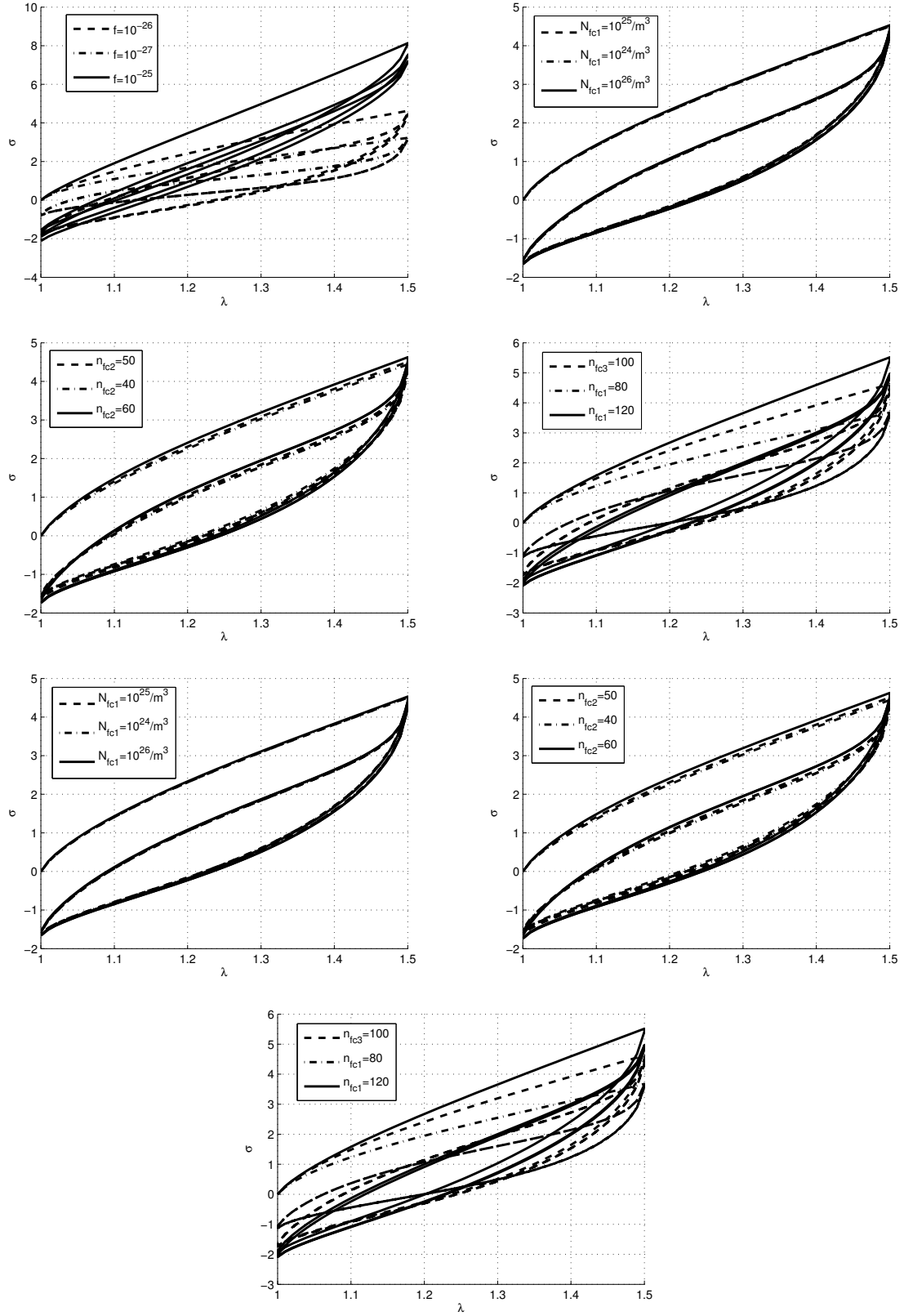| parameter	description
p	degree of approximation for the one dimensional diffusion equation
f	normalised bead friction power per unit volume
$N_{fc1}, N_{fc2}, N_{fc3}$	number of free chains per unit volume for different chain length
$n_{fc1}, n_{fc2}, n_{fc2}$	characteristic chain lengths

Figure 7.7.: Results of parameter study for viscosity, in each plot one parameter is variated, the remaining parameters are set to $p = 3, f = 10^{-26}, N_{fc1} = N_{fc2} = N_{fc3} = 10^{25}\,\mathrm{m}^{-3}$, $n_{fc1} = 20$, $n_{fc2} = 50$ and $n_{fc3} = 100$. The used elastic and damage parameter are written in table 7.2.

7.2.2. Fitting to Time-Dependent Test Data

In this section, the visco-elastic parameters are fitted to experimental data. A broad variety of test data for filled elastomer can be found in Dämgen [2006]. For the fitting, a uniaxial relaxation test is calculated. In the material test, the specimen is used for several loading speeds causing the problem that the Mullins effect has a significant influence in the first relaxation test. Therefore, for a good repeatability, the specimen is preconditioned, which means that the specimen is stretched in cyclic loading up to the precondition stretch of $\lambda = 1.6$.

This preconditioning has to be considered for the identification of the material model. A simple and correct way to apply the preconditioning in numerical simulation is to calculate the internal variables before the FE calculation, since the internal variables only depend on the maximal stretch, which is the precondition stretch in this case. The main calculation is started by using the precalculated internal variables.

The relaxation test is started with the jump from $\lambda = 1$ to $\lambda = 1.2$ at $t = 0s$. After a sufficiently long relation time, a step from $\lambda = 1.2$ to $\lambda = 1.4$ is performed. The second jump is timed in such a way that the maximal stretch is reached at $t = 300s$. Consequently, the jump with low loading speed starts earlier than with high loading speed.

The result is depicted in Figure 7.8. The material parameters for simulation are summarised in Table 7.4. A clear peak can be seen after the jump. For the loading speed of $\dot{\lambda} = 0.085\,\text{s}^{-1}$ and $\dot{\lambda} = 0.433\,\text{s}^{-1}$, the peak has almost the same height, because the step is faster than the diffusion of the elastomer chains. For low loading speeds, the diffusion of chains takes place during the loading step. The corresponding peak is much lower in the test and the simulation.

Table 7.4.: Fitted material parameter

parameter	description
p	3
f	$3.1 \times 10^{-25}\,\text{J}$
$N_{fc1}, N_{fc2}, N_{fc3}$	$3 \times 10^{24}\,\text{m}^{-3}, 2 \times 10^{24}\,\text{m}^{-3}, 2.3 \times 10^{24}\,\text{m}^{-3}$
$n_{fc1}, n_{fc2}, n_{fc2}$	$20, 50, 115$

7.2.3. Anisotropic Time-Depended Behaviour

The formulation of the viscous material law is isotropic in the initial state. However, due to the deformation, the internal variables generally evolve differently in each direction. This leads to an anisotropic viscous behaviour.

To show this behaviour, a specimen is first stretched in x direction. The study uses the viscous material parameter of Table 7.3 and a loading speed of $\dot{\lambda} = 0.433\,\text{s}^{-1}$. Directly after this, the specimen is stretched in y direction with the same loading speed. For the stretch in y direction, a higher stress during the loading can be observed in simulation, see Figure 7.9.
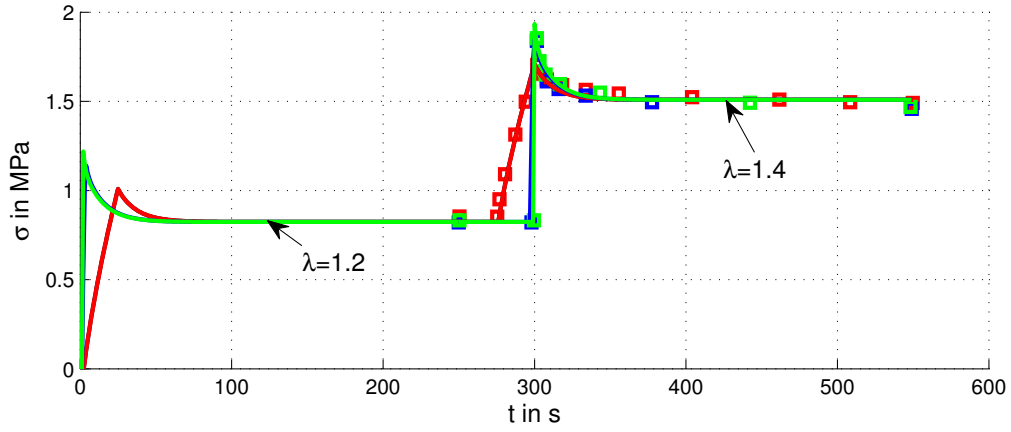
Figure 7.8.: Relaxation test, step form $\lambda = 1$ to $\lambda = 1.2$ and $\lambda = 1.2$ to $\lambda = 1.4$, loading speed $\dot{\lambda} = 0.00833\,\mathrm{s}^{-1}$ (red line), $\dot{\lambda} = 0.085\,\mathrm{s}^{-1}$ (blue line), $\dot{\lambda} = 0.433\,\mathrm{s}^{-1}$ (green line), test data (squares) form Dämgen [2006].

The specimen is now in an anisotropic state. During the increase of stretch in y direction, the curve converge to the loading in x direction, which can be explained by the relaxation of chains in x direction. After releasing the stretch, the specimen shows almost the same anisotropy in y direction as showed before in x direction.
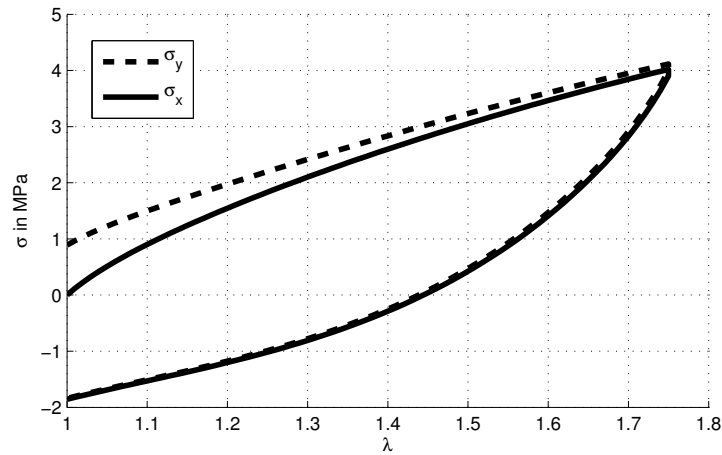

Figure 7.9.: Strain introduced anisotropic behaviour for loading in two directions

8. Conclusion

Elastomers play an important role in the automotive industry, especially in the tire industry. The requirements on elastomers are enormous since the tire is the only interface between the car and the road. Therefore, the need for improved elastomer materials and a better understanding is crucially demanded. Filling of elastomer leads to a broad band of material behaviour, such as the Mullins effect and frequency dependent damping.

In this thesis, a fully micro-mechanical motivated material model for filled elastomer is developed, including anisotropic damage (Mullins effect) and viscous effects. This model is applicable to a general elastomer material, which means that it can be used for filled and unfilled elastomer. An important fact is that all material parameters have a direct physical meaning in the micromechanics behaviour, thus making it possible to develop new materials by virtual testing and a better understanding of filled elastomer material.

The existing material models have been reviewed in this thesis. From given literature review, we know that many available material models describe the mechanical behaviour in a phenomenological way. Only a few material models are directly derived from the micromechanics, although no implementation of material tangent in FEM program has been reported. To overcome this problem, the existing micro-mechanical models were extended and transferred to a suitable form for FE implementation.

The material has been implemented based upon the idea of a network decomposition concept, whereby filled elastomers comprise the monomer chains and the filler particles. In this case, the material has been decomposed into chain-chain network, chain-filler network and free chains. This decomposition corresponds to the elastic, anisotropic damage (Mullins effect) and viscous response.

The elastic response has been modelled with the concept of entropy elasticity. If a chain of an elastomer specimen is stretched, the entropy decreases and consequently a force has to be applied to hold the entropy inequality. For the anisotropic Mullins effect, the model has been extended by including the chain-filler interaction. The loss of the stiffness can be described due to continuous debonding of chains from the filler particles during the virgin loading. Therefore, a distribution function for the chain length between the filler was used, as described in the existing literature and is modified for the computational efficient implementation in this thesis. The viscous effects have been modelled by the diffusion processes of free chains, described by a one-dimensional diffusion equation. From this equation, a relaxation time spectrum has been derived. The solution of this equation is turned into a computable form for the three-dimensional material law. The material description is the sum of the decomposed material chain-chain network for elastic response, chain-filler network for Mullins effect and free chains for frequency dependent damping.

The effect of each micro-mechanical parameter has been investigated in the parameter studies. In the next step, the material parameters have been fitted to material tests, like multi axial loading and relaxation tests. In multi axial loading, the modelling

capability has been shown in an expressive way. The permanent set could be modelled in a natural way without using any plasticity model. Furthermore, the reduced stiffness orthogonal to loading direction could be predicted correctly. Moreover, for viscous effects, the strain introduced anisotropy has been highlighted.

8.1. Outlook

The possibility to derive a material from microstructure has been shown in this thesis. A next step is to validate the statistical distribution of chains with the measured data from the existing elastomer material. Another interesting point is to model the quasi-static hysteresis, therefore it is important to gain a deeper look inside the filler particle clusters. A first step could be a mechanical description of the acting forces in the filler particles. Therefore a micro-mechanical model of the filler particle is necessary. Moreover, the influence of the temperature would be interesting.

It is known that the temperature has a big influence on the mechanical behaviour. For this reason the micro-mechanical relations have to be generalized to temperature dependency. The special interest lies in the temperature region where the mechanical behaviour changes rapidly. This could help to extend the temperature range of material usage.

A.
Numerical integration over a unit sphere

Table A.1.: Direction and weights for the 21×2 unit sphere integration schema, by Bazant and Oh [1986]

i	d_1	d_2	d_3	$w_i/2$
1	1.000000000000	0.000000000000	0.000000000000	0.0265214244093
2	0.000000000000	1.000000000000	0.000000000000	0.0265214244093
3	0.000000000000	0.000000000000	1.000000000000	0.0265214244093
4	0.707106781187	0.707106781187	0.000000000000	0.0199301476312
5	0.707106781187	-0.707106781187	0.000000000000	0.0199301476312
6	0.707106781187	0.000000000000	0.707106781187	0.0199301476312
7	0.707106781187	0.000000000000	-0.707106781187	0.0199301476312
8	0.000000000000	0.707106781187	0.707106781187	0.0199301476312
9	0.000000000000	0.707106781187	-0.707106781187	0.0199301476312
10	0.387907304067	0.387907304067	0.836095596749	0.0250712367487
11	0.387907304067	0.387907304067	-0.836095596749	0.0250712367487
12	0.387907304067	-0.387907304067	0.836095596749	0.0250712367487
13	0.387907304067	-0.387907304067	-0.836095596749	0.0250712367487
14	0.387907304067	0.836095596749	0.387907304067	0.0250712367487
15	0.387907304067	0.836095596749	-0.387907304067	0.0250712367487
16	0.387907304067	-0.836095596749	0.387907304067	0.0250712367487
17	0.387907304067	-0.836095596749	-0.387907304067	0.0250712367487
18	0.836095596749	0.387907304067	0.387907304067	0.0250712367487
19	0.836095596749	0.387907304067	-0.387907304067	0.0250712367487
20	0.836095596749	-0.387907304067	0.387907304067	0.0250712367487
21	0.836095596749	-0.387907304067	-0.387907304067	0.0250712367487

Literaturverzeichnis

Albrecht, J. and Collatz, L. (1958). Zur numerischen Auswertung mehrdimensionaler Integrale. *ZAMM - Journal of Applied Mathematics and Mechanics / Zeitschrift für Angewandte Mathematik und Mechanik*, 38(1-2):1–15.

Alder, B. J. and Wainwright, T. E. (1957). Phase transition for a hard sphere system. *The Journal of Chemical Physics*, 27(5):1208–1209.

Alger, M. (1996). *Polymer Science Dictionary.* Springer.

Baerns, M., Behr, A., Brehm, A., Gmehling, J., Hofmann, H., Onken, U., Renken, A., Hinrichsen, K.-O., and Palkovits, R. (2013). *Technische Chemie.* Wiley-VCH.

Bathe, K. J. (2006). *Finte Element Procedures.* Prentice Hall, Pearson Education.

Bazant, P. and Oh, B. H. (1986). Efficient numerical integration on the surface of a sphere. *ZAMM - Journal of Applied Mathematics and Mechanics / Zeitschrift für Angewandte Mathematik und Mechanik*, 66(1):37–49.

Bazant, Z. P. and Oh, B. H. (1985). Microplane model for progressive fracture of concrete and rock. *Journal of Engineering Mechanics*, 111(4):559–582.

Besdo, D. and Ihlemann, J. (2003). A phenomenological constitutive model for rubberlike materials and its numerical applications. *International Journal of Plasticity*, 19(7):1019 – 1036.

Blum, G. W., Shelton, J. R., and Winn, H. (1951). Rubber oxidation and aging studies safe limits of sample thickness. *Rubber Chem. Technol.*, 24:999–1016.

Bonet, J. and Wood, R. D. (2008). *Nonlinear continuum mechanics for finite element analysis.* Cambridge University Press, 2 edition.

Boukamel, A., Meo, S., Debordes, O., and Jaeger, M. (2001). A thermo-viscoelastic model for elastomeric behaviour and its numerical application. *Archive of Applied Mechanics*, 71:785–801. 10.1007/s004190100191.

Bueche, F. (1960). Molecular basis for the mullins effect. *Journal of Applied Polymer Science*, 4(10):107–114.

Bueche, F. (1961). Mullins effect and rubber–filler interaction. *Journal of Applied Polymer Science*, 5(15):271–281.

Cantournet, S., Desmorat, R., and Besson, J. (2009). Mullins effect and cyclic stress softening of filled elastomers by internal sliding and friction thermodynamics model. *International Journal of Solids and Structures*, 46(11-12):2255 – 2264.

Chauvin, J. (1999). François fresneau : un saintongeais méconnu, inventeur de l'arbre à caoutchouc. *Le Picton*, 95:1–10.

Coleman, B. D. and Gurtin, M. E. (1967). Thermodynamics with internal state variables. *The Journal of Chemical Physics*, 47(2):597–613.

Dal, H. and Kaliske, M. (2009). Bergström–Boyce model for nonlinear finite rubber viscoelasticity: theoretical aspects and algorithmic treatment for the FE method. *Computational Mechanics*, 44:809–823.

Dargazany, R. and Itskov, M. (2009). A network evolution model for the anisotropic Mullins effect in carbon black filled rubbers. *International Journal of Solids and Structures*, 46(16):2967 – 2977.

Doi, M. and Edwards, S. F. (1986). *The Theory of Polymer Dynamics*. Oxford Science Publications.

Dorfmann, A. and Ogden, R. W. (2004). A constitutive model for the Mullins effect with permanent set in particle-reinforced rubber. *International Journal of Solids and Structures*, 41(7):1855 – 1878.

Drozdov, A. and Christiansen, J. (2009). Thermo-viscoplasticity of carbon black-reinforced thermoplastic elastomers. *International Journal of Solids and Structures*, 46(11):2298 – 2308.

Dämgen, M. (2006). *Experimentelle Untersuchungen zum elastischen und inelastischen Verhalten von Elastomeren*. PhD thesis, Gottfried Wilhelm Leinbniz Universität Hannover.

Einstein, A. (1906). Eine neue Bestimmung der Molekul-Dimension (a new determination of the molecular dimensions). *Ann. d. Physik*, 19(2):289–306.

Einstein, A. (1911). Berichtigung zu meiner Arbeit: Eine neue Bestimmung der Molekul-Dimension (correction of my work: A new determination of the molecular dimensions). *Annalen der Physik*, 34(3):591–592.

Flory, P. J. (1989). *Statistical Mechanics of Chain Molecules*. Hanser.

Gent, A. N. (1996). A new constitutive relation for rubber. *Rubber Chemistry and Technology*, 69:59–61.

Gibbs, J. H. and DiMarzio, E. A. (1958). Nature of the glass transition and the glassy state. *The Journal of Chemical Physics*, 28(3):373–383.

Goodyear, C. (1844). Improvement in india-rubber fabrics.

Govindjee, S. and Simo, J. (1991). A micro-mechanically based continuum damage model for carbon black-filled rubbers incorporating Mullins' effect. *Journal of the Mechanics and Physics of Solids*, 39(1):87 – 112.

Guth, E. and Simha, R. (1936). Untersuchungen über die Viskosität von Suspensionen und Lösungen. 3. Über die Viskosität von Kugelsuspensionen. *Kolloid-Zeitschrift*, 74(3):266–275.

Göktepe, S. and Miehe, C. (2005). A micro–macro approach to rubber-like materials. Part III: The micro-sphere model of anisotropic Mullins-type damage. *Journal of the Mechanics and Physics of Solids*, 53(10):2259 – 2283.

Harwood, J. A. C., Mullins, L., and Payne, A. R. (1965). Stress softening in natural rubber vulcanizates. Part II. stress softening effects in pure gum and filler loaded rubbers. *Journal of Applied Polymer Science*, 9(9):3011–3021.

Hashin, Z. (1962). The elastic moduli of hetrogeneous materials. *Journal of Applied Mechanics*, 29:143–150.

Haupt, P. (1985). On the concept of an intermediate configuration and its application to a representation of viscoelastic-plastic material behavior. *International Journal of Plasticity*, 4:303–316.

Heinrich, G. and Kaliske, M. (1997). Theoretical and numerical formulation of a molecular constitutive tube-model of rubber elasticity. *Computational and Theoretical Polymer Science*, 7:227–241.

Hiemenz, P. C. and Lodge, T. P. (2007). *Polymer Chemistry*. CRC Press.

Hill, R. (1963). Elastic properties of reinforced solids: some theoretical principles. *Journal of the Mechanics and Physics of Solids*, 11:357–372.

Holzapfel, G. A. (2000). *Nonlinear Solid Mechanics*. Wiley.

Holzapfel, G. A. and Simo, J. C. (1996). A new viscoelastic constitutive model for continuous media at finite thermomechanical changes. *International Journal of Solids and Structures*, 33(20-22):3019 – 3034.

Huber, G. and Vilgis, T. A. (1998). Polymer adsorption on heterogeneous surfaces. *The European Physical Journal B*, 3(2):217–223.

Itskov, M. (2007). *Tensor Algabra and Tensor Analysis for Engineers, With Application to Continuum Mechanics*. Springer.

Itskov, M., Ehret, A., Makovska, R., and Weinhold, G. (2010). A thermodynamically consistent phenomenological model of the anisotropic Mullins effect. *ZAMM - Journal of Applied Mathematics and Mechanics / Zeitschrift für Angewandte Mathematik und Mechanik*, 90(5):370–386.

James, H. M. and Guth, E. (1943). Theory of the elastic properties of rubber. *The Journal of Chemical Physics*, 11(10):455–481.

Kaliske, M. and Heinrich, G. (1999). An extended tube-model for rubber elasticity: Statistical-mechanical theory and finite element implementation. *Rubber Chemistry and Technology*, 72(4):602–632.

Klueppel, M. (2003). The role of disorder in filler reinforcement of elastomers on various length scales. In *Filler-Reinforced Elastomers/Sanning Force Microscopy*, pages 1–86. Springer.

Kröner, E. (1977). Bounds for effective elastic moduli of disordered materials. *Journal of the Mechanics and Physics of Solids*, 25:137–157.

Kuhn, W. and Grün, F. (1942). Beziehungen zwischen elastischen Konstanten und Dehnungsdoppelbrechung hochelastischer Stoffe. *Kolloid-Zeitschrift*, 101(3):248–271.

Lemaitre, J. and Desmorat, R. (2005). *Engineering Damage Mechanics: Ductile, Creep, Fatigue and Brittle Failures*. Springer Berlin Heidelberg New York.

Lion, A. (1997). A physically based method to represent the thermo-mechanical behaviour of elastomers. *Acta Mechanica*, 123(1-4):1–25.

Lubliner, J. (1969). On fading memory in materials of evolutionary type. *Acta Mechanica*, 8:75–81.

Malvern, L. E. (1969). *Introduction to the Mechanics of a Contiuous Medium*. Prentice-Hall.

Marlow, R. (2003). A general first-invariant hyperelastic constitutive model. *Constitutive Models for Rubber*, pages 157–160.

Marsden, J. E. and Hughes, T. J. R. (1983). *Mathematical Foundations of Elasticity*. Pretice-Hall.

Martinez, J., Boukamel, A., Méo, S., and Lejeunes, S. (2011). Statistical approach for a hyper-visco-plastic model for filled rubber: Experimental characterization and numerical modeling. *European Journal of Mechanics - A/Solids*, 30(6):1028 – 1039.

McLeish, T. C. B. and Larson, R. G. (1998). Molecular constitutive equations for a class of branched polymers: The pom-pom polymer. *Journal of Rheology*, 42(1):81–110.

Miehe, C. (1994). Aspects of the formulation and finite element implementation of large strain isotropic elasticity. *International Journal for Numerical Methods in Engineering*, 37(12):1981–2004.

Miehe, C. (1996). Numerical computation of algorithmic (consistent) tangent moduli in large-strain computational inelasticity. *Computer Methods in Applied Mechanics and Engineering*, 134(3–4):223 – 240.

Miehe, C. and Göktepe, S. (2005). A micro–macro approach to rubber-like materials. Part II: The micro-sphere model of finite rubber viscoelasticity. *Journal of the Mechanics and Physics of Solids*, 53(10):2231 – 2258.

Miehe, C., Göktepe, S., and Lulei, F. (2004). A micro-macro approach to rubber-like materials. Part I: The non-affine micro-sphere model of rubber elasticity. *Journal of the Mechanics and Physics of Solids*, 52(11):2617 – 2660.

Mooney, M. (1940). A theory of large elastic deformation. *Journal of Applied Physics*, 11(9):582 –592.

Mullins, L. (1969). Softening of rubber by deformation. *Rubber Chemistry and Technology*, 42(1):339–362.

Mullins, L. and Tobin, N. R. (1965). Stress softening in rubber vulcanizates. Part I. Use of a strain amplification factor to describe the elastic behavior of filler-reinforced vulcanized rubber. *Journal of Applied Polymer Science*, 9(9):2993–3009.

Nasdala, L., Kaliske, M., and Wei, Y. (2005). Simulation of inelastic rubber material using a force field based FE approach. *Constitutive Models for Rubber IV*.

Ogden, R. (1973). Large deformation isotropic elasticity - on the correlation of theory and experiment for incompressible rubberlike solids. *Rubber Chemistry and Technology*, 46(2):398–416.

Ogden, R. (1984). *Non-Linear Elastic Deformations*. Dover Publications.

Ogden, R. and Roxburgh, D. (1999). A pseudo–elastic model for the Mullins effect in filled rubber. *Proceedings of the Royal Society of London. Series A: Mathematical, Physical and Engineering Sciences*, 455(1988):2861–2877.

O'Neil, G. A., Wisnudel, M. B., and Torkelson, J. M. (1996). A critical experimental examination of the gel effect in free radical polymerization: Do entanglements cause autoacceleration? *Macromolecules*, 29(23):7477–7490.

Pawelski, H. (2001). Softening behaviour of elastomeric media after loading in changing directions. In *Constitutive Models For Rubber 2*, pages 27–36.

Payne, A. R. (1962). The dynamic properties of carbon black-loaded natural rubber vulcanizates. Part I. *Journal of Applied Polymer Science*, 6(19):57–63.

Plauson, H. (1937). Process for polymerizing acrylic mixtures of acrylic esters with vinyl esters (us patent).

Rault, J., Marchal, J., Judeinstein, P., and Albouy, P. A. (2006). Stress-induced crystallization and reinforcement in filled natural rubbers: 2H NMR study. *Macromolecules*, 39(24):8356–8368.

Reese, S. (2003). A micromechanically motivated material model for the thermoviscoelastic material behaviour of rubber-like polymers. *International Journal of Plasticity*, 19(7):909 – 940.

Reese, S. and Govindjee, S. (1997). Theoretical and numerical aspects in the thermo-viscoelastic material behaviour of rubber-like polymers. *Mechanics of Time-Dependent Materials*, 1:357–396. 10.1023/A:1009795431265.

Reuss, A. (1929). A calculation of the bulk modulus of polycrystalline materials. *Zeitschrift Angewandte - Mathematische Methoden*, 9:49–81.

Rivlin, R. S. (1948). Large elastic deformations of isotropic materials. IV. Further developments of the general theory. *Philosophical Transactions of the Royal Society of London. Series A, Mathematical and Physical Sciences*, 241(835):379–397.

Rivlin, R. S. and Saunders, D. W. (1951a). Large elastic deformations of isotropic materials VII. *Philosophical Transactions of the Royal Society of London. Series A, Mathematical and Physical Sciences*, 243:251–288.

Rivlin, R. S. and Saunders, D. W. (1951b). Large elastic deformations of isotropic materials. VII. Experiments on the deformation of rubber. *Philosophical Transactions of the Royal Society of London. Series A, Mathematical and Physical Sciences*, 243(865):251–288.

Rouse, P. E. (1953). A theory of the linear viscoelastic properties of dilute solutions of coiling polymers. *The Journal of Chemical Physics*, 21(7):1272–1280.

Röthemeyer, F. and Sommer, F. (2013). *Kautschuktechnologie: Werkstoffe - Verarbeitung - Produkte*. Hanser Verlag.

Simo (1987). On a fully three-dimensional finite-strain viscoelastic damage model: Formulation and computational aspects. *Computer Methods In Applied Mechanics And Engineering*, 60:153–173.

Simo, J. C. and Hughes, T. J. R. (2000). *Computational Inelasticity*. Springer.

Suwannachit, A. and Nackenhorst, U. (2013). A novel approach for thermomechanical analysis of stationary rolling tires within an ALE–kinematic framework. *Tire Science and Technology*, 41(3):174–195.

Tang, S., Greene, M. S., and Liu, W. K. (2012). Two-scale mechanism-based theory of nonlinear viscoelasticity. *Journal of the Mechanics and Physics of Solids*, 60(2):199 – 226.

Taylor, G. I. (1938). Plastic strain in metals. *Lecturenotes: Institute of Metals*.

Toki, S., Hsiao, B. S., Amnuaypornsri, S., and Sakdapipanich, J. (2009). New insights into the relationship between network structure and strain-induced crystallization in un-vulcanized and vulcanized natural rubber by synchrotron X-ray diffraction. *Polymer*, 50(9):2142 – 2148.

Treloar, L. R. G. (1943). The elasticity of a network of long-chain molecules. I. *Rubber Chemistry and Technology*, 16:746–751.

Treloar, L. R. G. (1954). The photoelastic properties of short-chain molecular networks. *Trans. Faraday Soc.*, 50:881–896.

Treloar, L. R. G. (1975). *The Phyiscs of Rubber Elasticity*. Oxford University Press.

Truesdell, C. and Noll, W. (1965). *The Non-Linear Field Theories of Mechanics*. Springer.

van der Linden, C. C., van Lent, B., Leermakers, F. A. M., and Fleer, G. J. (1994). Adsorption of polymers on heterogeneous surfaces. *Macromolecules*, 27(7):1915–1921.

Voigt, W. (1889). Bestimmung der Elasticitäts- Constanten für Kalkspats. *Nachrichten von der Königl. Gesellschaft der Wissenschaften und der Georg-Augusts-Universitöt zu Göttingen*, (1889):483–519.

Wriggers, P. (2008). *Nonlinear Finite Element Methods*. Springer Berlin Heidelberg.

Yeoh, O. H. (1993). Some forms of the strain energy function for rubber. *Rubber Chemistry and Technolog*, 66(5):754–771.

Zeng, Q., Yu, A., and Lu, G. (2008). Multiscale modeling and simulation of polymer nanocomposites. *Progress in Polymer Science*, 33(2):191 – 269.

Zienkiewicz, O., Taylor, R., and Zhu, J. (2005). *The Finite Element Method: It's Basis and Fundamentals*. Elsevier Ltd.

Lebenslauf

Persönliche Daten

Ole Stegen

geboren am 30. August 1984 in Hamburg

Schulbildung

1991–1995   Grundschule Dassendorf

1995–2004   Integrierte Gesamtschule Geesthacht

Zivildienst

09/2004–06/2005   Zivildienst bei den Jugendzentrum Geesthacht

Studium

2005–2009   Studium des Maschinenbaus
an der HAW Hamburg
Abschluss: Diplon Ingenieur (FH)

2009–2011   Studium der Computergestützten Ingenieurwissenschaften
an der Leibniz Universität Hannover
Abschluss Master of Science

Berufstätigkeit

10/2011–09/2014   Wissenschaftlicher Mitarbeiter am Institut für Baumechanik
und Numerische Mechanik der Leibniz Universität Hannover

Forschungs- und Seminarberichte

Institut für Baumechanik und Numerische Mechanik
Gottfried Wilhelm Leibniz Universität Hannover

Bisher in dieser Schriftenreihe erschienene Berichte:

S 73/1   Seminar über Thermodynamik und Kontinuumsmechanik, Hannover 1973

F 75/1   "Die Spannungsberechnung im Rahmen der Finite–Element–Methode",
R. Ahmad, Dissertation, April 1975

F 76/1   "Zur Theorie und Anwendung der Stoffgleichungen elastisch–plastisch–viskoser Werkstoffe",
H. Mentlein, Dissertation, April 1976

S 77/1   Seminar über lineare und geometrisch nichtlineare Schalentheorie einschließlich Stabilitätstheorie, Hannover 1977

F 77/2   "Beitrag zur Berechnung von Gründungsplatten mit Hilfe der Finite–Element–Methode",
H. Meyer, Dissertation, Juli 1977

F 77/3   "Zur Berechnung der Eigenfrequenzen und Eigenschwingungsformen räumlich vorgekrümmter und vorverwundener Stäbe",
J. Möhlenkamp, Dissertation, Dezember 1977

F 77/4   "Zur Theorie und Berechnung geometrisch und physikalisch nichtlinearer Kontinua mit Anwendung der Methode der finiten Elemente",
J. Paulun, Dissertation, Dezember 1977

S 78/1   2. Seminar über Thermodynamik und Kontinuumsmechanik,
Hannover 1978

F 79/1   "Theoretische und numerische Behandlung geometrisch nichtlinearer viskoplastischer Kontinua",
K.–D. Klee, Dissertation, Februar 1979

F 79/2   "Zur Konstruierbarkeit von Variationsfunktionalen für nichtlineare Probleme der Kontinuumsmechanik",
J. Siefer, Dissertation, Oktober 1979

F 80/1   "Theoretische und numerische Behandlung gerader Stäbe mit endlichen Drehungen",
M. Kessel, Dissertation, Februar 1980

F 81/1   "Zur Berechnung von Kontakt– und Stoßproblemen elastischer Körper mit Hilfe der Finite–Element–Methode",
P. Wriggers, Dissertation, Januar 1981

F 81/2   "Stoffgleichungen für Steinsalze unter mechanischer und thermischer Beanspruchung",
J. Olschewski, E. Stein, W. Wagner, D. Wetjen, geänderte Fassung eines Zwischenberichtes zum BMFT–Forschungsvorhaben KWA 1608/5

F 82/1   "Konvergenz und Fehlerabschätzung bei der Methode der Finiten Elemente",
R. Rohrbach, E. Stein, Abschlußbericht eines VW–Forschungsvorhabens, Februar 1982

F 82/2   "Alternative Spannungsberechnung in Finite–Element–Verschiebungsmodellen",
C. Klöhn, Dissertation, November 1982

F 83/1   Seminar über nichtlineare Stabtheorie, Hannover 1983

F 83/2   "Beiträge zur nichtlinearen Theorie und inkrementellen Finite–Element– Berechnung dünner elastischer Schalen",
A. Berg, Dissertation, Juli 1983

F 83/3   "Elastoplastische Plattenbiegung bei kleinen Verzerrungen und großen Drehungen",
J. Paulun, Habilitation, September 1983

F 83/4   "Geometrisch nichtlineare FE–Berechnung von Faltwerken mit plastisch / viskoplastischem Deformationsverhalten",
M. Krog, Dissertation, Dezember 1983

F 85/1   Verleihung der Ehrendoktorwürde des Fachbereichs Bauingenieur– und Vermessungswesen der Universität Hannover an die Herren Prof. Dr. Drs. h.c. J.H. Argyris, Dr.–Ing. H.Wittmeyer

F 85/2   "Eine geometrisch nichtlineare Theorie schubelastischer Schalen mit Anwendung auf Finite–Element–Berechnungen von Durchschlag– und Kontaktproblemen",
W. Wagner, Dissertation, März 1985

F 85/3   "Geometrisch/physikalisch nichtlineare Probleme — Struktur und Algorithmen — ",
GAMM–Seminar im Februar 1985 in Hannover

F 87/1   "Finite–Elemente–Berechnungen ebener Stabtragwerke mit Fließgelenken und großen Verschiebungen",
R.Kahn, Dissertation, Oktober 1987

F 88/1   "Theorie und Numerik schubelastischer Schalen mit endlichen Drehungen unter Verwendung der Biot–Spannungen",
F. Gruttmann, Dissertation, Juni 1988

F 88/2   "Optimale Formgebung von Stabtragwerken mit Nichtlinearitäten in der Zielfunktion und in den Restriktionen unter Verwendung der Finite-Element-Methode",
V. Berkhahn, Dissertation, Oktober 1988

F 88/3   "Beiträge zur Theorie und Numerik großer plastischer und kleiner elastischer Deformationen mit Schädigungseinfluß",
R. Lammering, Dissertation, November 1988

F 88/4   "Konsistente Linearisierungen in der Kontinuumsmechanik und ihrer Anwendung auf die Finite–Elemente–Methode",
P. Wriggers, Habilitation, November 1988

F 88/5   "Mathematische Formulierung und numerische Methoden für Kontaktprobleme auf der Grundlage von Extremalprinzipien",
D. Bischoff, Habilitation, Dezember 1988

F 88/6   "Zur numerischen Behandlung thermomechanischer Prozesse",
C. Miehe, Dissertation, Dezember 1988

F 89/1   "Zur Stabilität und Konvergenz gemischter finiter Elemente in der linearen Elastizitätstheorie",
R. Rolfes, Dissertation, Juni 1989

F 89/2   "Traglastberechnungen von Faltwerken mit elastoplastischen Deformationen",
K.-H. Lambertz, Dissertation, Oktober 1989

F 89/3   "Transientes Kriechen und Kriechbruch im Steinsalz",
U. Heemann, Dissertation, November 1989

F 89/4   "Materialgesetze zum Verhalten von Betonkonstruktionen bei harten Stößen",
E. Stein, P. Wriggers, T. Vu Van & T. Wedemeier, Dezember 1989

F 89/5   "Lineare Konstruktion und Anwendungen von Begleitmatrizen",
C. Carstensen, Dissertation, Dezember 1989

F 90/1   "Zur Berechnung prismatischer Stahlbetonbalken mit verschiedenen Querschnittsformen für allgemeine Beanspruchungen",
H. N. Lucero–Cimas, Dissertation, April 1990

F 90/2   "Zur Behandlung von Stoß- Kontaktproblemen mit Reibung unter Verwendung der Finite–Element–Methode",
T. Vu Van, Dissertation, Juni 1990

F 90/3   "Netzadaption und Mehrgitterverfahren für die numerische Behandlung von Faltwerken",
L. Plank, Dissertation, September 1990

F 90/4   "Beiträge zur Theorie und Numerik finiter inelastischer Deformationen",
N. Müller–Hoeppe, Dissertation, Oktober 1990

F 90/5 "Beiträge zur Theorie und Numerik von Materialien mit innerer
Reibung am Beispiel des Werkstoffes Beton",
T. Wedemeier, Dissertation, Oktober 1990

F 91/1 "Zur Behandlung von Stabilitätsproblemen der Elastostatik mit der Methode der
Finiten Elemente",
W. Wagner, Habilitation, April 1991

F 91/2 "Mehrgitterverfahren und Netzadaption für lineare und nichtlineare statische Finite–
Elemente–Berechnungen von Flächentragwerken",
W. Rust, Dissertation, Oktober 1991

F 91/3 "Finite Elemente Formulierungen im Trefftzschen Sinne für dreidimensionale
anisotrop–elastische Faserverbundstrukturen",
K. Peters, Dissertation, Dezember 1991

F 92/1 "Einspielen und dessen numerische Behandlung von Flächentragwerken aus ideal plas-
tischem bzw. kinematisch verfestigendem Material",
G. Zhang, Dissertation, Februar 1992

F 92/2 "Strukturoptimierung stabilitätsgefährdeter Systeme mittels analytischer
Gradientenermittlung",
A. Becker, Dissertation, April 1992

F 92/3 "Duale Methoden für nichtlineare Optimierungsprobleme in der Strukturmechanik",
R. Mahnken, Dissertation, April 1992

F 93/1 "Kanonische Modelle multiplikativer Elasto–Plastizität. Thermodynamische For-
mulierung und numerische Implementation",
C. Miehe, Habilitation, Dezember 1993

F 93/2 "Theorie und Numerik zur Berechnung und Optimierung von Strukturen aus
isotropen, hyperelastischen Materialien",
F.–J. Barthold, Dissertation, Dezember 1993

F 94/1 "Adaptive Verfeinerung von Finite-Element-Netzen für Stabilitätsprobleme von
Flächentragwerken",
E. Stein, B. Seifert, W. Rust, Forschungsbericht, Oktober 1994

F 95/1 "Adaptive Verfahren für die Formoptimierung von Flächentragwerken unter Berück-
sichtigung der CAD–FEM–Kopplung",
A. Falk, Dissertation, Juni 1995

F 96/1 "Theorie und Numerik dünnwandiger Faserverbundstrukturen",
F. Gruttmann, Habilitation, Januar 1996

F 96/2 "Zur Theorie und Numerik finiter elastoplastischer Deformationen von Schalenstruk-
turen",
B. Seifert, Dissertation, März 1996

F 96/3 "Theoretische und algorithmische Konzepte zur phänomenologischen Beschreibung
anisotropen Materialverhaltens",
J. Schröder, Dissertation, März 1996

F 96/4 "Statische und dynamische Berechnungen von Schalen endlicher elastischer Deforma-
tionen mit gemischten finiten Elementen",
P. Betsch, Dissertation, März 1996

F 96/5 "Kopplung von Finiten Elementen und Randelementen für ebene Elastoplastizität mit
Implementierung auf Parallelrechnern",
M. Kreienmeyer, Dissertation, März 1996

F 96/6 "Theorie und Numerik dimensions- und modelladaptiver Finite-Elemente-Methoden
von Flächentragwerken",
S. Ohnimus, Dissertation, Juni 1996

F 96/7 "Adaptive Finite Elemente Methoden für MIMD-Parallelrechner zur Behandlung von
Strukturproblemen mit Anwendung auf Stabilitätsprobleme",
O. Klaas, Dissertation, Juli 1996

F 96/8 "Institutsbericht 1971–1996 aus Anlaß des 25-jährigen Dienstjubiläums von Prof. Dr.-
Ing. Dr.-Ing. E.h. Dr. h.c. mult. Erwin Stein, Dezember 1996

F 97/1 "Modellierung und Numerik duktiler kristalliner Werkstoffe",
P. Steinmann, Habilitation, August 1997

F 97/2   "Formoptimierung in der Strukturdynamik",
L. Meyer, Dissertation, September 1997

F 97/3   "Modellbildung und Numerik für Versagensprozesse in Gründungen von Caisonwellenbrechern",
M. Lengnick, Dissertation, November 1997

F 98/1   "Adaptive gemischte finite Elemente in der nichtlinearen Elastostatik und deren Kopplung mit Randelementen",
U. Brink, Dissertation, Februar 1998

F 98/2   "Theoretische und numerische Aspekte zur Parameteridentifikation und Modellierung bei metallischen Werkstoffen",
R. Mahnken, Habilitation, Juli 1998

F 98/3   "Lokalisierung und Stabilität der Deformation wassergesättigter bindiger und granularer Böden",
J. M. Panesso, Dissertation, August 1998

F 98/4   "Theoretische und numerische Methoden in der angewandten Mechanik mit Praxisbeispielen",
R. Mahnken (Hrsg.), Festschrift anlässlich der Emeritierung von Prof. Dr.–Ing. Dr.–Ing. E.h. h.c. mult. Erwin Stein, November 1998

F 99/1   "Eine h-adaptive Finite–Element–Methode für elasto–plastische Schalenprobleme in unilateralem Kontakt",
C.-S. Han, Dissertation, Juli 1999

F 00/1   "Ein diskontinuierliches Finite–Element–Modell für Lokalisierungsversagen in metallischen und granularen Materialien",
C. Leppin, Dissertation, März 2000

F 00/2   "Untersuchungen von Strömungen in zeitlich veränderlichen Gebieten mit der Methode der Finiten Elemente",
H. Braess, Dissertation, März 2000

F 00/3   "Theoretische und algorithmische Beiträge zur Berechnung von Faserverbundschalen",
J. Tessmer, Dissertation, März 2000

F 00/4   "Theorie und Finite-Element-Methode für die Schädigungsbeschreibung in Beton und Stahlbeton",
D. Tikhomirov, Dissertation, August 2000

F 01/1   "A C1 - continuous formulation for finite deformation contact",
L. Krstulovic-Opara, Dissertation, Januar 2001

F 01/2   "Strain Localisation Analysis for Fully and Partially Saturated Geomaterials",
H. Zhang, Dissertation, Januar 2001

F 01/3   "Meso-makromechanische Modellierung von Faserverbundwerkstoffen mit Schädigung",
C. Döbert, Dissertation, April 2001

F 01/4   "Thermomechanische Modellierung gummiartiger Polymerstrukturen",
S. Reese, Habilitation, April 2001

F 01/5   "Thermomechanisches Verhalten von Gummimaterialien während der Vulkanisation – Theorie und Numerik –",
M. André, Dissertation, April 2001

F 01/6   "Adaptive FEM für elastoplastische Deformationen – Algorithmen und Visualisierung",
M. Schmidt, Dissertation, Juni 2001

F 01/7   "Verteilte Algorithmen für h-, p- und d-adaptive Berechnungen in der nichtlinearen Strukturmechanik ",
R. Niekamp, Dissertation, Juni 2001

F 01/8   "Theorie und Numerik zur Berechnung und Optimierung von Strukturen mit elastoplastischen Deformationen",
K. Wiechmann, Dissertation, Juli 2001

F 01/9   "Direct Computation of Instability Points with Inequality Contraints using the Finite Element Method",
H. Tschöpe, Dissertation, September 2001

F 01/10   "Theorie und Numerik residualer Fehlerschätzer für die Finite-Elemente-Methode unter Verwendung äquilibrierter Randspannungen",
S. Ohnimus, Habilitation, September 2001

F 02/1   "Adaptive Algorithmen für thermo-mechanisch gekoppelte Kontaktprobleme",
A. Rieger, Dissertation, August 2002

F 02/2   "Consistent coupling of shell- and beam-models for thermo-elastic problems",
K. Chavan, Dissertation, September 2002

F 03/1   "Error-controlled adaptive finite element methods in large strain hyperelasticity and fracture mechanics",
M. Rüter, Dissertation, Mai 2003

F 03/2   "Formulierung und Simulation der Kontaktvorgänge in der Baugrund-Tragwerks-Interaktion",
A. Haraldsson, Dissertation, Juni 2003

F 03/3   "Concepts for Nonlinear Orthotropic Material Modeling with Applications to Membrane Structures",
T. Raible, Dissertation, Juni 2003

F 04/1   "On Single- and Multi-Material arbitrary Lagrangian-Eulerian Approaches with Application to Micromechanical Problems at Finite Deformations",
D. Freßmann, Dissertation, Oktober 2004

F 04/2   "Computational Homogenization of Microheterogeneous Materials at Finite Strains Including Damage",
S. Löhnert, Dissertation, Oktober 2004

F 05/1   "Numerical Micro-Meso Modeling of Mechanosensation driven Osteonal Remodeling in Cortical Bone",
C. Lenz, Dissertation, Juli 2005

F 05/2   "Mortar Type Methods Applied to Nonlinear Contact Mechanics",
K.A. Fischer, Dissertation, Juli 2005

F 05/3   "Models, Algorithms and Software Concepts for Contact and Fragmentation in Computational Solid Mechanics",
C. Hahn, Dissertation, November 2005

F 06/1   "Computational Homogenization of Concrete",
S. Moftah, Dissertation, Januar 2006

F 06/2   "Reduction Methods in Finite Element Analysis of Nonlinear Structural Dynamics",
H. Spiess, Dissertation, Februar 2006

F 06/3   "Theoretische und algorithmische Konzepte zur Beschreibung des beanspruchungsadaptiven Knochenwachstums",
B. Ebbecke, Dissertation, März 2006

F 06/4   "Experimentelle Untersuchungen an elastomeren Werkstoffen",
M. Dämgen, Dissertation, Dezember 2006

F 07/1   "Numerische Konzepte zur Behandlung inelastischer Effekte beim reibungsbehafteten Rollkontakt",
M. Ziefle, Dissertation, Februar 2007

F 07/2   "Begleitbuch zur Leibniz-Ausstellung",
Hrsg: E. Stein, P. Wriggers, 2007

F 07/3   "Modellierung und Simulation der hochfrequenten Dynamik rollender Reifen",
M. Brinkmeier, Dissertation, Juni 2007

F 07/4   "Computational Homogenization of micro-structural Damage due to Frost in Hardened Cement Paste",
M. Hain, Dissertation, Juli 2007

F 07/5   "Elektromechanisch gekoppelte Kontaktmodellierung auf Mikroebene",
T. Helmich, Dissertation, August 2007

F 07/6   "Dreidimensionales Diskrete Elemente Modell für Superellipsoide",
C. Lillie, Dissertation, Oktober 2007

F 07/7   "Adaptive Methods for Continuous and Discontinuous Damage Modeling in Fracturing Solids",
S.H. Reese, Dissertation, Oktober 2007

F 08/1   "Student Projects of Micromechanics",
Hrsg: U. Nackenhorst, August 2008

F 09/1   "Theory and Computation of Mono- and Poly- crystalline Cyclic Martensitic Phase Transformations",
G. Sagar, Dissertation, August 2009

F 09/2   "Student projects of Micromechanics",
D. Balzani and U. Nackenhorst, Course Volume, October 2009

F 09/3   "Multiscale Coupling based on the Quasicontinuum Framework, with Application to Contact Problems",
W. Shan, Dissertation, November 2009

F 10/1   "A Multiscale Computational Approach for Microcrack Evolution in Cortical Bone and Related Mechanical Stimulation of Bone Cells",
D. Kardas, Dissertation, September 2010

F 12/1   "Ein physikalisch motiviertes Reifen-Fahrbahnmodell für die Gesamtfahrzeugsimulation",
R. Chiarello, Dissertation, Februar 2012

F 13/1   "Thermomechanical Analysis of Tire Rubber Compounds in Rolling Contact",
A. Suwannachit, Dissertation, September 2012

F 13/2   "Towards a Finite Element Model for Fluid Flow in the Human Hip Joint",
K. Fietz, Dissertation, September 2013

F 14/1   "Micro-Mechanically Based Damage Analysis of Ultra High Performance Fibre Reinforced Concrete Structures with Uncertainties",
A. Hürkamp, Dissertation, December 2013

F 14/2   "Numerical Solution of High-Dimensional Fokker-Planck Equations with Discontinuous Galerkin Methods",
F. Loerke, Dissertation, Dezember 2013

F 14/3   "Numerische Simulation probabilistischer Schädigungsmodelle mit der Stochastischen Finite Elemente Methode",
P. Jablonski, Dissertation, September 2014

F 15/1   "On a Finite Element Approach for the Solution of a Mechanically Stimulated Biochemical Fracture Healing Model",
A. Sapotnick, Dissertation, September 2015